UNDERWATER TARGET DETECTION WITH HYPERSPECTRAL IMAGERY FOR SEARCH AND RESCUE OPERATIONS

A THESIS SUBMITTED TO

THE GRADUATE SCHOOL OF INFORMATICS OF

THE MIDDLE EAST TECHNICAL UNIVERSITY

BY

İSA CEM EKEN

IN PARTIAL FULFILLMENT OF THE REQUIREMENTS FOR THE DEGREE OF

MASTER OF SCIENCE

IN

THE DEPARTMENT OF INFORMATION SYSTEMS

DECEMBER 2017

UNDERWATER TARGET DETECTION WITH HYPERSPECTRAL IMAGERY FOR SEARCH AND RESCUE OPERATIONS

Submitted by İsa Cem EKEN in partial fulfillment of the requirements for the degree of **Master of Science in Information Systems Department, Middle East Technical University** by,

Prof. Dr. Deniz ZEYREK BOZŞAHIN
Dean, **Graduate School of Informatics** _____

Prof. Dr. Yasemin YARDIMCI ÇETİN
Head of Department, **Information Systems** _____

Prof. Dr. Yasemin YARDIMCI ÇETİN
Supervisor, **Information Systems Dept., METU** _____

Examining Committee Members:

Prof. Dr. Sevgi ÖZKAN YILDIRIM
Information Systems Dept., METU _____

Prof. Dr. Yasemin YARDIMCI ÇETİN
Information Systems Dept., METU _____

Assoc. Prof. Dr. Selim AKSOY
Computer Engineering Dept., Bilkent University _____

Prof. Dr. Kemal LEBLEBİCİOĞLU
Electric-Electronic Eng. Dept., METU _____

Assist. Prof. Dr. Yakup ÖZKAZANÇ
Electric-Electronic Eng. Dept., Hacettepe University _____

Date: *14 December 2017*

I hereby declare that all information in this document has been obtained and presented in accordance with academic rules and ethical conduct. I also declare that, as required by these rules and conduct, I have fully cited and referenced all material and results that are not original to this work.

Name, Last name : İsa Cem EKEN

Signature : _____

ABSTRACT

UNDERWATER TARGET DETECTION WITH HYPERSPECTRAL IMAGERY FOR SEARCH AND RESCUE OPERATIONS

EKEN, İsa Cem

MSc., Department of Information Systems

Supervisor: Prof. Dr. Yasemin YARDIMCI ÇETİN

December 2017, 127 pages

Fast and precise target detection is an issue in underwater object detection applications such as search and rescue, mine detection, archeological remains, etc. Hyperspectral imaging could be effective in determining different components in a selected region thanks to its ability to provide detailed spectral information. The detection of underwater objects with their above-water reflectance signature may not be efficient because of the reflectance changes due to water column. The detection should be conducted with the reflectance signature affected by the water column. To simulate object reflectance under a specific water column, water column correction algorithms can be taken into consideration. Once underwater spectral reflectance is obtained, their effect on the detection performance can be observed.

In this thesis, the effect of water column to an object reflectance is investigated. The water column correction algorithms are utilized to create underwater object spectrum from above-water object reflectance. The effect of underwater target spectrum to object detection is also investigated. The materials used for the study are related to search and rescue operations to be evaluated according to their capability of detection in such scenarios. To increase reaction speed in search and rescue operations, the algorithms used for water column correction and target detection are applied to each material to evaluate the optimum water column correction – target detection algorithm pair for material types.

Keywords: Hyperspectral Imagery, Underwater, Target Detection, Search and Rescue.

ÖZ

ARAMA KURTARMA FAALİYETLERİ İÇİN HİPERSPEKTRAL GÖRÜNTÜLEME İLE SU ALTI NESNE TESPİTİ

EKEN, İsa Cem

Yüksek Lisans, Bilişim Sistemleri Bölümü

Tez Yöneticisi: Prof. Dr. Yasemin YARDIMCI ÇETİN

Aralık 2017, 127 sayfa

Arama kurtarma, mayın tespiti, arkeolojik çalışma faaliyetleri gibi su altı nesne tespiti uygulamalarında hızlı ve hassas tespitin yapılabilmesi sorunlu bir konudur. Hiperspektral görüntüleme ayrıntılı spektral bilgi sağlayabilmesi sayesinde ilgili bölgedeki farklı bileşenleri etkili bir şekilde ayırt edilebilmektedir. Sualtında bulunan nesnelerin tespiti için, nesnenin su üzerindeki imzasının kullanılması, su kütlesinin yansımaya etkisinden dolayı verimli olmayabilir. Nesne tespiti, su kütlesi tarafından etki edilmiş yansıma imzası ile yapılmalıdır. Nesne imzalarının belirli bir su kütlesi altındaki yansımalarını benzetmek için, su kütlesini düzelten algoritmalar dikkate alınabilir. Su altı yansıması elde edildikten sonra, nesne tespitine olan etkisi gözlemlenebilir.

Bu tezde su katmanının bir nesne yansımasına etkisi araştırıldı. Su üzerindeki imzadan sualtı nesne yansıması oluşturmak için su kütlesi düzeltme algoritmaları kullanıldı. Sualtı hedef imzasının hedef tespitine olan etkisi de incelendi. Tezde kullanılan nesneler arama kurtarma faaliyetlerindeki tespit performanslarını ölçmek maksadıyla ilgili senaryolarda karşılaşılan nesnelerden seçilmiştir. Arama kurtarma faaliyetlerindeki reaksiyon hızını artırmak için su kütlesinin etkisini düzeltme ve nesne tepiti algoritmaları her nesneye uygulanmış, optimum su kütlesi düzeltme - nesne tespiti algoritma çiftleri değerlendirilmiştir.

Anahtar Sözcükler: Hiperspektral Görüntüleme, Su altı, Nesne Tespiti, Arama Kurtarma.

To My Family

ACKNOWLEDGMENTS

First of all, I would like to express my gratitude to my thesis supervisor Prof. Dr. Yasemin YARDIMCI ÇETİN for her extensive support, guidance and motivation through the thesis period.

I also thank my thesis jury members Prof. Dr. Sevgi ÖZKAN YILDIRIM, Assoc. Prof. Dr. Selim AKSOY, Prof. Dr. Kemal LEBLEBİCİOĞLU and Assist. Prof. Dr. Yakup ÖZKAZANÇ for their suggestions and reviewing my work.

I would also like to thank Yusuf GÜR, Didem ÖZIŞIK BAŞKURT, Okan Bilge ÖZDEMİR and Fatih ÖMRÜUZUN for their support in data collection, technical troubleshooting and guidance.

Finally, I would like to thank my beloved wife Dilek EKEN and my son Umut EKEN for their endless support, patience and love through the thesis period.

TABLE OF CONTENTS

ABSTRACT iv
ÖZ v
ACKNOWLEDGMENTS vii
TABLE OF CONTENTS viii
LIST OF TABLES x
LIST OF FIGURES xi
LIST OF ABBREVIATIONS xvi
CHAPTERS
INTRODUCTION 1
1.1. Motivation 1
1.2. Scope of the Thesis 2
1.3. Outline of the Thesis 2
2. BACKGROUND 3
2.1. Hyperspectral Imagery 3
2.2. Effect of Water in Hyperspectral Imagery 4
2.2.1 Inherent Optical Properties 4
2.2.2 Apparent Optical Properties 4
2.3. Literature Review 5
2.3.1 Water Column Correction Algorithms 6
2.3.2 Hyperspectral Object Detection Studies 10
3. METHODOLOGY 13
3.1. Approach to the Problem 13
3.2. Choosing Water Column Correction and Target Detection Algorithms 15
4. EXPERIMENTS AND RESULTS 19
4.1. Simulated and Real Data 19

4.2. Evaluating the Performance of Water Column Correction Algorithms in Spectral Signatures 21
4.2.1 Simulation Comparison 21
4.2.2 Real Data Comparison 23
4.3. Evaluating the Performance of Water Column Correction Algorithms in Target Detection 26
4.3.1 Simulation Comparison 26
4.3.2 Real Data Comparison 31
5. CONCLUSION AND FUTURE WORK 37
5.1. Results of the Study 37
5.2. Future Work 40
REFERENCES 41
APPENDICES 45
APPENDIX A 45
APPENDIX B 49
APPENDIX C 55
APPENDIX D 63
APPENDIX E 67
APPENDIX F 117

LIST OF TABLES

Table 1: Outputs of the water column correction algorithms.....15
Table 2: Angles between simulated and obtained signatures with inverted parameters in simulated data.....24
Table 3: Angles between simulated and obtained signatures with inverted parameters in real data 25
Table 4: Performance Evaluation of White Cotton Fabric in 1 meter Depth.....28
Table 5: Detection performance of simulated materials with ACE 29
Table 6: Detection performance of simulated materials with SAM.....30
Table 7: Detection performance of white cotton fabric with F-measure 33
Table 8: Detection performance of real materials with ACE.....34
Table 9: Detection performance of real materials with SAM 35
Table 10: Overall Evaluation of Real Data 38
Table 11: Overall Evaluation of Simulated Data 39

LIST OF FIGURES

Figure 1: Band coverage of multispectral and hyperspectral sensors over the electromagnetic spectrum....3
Figure 2: Hyperspectral Cube 4
Figure 3: Absorption and backscattering coefficients of pure water 5
Figure 4: Reflectance and attenuation coefficient of pure water 5
Figure 5: Flowchart of Target Detection with Simulated Data....13
Figure 6: Flowchart of Target Detection with Real Data....14
Figure 7: Observed Ratio of Dry-Wet Reflectance Transition 19
Figure 8: Simulation Scenes....20
Figure 9: Reflectance Changes of Materials in Dry, Pure and Turbid Water....22
Figure 10: Simulated and Inverted Reflectance of Sheet Metal with MEA and LEA Algorithms in 1 meter depth 23
Figure 11: Observed Reflectance Changes of Sheet Metal and Concrete in different depths 24
Figure 12: Observed Reflectance Changes of Sheet Metal and Concrete in different depths 25
Figure 13: Detection Results of White Cotton Fabric with Different Target Reflectance 27
Figure 14: Detection Results of White Cotton Fabric with Different Target Reflectance (Real Data) 32
Figure 15: Signature comparison of sheet metal from laboratory and outside environments....45
Figure 16: Signature comparison of concrete from laboratory and outside environments 46
Figure 17: Signature comparison of red cotton fabric from laboratory and outside environments....46
Figure 18: Signature comparison of green cotton fabric from laboratory and outside environments....47
Figure 19: Signature comparison of white cotton fabric from laboratory and outside environments....47
Figure 20: Signature comparison of black cotton fabric from laboratory and outside environments....48
Figure 21: Signature comparison of sheet metal (Dry-Wet)....49
Figure 22: Signature comparison of concrete (Dry-Wet) 50
Figure 23: Signature comparison of red cotton fabric (Dry-Wet)....50
Figure 24: Signature comparison of green cotton fabric (Dry-Wet)....51
Figure 25: Signature comparison of sheet metal (Dry-Wet-Underwater)....51

Figure 26: Signature comparison of concrete (Dry-Wet-Underwater) 52
Figure 27: Signature comparison of red cotton fabric (Dry-Wet-Underwater).....52
Figure 28: Signature comparison of green cotton fabric (Dry-Wet-Underwater).....53
Figure 29: Simulated and Inverted Reflectance of Sheet Metal in Various Depths 56
Figure 30: Simulated and Inverted Reflectance of Concrete in Various Depths 57
Figure 31: Simulated and Inverted Reflectance of White Cotton Fabric in Various Depths.....58
Figure 32: Simulated and Inverted Reflectance of Black Nylon Fabric in Various Depths 59
Figure 33: Simulated and Inverted Reflectance of Blue Nylon Fabric in Various Depths 60
Figure 34: Simulated and Inverted Reflectance of Green Nylon Fabric in Various Depths 61
Figure 35: Simulated and Inverted Reflectance of Red Nylon Fabric in Various Depths 62
Figure 36: Simulated and Inverted Reflectance of Sheet Metal, Concrete, White and Black Cotton Fabric (0.3m depth).....63
Figure 37: Simulated and Inverted Reflectance of Cotton Fabric with Colors of Red, Green, Blue(0.3m depth).....64
Figure 38: Simulated and Inverted Reflectance of Blue Denim (0.3m depth).....65
Figure 39: Detection Results of Sheet Metal with Different Target Reflectance(0.1m depth).....68
Figure 40: Detection Results of Sheet Metal with Different Target Reflectance (0.2m depth).....69
Figure 41: Detection Results of Sheet Metal with Different Target Reflectance (0.3m depth).....70
Figure 42: Detection Results of Sheet Metal with Different Target Reflectance (1m depth).....71
Figure 43: Detection Results of Sheet Metal with Different Target Reflectance (2m depth).....72
Figure 44: Detection Results of Sheet Metal with Different Target Reflectance (5m depth).....73
Figure 45: Detection Results of Sheet Metal with Different Target Reflectance (10m depth).....74
Figure 46: Detection Results of Concrete with Different Target Reflectance (0.1m depth) 75
Figure 47: Detection Results of Concrete with Different Target Reflectance (0.2m depth) 76
Figure 48: Detection Results of Concrete with Different Target Reflectance (0.3m depth) 77

Figure 49: Detection Results of Concrete with Different Target Reflectance (1m depth) 78
Figure 50: Detection Results of Concrete with Different Target Reflectance (2m depth) 79
Figure 51: Detection Results of Concrete with Different Target Reflectance (5m depth) 80
Figure 52: Detection Results of Concrete with Different Target Reflectance (10m depth) 81
Figure 53: Detection Results of White Cotton Fabric with Different Target Reflectance (0.1m depth) 82
Figure 54: Detection Results of White Cotton Fabric with Different Target Reflectance (0.2m depth) 83
Figure 55: Detection Results of White Cotton Fabric with Different Target Reflectance (0.3m depth) 84
Figure 56: Detection Results of White Cotton Fabric with Different Target Reflectance (1m depth) 85
Figure 57: Detection Results of White Cotton Fabric with Different Target Reflectance (2m depth) 86
Figure 58: Detection Results of White Cotton Fabric with Different Target Reflectance (5m depth) 87
Figure 59: Detection Results of White Cotton Fabric with Different Target Reflectance (10m depth) 88
Figure 60: Detection Results of Black Nylon Fabric with Different Target Reflectance (0.1m depth) 89
Figure 61: Detection Results of Black Nylon Fabric with Different Target Reflectance (0.2m depth) 90
Figure 62: Detection Results of Black Nylon Fabric with Different Target Reflectance (0.3m depth) 91
Figure 63: Detection Results of Black Nylon Fabric with Different Target Reflectance (1m depth) 92
Figure 64: Detection Results of Black Nylon Fabric with Different Target Reflectance (2m depth) 93
Figure 65: Detection Results of Black Nylon Fabric with Different Target Reflectance (5m depth) 94
Figure 66: Detection Results of Black Nylon Fabric with Different Target Reflectance (10m depth) 95
Figure 67: Detection Results of Blue Nylon Fabric with Different Target Reflectance (0.1m depth) 96
Figure 68: Detection Results of Blue Nylon Fabric with Different Target Reflectance (0.2m depth) 97

Figure 69: Detection Results of Blue Nylon Fabric with Different Target Reflectance (0.3m depth) 98
Figure 70: Detection Results of Blue Nylon Fabric with Different Target Reflectance (1m depth) 99
Figure 71: Detection Results of Blue Nylon Fabric with Different Target Reflectance (2m depth) 100
Figure 72: Detection Results of Blue Nylon Fabric with Different Target Reflectance (5m depth) 101
Figure 73: Detection Results of Blue Nylon Fabric with Different Target Reflectance (10m depth) 102
Figure 74: Detection Results of Green Nylon Fabric with Different Target Reflectance (0.1m depth) 103
Figure 75: Detection Results of Green Nylon Fabric with Different Target Reflectance (0.2m depth) 104
Figure 76: Detection Results of Green Nylon Fabric with Different Target Reflectance (0.3m depth) 105
Figure 77: Detection Results of Green Nylon Fabric with Different Target Reflectance (1m depth) 106
Figure 78: Detection Results of Green Nylon Fabric with Different Target Reflectance (2m depth) 107
Figure 79: Detection Results of Green Nylon Fabric with Different Target Reflectance (5m depth) 108
Figure 80: Detection Results of Green Nylon Fabric with Different Target Reflectance (10m depth) 109
Figure 81: Detection Results of Red Nylon Fabric with Different Target Reflectance (0.1m depth) 110
Figure 82: Detection Results of Red Nylon Fabric with Different Target Reflectance (0.2m depth) 111
Figure 83: Detection Results of Red Nylon Fabric with Different Target Reflectance (0.3m depth) 112
Figure 84: Detection Results of Red Nylon Fabric with Different Target Reflectance (1m depth).....113
Figure 85: Detection Results of Red Nylon Fabric with Different Target Reflectance (2m depth).....114
Figure 86: Detection Results of Red Nylon Fabric with Different Target Reflectance (5m depth).....115
Figure 87: Detection Results of Red Nylon Fabric with Different Target Reflectance (10m depth) 116
Figure 88: Detection Results of Sheet Metal with Different Target Reflectance 118
Figure 89: Detection Results of Concrete with Different Target Reflectance 119
Figure 90: Detection Results of Black Cotton with Different Target Reflectance 120

Figure 91: Detection Results of Blue Cotton Inverted from Green Cotton with Different Target Reflectance 121
Figure 92: Detection Results of Blue Cotton Inverted from Red Cotton with Different Target Reflectance 122
Figure 93: Detection Results of Green Cotton Inverted from Blue Cotton with Different Target Reflectance 123
Figure 94: Detection Results of Green Cotton Inverted from Red Cotton with Different Target Reflectance 124
Figure 95: Detection Results of Red Cotton Inverted from Blue Cotton with Different Target Reflectance 125
Figure 96: Detection Results of Red Cotton Inverted from Green Cotton with Different Target Reflectance 126
Figure 97: Detection Results of Blue Denim Inverted from Blue Cotton with Different Target Reflectance 127

LIST OF ABBREVIATIONS

ACE	Adaptive Coherence Estimator (Signed)
AOP	Apparent optical property
IOP	Inherent Optical Property
LEA	The model proposed by Lee et al.
MEA	The model proposed by Maritorena et al.
SAM	Spectral Angle Mapper
SAR	Search and Rescue
WCC	Water Column Correction

CHAPTER 1

INTRODUCTION

1.1. Motivation

Underwater object detection applications can be seen in various areas such as archeology, defense, coral reef studies and Search&Rescue. Underwater Search and Rescue (SAR) operations are common in our country. Coastal waters, dam lakes and other natural lakes are common incident areas for SAR operations. In practice, the search methods for the victims in these incidents are conducted with physical search and sonar devices from rescue boats. The physical search methods are commonly in the form of searching the incident area with physical touch, search tools, etc. along the search lines planned by the SAR team leader. In this form of SAR activities, the possibility of target finding takes a significant amount of time and work force. The sonar devices are also difficult to operate in practice as there are significant amount of noise activities and false positives as the sonar detection is related to the response of the acoustic signals returning from obstacles under the water.

Hyperspectral imaging has the benefit to determine the characteristics of materials and help to detect the right material. If this imaging technique applies to SAR operations, target detection can be done in less time and work force. But unfortunately, the water affects hyperspectral imaging in a critical way that needs to be corrected or reduced. The detection of underwater objects with their above-water (dry) reflectance signature may not be efficient because of the reflectance changes due to water column. The detection should be conducted with the reflectance signature affected by the water column. To simulate object reflectance under a specific water column, water column correction algorithms can be taken into consideration. Once underwater spectral reflectance is obtained, their effect on the detection performance can be observed.

Furthermore with hyperspectral imagery, materials can be evaluated according to their capability of detection. With this type of evaluation, SAR teams can focus on the most detectable materials and increase the possibility of target detection and reduce the detection time.

1.2. Scope of the Thesis

The goal of the thesis is to investigate the enhancement of underwater target detection for search and rescue missions. For this purpose, effect of water on material reflectance is studied with two known water column correction algorithms first. Furthermore the detection performances of water column correction algorithms are also compared in object detection phase with two detection algorithms. The water column correction and the detection algorithms are explained in the following chapters.

While investigating the improvement in target detection, the materials are also evaluated in their positive contribution to SAR operations.

1.3. Outline of the Thesis

The thesis is structured in five chapters namely, “Introduction”, “Background”, “Methodology”, “Experiments and Results”, and “Conclusion and Future Work”. The motivation, scope and the outline of the thesis is described in the introduction section. Hyperspectral imagery, effect of water, and literature survey for underwater target detection is described in the background section. The methodology and the data preparation stage are described in the methodology section. Simulated and real data experiments and their results are described in the experiments and results section. The conclusion and the further studies are described in the conclusions and future work section. The appendices include large scale data illustrations and research in the related parts of the former chapters.

CHAPTER 2

BACKGROUND

2.1. Hyperspectral Imagery

Hyperspectral imaging is an imaging technique that gathers extensive information from the electromagnetic spectrum. While multispectral imaging takes a selected set of bands from the visible area of electromagnetic spectrum (400nm-700nm), hyperspectral imaging collects hundreds of contiguous bands from the same spectral coverage. Figure 1 shows sample band coverage of hyperspectral and multispectral imaging over the electromagnetic spectrum.

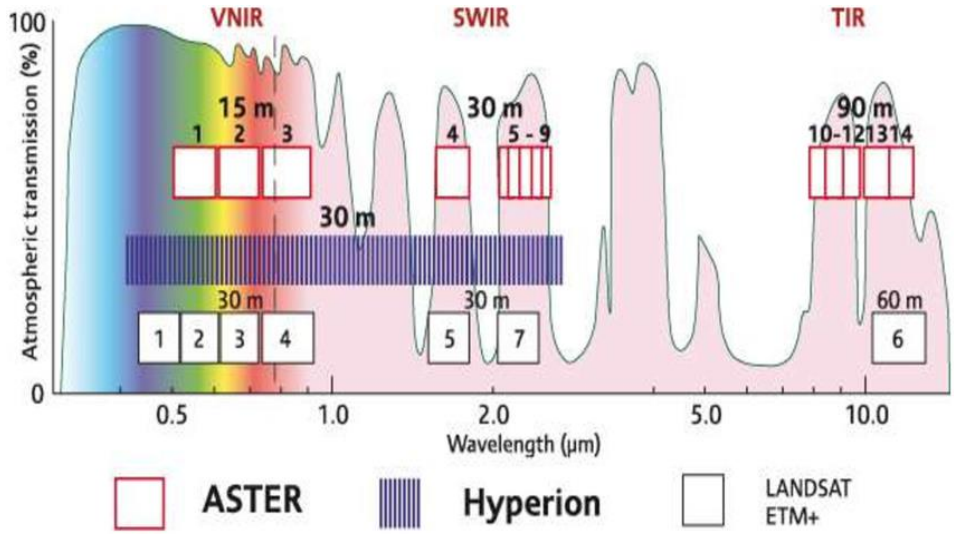

Figure 1: Band coverage of multispectral and hyperspectral sensors over the electromagnetic spectrum (Pour & Hashim, 2014)

As seen in Figure 1, contrary to multispectral imagery, hyperspectral imaging creates a continuous measurement in the related band coverage. This ability has the advantage of providing unique signatures for different material types. Thus several signal processing algorithms can be applied to detect the target material effectively.

Hyperspectral imaging has three dimensional data structure, two dimensions of spatial component and a dimension of spectral component. This three dimensional

representation is called hyperspectral cube (Manolakis, Marden, & Shaw, 2003). Figure 2 shows the representation of a hyperspectral cube.

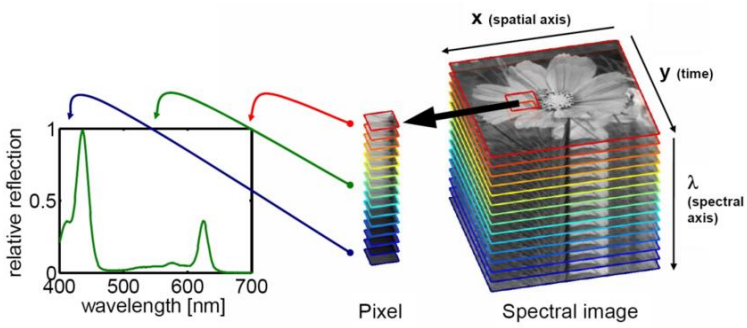

Figure 2: Hyperspectral cube (Polder & Pekkeriet, 2013)

2.2. Effect of Water in Hyperspectral Imagery

In this section, the water properties related to the hyperspectral imaging are discussed.

2.2.1 Inherent Optical Properties

Inherent optical properties (IOPs) are the optical properties of water that is related only to the water body (Mobley C. , 1994). These properties are the quality measurements of the water which affect the reflectance in water for target detection. Typical IOPs are absorption and scattering coefficients.

Absorption is the fragment of incident power that is absorbed in the water column. Scattering is the fragment of the incident power that is scattered in the water column (Mobley C. , 1994). These two optical properties are related to the water quality (pure, turbid, etc.) with the active optical components within the water. The active components in water are phytoplankton, algae, colored dissolved organic matter (Jay & Guillaume, 2010). Figure 3 shows the absorption and backscattering coefficients of pure water. The absorption and backscattering coefficients are obtained from (Pope & Fry, 1997) and (Richardson & LeDrew, 2006) respectively.

2.2.2 Apparent Optical Properties

Apparent optical properties are the optical properties of water that are related with both water body and the geometric (directional) structure of the ambient light field (Mobley C. , 1994). Typical AOPs are irradiance reflectance, remote sensing reflectance, attenuation coefficients and distribution functions.

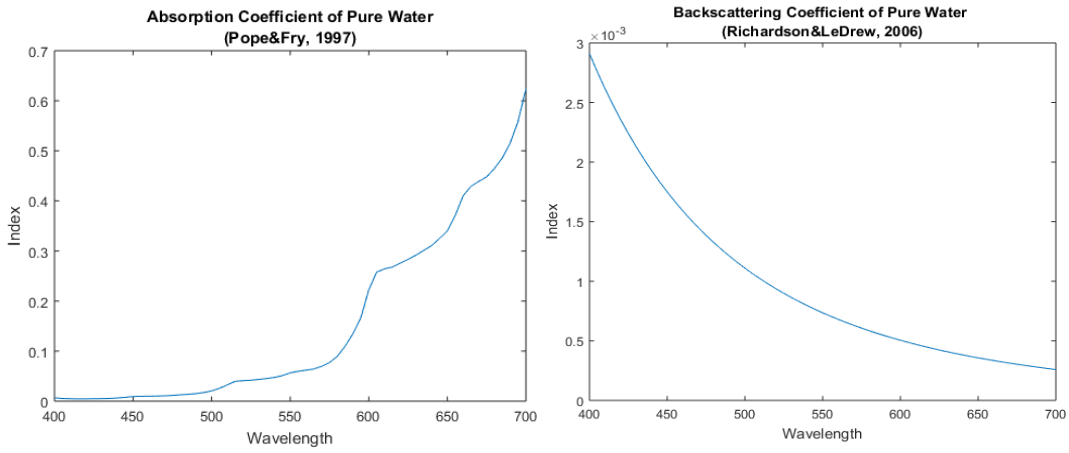

Figure 3: Absorption and backscattering coefficients of pure water

Irradiance reflectance is the ratio of upwelling irradiance to downwelling irradiance in water. Remote sensing reflectance is the ratio of water leaving radiance to downwelling irradiance. Attenuation coefficients are the coefficients to represent the attenuation rate of the radiance/irradiance in the water medium (Mobley C. , 1994). Figure 4 shows the reflectance and attenuation coefficient of pure water. The reflectance and attenuation coefficient of pure water are modeled from the absorption and backscattering coefficients with the algorithm of (Lee, Carder, Mobley, Steward, & Patch, 1999) which will be discussed in the next chapters.

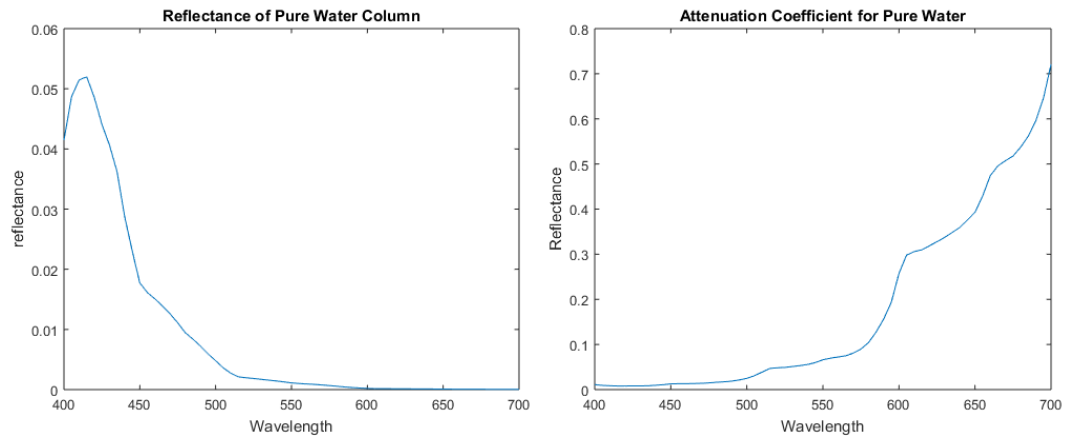

Figure 4: Reflectance and attenuation coefficient of pure water

Distribution functions are the indicators of diffuseness of light field in downward or upward flow (Preisendorfer, 1976).

2.3. Literature Review

In this part, water column correction algorithms and underwater target detection studies in the literature are investigated.

2.3.1 Water Column Correction Algorithms

(Zoffoli, Frouin, & Kampel, 2014) made a study on the water column correction algorithms for coral reef studies. They categorized the algorithms into five categories according to their solution to water column correction which are explained below.

a) Band Combination Algorithms

These algorithms linearise the depth effect in their proposed reflectance algorithms, plot these linearised functions between different spectral bands and classify the bottom types according to their offset in the plot area. The result of these algorithms is not the bottom reflectance spectra but the bottom classification according to their plotted depth functions. The most common algorithm for this type is produced by (Lyzenga, 1978). In his study, he represented the reflectance as

$$L_i = L_{si} + K_i p_i e^{(-k_i f h)} \tag{1}$$

Where L_i is the measured radiance for band i, L_{si} is the deep water reflectance, p_i is the bottom reflectance, h is the depth and k_i is the attenuation coefficient, f is the geometric factor for path length through the water and K_i is a constant for atmosphere – water surface transmittance. From this reflectance algorithm, he assumed that the function which linearises the water depth effect can be described as

$$X_i = \ln(L_i - L_{si}) \tag{2}$$

The result variables of this function are related linearly for a given bottom reflectance. If two linear functions of water depth for two bands (i, j) are plotted, the pixels for a same bottom type will be on a straight line on this plot. Another bottom type will be over or under this straight line according to their reflectance measures. With a selected threshold between those different offset lines, bottom type classification can be obtained without the knowledge of depth information (Lyzenga, 1981).

Other algorithms related to this type are the modifications of Lyzenga's Algorithm. (Sagawa, et al., 2010) added radiometric correction Lyzenga's algorithm and studied on turbid water type.

b) Model-Based Algebraic Algorithms

These algorithms model the effect of water on immersed material reflectance with optical properties of water and depth. They retrieve bottom reflectance which can be used in underwater target detection. All the parameters except depth (h) is wavelength dependent in the next formulas. To enable formulation simplicity, the wavelength notation is neglected.

(Gordon & Brown, 1974) developed a model that irradiance reflectance (r) for a given bottom albedo (p) is

$$r = r_1 + \frac{pr_2}{1 - pr_{2:1}} \tag{3}$$

where (r_1) is the reflectance of photons that do not strike the bottom, (r_2) is the reflectance of photons that strike the bottom once for bottom albedo equals to 1, and $(r_{2:1})$ is the ratio of the number of photons that strike the bottom twice to the number of photons that strike the bottom once for bottom albedo equals to 1. They made assumptions regarding that water column is flat, homogenous and a Lambertian bottom lies beneath it.

(Maritorena, Morel, & Gentili, 1994) (hereafter referred as MEA) developed a model which defines the irradiance reflectance just under the water surface (r) as the sum of the reflectance of water column (r_∞) and exponential effect of the attenuation coefficient (k) and depth (h) to the contrast between bottom albedo (p) and (r_∞):

$$r = r_\infty + (p - r_\infty)e^{-2kh} \tag{4}$$

If the water is assumed to be homogenous in the related area, these parameters will be same for all objects in the search area. Although the attenuation coefficients in upwelling and downwelling radiance are different, the coefficients are assumed to be equal because the upwelling attenuation coefficient cannot be easily calculated and hence it is placed as ($2k$) in Formula 4. The results of the model are compared to Monte Carlo simulation results and good match were obtained according to (Maritorena, Morel, & Gentili, 1994).

(Bierwirth, Lee, & Burne, 1993) proposed a method that unmixes the exponential influence of depth in each pixel. The outputs of the method are the subsurface reflectance image corresponding to input bands and a grayscale depth image. Their method was successfully tested in a real situation and it represented a valuable tool for the analysis and management of coastal zones. For the method be effective, IOPs should be estimated.

(Lee, Carder, Mobley, Steward, & Patch, 1999)(hereafter referred as LEA) also assumed that the remote sensing reflectance is related to (r_∞), (p), (k) and (h). They detailed the assumptions of (k) in MEA and proposed the model below:

$$r_{rs} = r_\infty(1 - e^{\{[-(k_d + k_{uc})h]\}}) + \frac{p}{\pi}(e^{[-(k_d + k_{ub})h]}) \tag{5}$$

One of the most significant difference between LEA and MEA is that the downwelling attenuation coefficient (k_d), upwelling attenuation coefficient of the

water column (k_{uc}) and upwelling attenuation coefficient of bottom (k_{ub}) is separated. Also because the bottom material is Lambertian reflector, the bottom irradiance reflectance is divided by (π) . When we separate the attenuation coefficients to Inherent Optical Properties of water and the distribution functions of attenuation coefficients, the resulting parameters will be as below:

$$k_d = D_d k \, , k_{uc} = D_{uc} k \, , k_{ub} = D_{ub} k \tag{6}$$

$$D_d = 1/\cos(\theta_w) \tag{7}$$

(θ_w) is solar zenith angle, and it makes (D_d) a constant. After these adjustments, remote sensing reflectance obtained just under the surface of the water column is:

$$r_{rs} = r_\infty (1 - e^{\left\{-[\frac{1}{\cos(\theta_w)} + D_{uc}]kh\right\}}) + \frac{p}{\pi}(e^{\left\{-[\frac{1}{\cos(\theta_w)} + D_{uc}]kh\right\}}) \tag{8}$$

With various Hydrolight simulation repetitions, a semi analytical model is obtained from LEA model. With simulation results, the reflectance of water column (r_∞),

$$r_\infty \approx (0.084 + 0.17u)u \tag{9}$$

the upwelling water and bottom photon distribution functions (D_{uc}, D_{ub}),

$$D_{uc} \approx 1.03(1 + 2.4u)^{0.5}, D_{ub} \approx 1.04(1 + 5.4u)^{0.5} \tag{10}$$

is obtained. Inherent optical properties (u, k) are formulized as:

$$u = b_b / (a_t + b_b), k = a_t + b_b \tag{11}$$

and the change of these parameters with water quality can be observed. Here (a_t) is the absorption and (b_b) is the backscattering parameter of water. Another property of LEA model is that we can obtain the reflectance just above the water surface. The water-air inference obtained from Hydrolight simulation results is:

$$R_{rs} \approx \frac{0.5 r_{rs}}{1 - 1.5 r_{rs}} \tag{12}$$

c) Optimization/Matching Algorithms

These algorithms use the reflectance of the material that is searched and creates a collection of spectra with all the possible conditions that the material reflectance can face. After creating the collection, the most suited reflectance is chosen and classification of the related area is performed.

(Louchard, Reid, Stephens, Davis, Leathers, & Downes, 2003) proposed a method that the classification of the bottom of a study area can be performed by first measuring the spectral properties of study area (bottom reflectance, IOPs, water depth), create a simulation library with these inputs in Hydrolight simulator, and select the most fitting simulated spectra for each pixel and make a bottom type and bathymetric map of the study area. The authors found good results in bottom type classification by visual inspection and bathymetric results which have a mean accuracy of %83 with ground truth. They indicate that enhancing the simulation library can be effective in enhancing the success of the method.

(Mobley, et al., 2005) developed a spectrum matching and look-up table methodology that can retrieve information related to study area from hyperspectral imagery. They first created a reflectance lookup table including different water depths, bottom reflectance, and IOPs using Hydrolight simulator. Then they compared the table with specific image pixels from the study area. The depth and IOPs information of the closest matched reflectance is assumed to be related to the whole study area. Later, the related reflectance measures are compared with other pixels of the study area. The result is the bottom classification of the study area. The authors found good results in bottom type classification by visual inspection. They also have a depth estimation error of %5. The restriction of the method is that the computation time of the process requires a few hours to operate.

(Klonowski, Fearns, & Lynch, 2007) used a collection of simulation reflectance created by Hydrolight simulator with the IOPs inverted by the LEA model. They also collected in-situ measurements of the bottom reflectance and depth to validate their model.

(Brando, Anstee, Wettle, Dekker, Phinn, & Roelfsema, 2009) proposed the semi-analytical model for bathymetry, un-mixing, and concentration assessment (SAMBUCA) which uses LEA for estimating bathymetry, reflectance of bottom composition, and IOPs of the water column. They made some modifications to LEA to express the bottom albedo as a linear mixture of two material types. The required parameters of IOPs of water need to be obtained from in-situ measurements or from the literature. With these inputs, SAMBUCA models a reflectance for different values of inputs, compares them with remote sensing data and finds the most likely spectrum which yields the best solution. This procedure is performed pixel by pixel and the result is a bathymetric map. The overall performance for bathymetric retrieval is %87.

(Hedley, Roelfsema, & Phinn, 2009) developed an adaptive look-up tree (ALUT) method which is post-processed into a binary search partitioning tree. With the construction of the ALUT, execution time of the look-up table matching process is decreased. They used the process and had the bathymetric estimation error of %9. They did not provide the performance of bottom reflectance estimation.

d) Water Column Correction for Multi-Temporal Studies

The image of a scene gathered by a sensor in different time periods can be different because of the changes in water quality, light incident on the study area and atmospheric effects. To correct the difference between the pixels of the same scene taken in different periods, (Schott, Salvaggio, & Volchok, 1988) used pseudo-invariant feature (PIF) technique. This technique uses the PIF pixels, which are white and dark pixels of the scene, plots them on the relevant pixels in the other image taken in a different time period and obtains a gain and offset for the pixels in each band. With this assumption that the pixels are constant over time, two images can be calibrated. (Michalek, Wagner, Luczkovich, & Staffle, 1993) used a method called change vector analysis. They took bare soil, mangrove forest and deep water pixels of two images of the same scene taken in different times, calculated linear relationship between them and calibrated the images.

e) Geomorphologic Approach

When the water depth is different in the scene, different materials in different depth can have very similar reflectance spectra due to the water column effect. (Bertel, et al., 2008) used a geomorphologic approach to separate different cover types with same reflectance spectra. They divided the scene to five geomorphologic zones, made classifications using spectral angle mapper with thresholds obtained by field observations. They obtained a classification accuracy of %73, but the method they used did not retrieve bottom reflectance.

2.3.2 Hyperspectral Object Detection Studies

Some studies concentrated on underwater object detection with hyperspectral imagery. (Burt, 2012) made a study on sea mine detection with hyperspectral imagery. He used two detection algorithms, RX anomaly detector and Mixture Tuned Matched Filter (MTMF) to detect 3 surface and 3 submerged targets which submerged in 1, 2 and 3 meters respectively. In RX anomaly detector, he could not detect submerged targets. In MTMF, he used 2 meter submerged target as the input target spectrum and detected the submerged targets. Because he did not investigate the effect of water in underwater target detection directly, it would be difficult to give input target spectrum if there was a scenario with no information of the target pixels and therefore detect subsurface targets. He also gave some practical advices such as the image gathering time for sea surface target detection scenarios should not be in direct sunlight hours to avoid glint effects, and for detection scenarios, an example target material should be located near the search area for better target signature gathering.

(Jay & Guillaume, 2010) showed that with using water column correction algorithms, detection for underwater targets can be enhanced. In their study they investigated the effect of water in simulated and real data. For simulated data, they used different materials in different depths ranged in 0.1 m to 30 m. For real data,

they used black and white tarpaulins in 4.7 and 6.7 meters depth. They showed that the addition of water column correction to target detection enhances the process.

(Gillis, 2016) designed a framework for underwater target detection with hyperspectral imagery. The steps of his framework are:

1. IOPs estimation using water column correction algorithms
2. Target space construction with the estimated IOPs and different depths
3. Nonlinear dimensionality reduction
4. Detection

In his study, he embedded synthetic target pixels to a hyperspectral image and applied his framework. He omitted the detection process for simplicity. Instead, he used the projected data obtained after nonlinear dimensionality reduction as a detection statistic. The study shows that nonlinear dimensionality reduction gives positive contributions to simplify detection process but it has a significant computation cost.

CHAPTER 3

METHODOLOGY

3.1. Approach to the Problem

In this study, object detection will be investigated with real and simulated data. With simulated data, the problem will be investigated for clean water in depths between 0.1 – 10 meters. Figure 5 shows the general flowchart for the detection of simulated underwater objects for SAR missions.

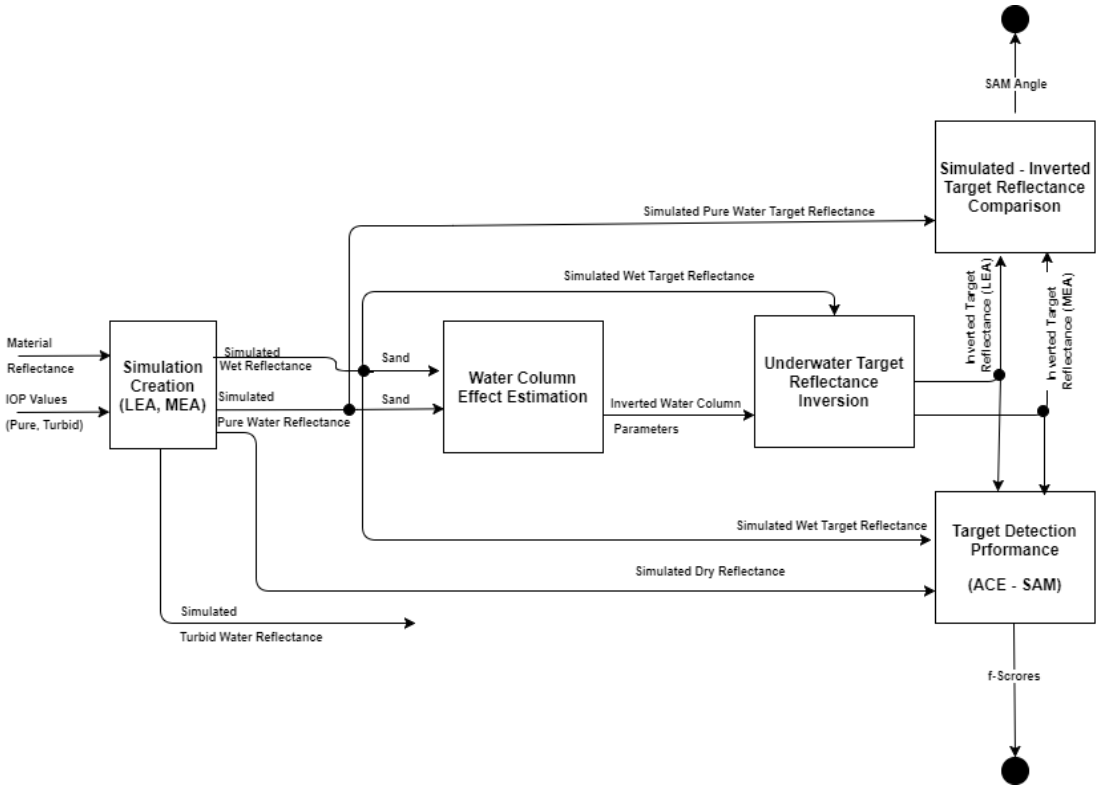

Figure 5: Flowchart of Target Detection with Simulated Data

As seen in Figure 5, first step is the creation of the simulation. The simulation method of (Jay & Guillaume, 2010) is exampled. Different material types with differing size will be put on sand background. The materials will be the ones that can be encountered in SAR operations such as sheet metal, concrete, white cotton fabric, nylon fabric with colors red, green, blue, black and blue denim. Further information for the simulation preparation is explained in the following chapter.

The second step is the estimation of water column effect. In this step, the difference between the wet reflectance and related depth reflectance of background (sand) will be compared with water column correction algorithms and parameters for these algorithms will be inverted.

The third step is applying the inverted parameters to wet reflectance of target data and simulate the target spectrum in related depth. The input reflectance to water column correction algorithms will be the wet reflectance of target material. The output reflectance from the water column correction algorithms will be the inverted reflectance of target material. The difference between the target spectrum and the inverted target spectrum will be investigated.

The last step is using the inverted target spectra for detecting underwater target. In this step, detection with dry, wet and inverted spectra with different water column correction algorithms will be compared and the effect of using water column corrected spectra will be evaluated.

Figure 6 shows the general flowchart for the detection of real underwater objects for SAR missions.

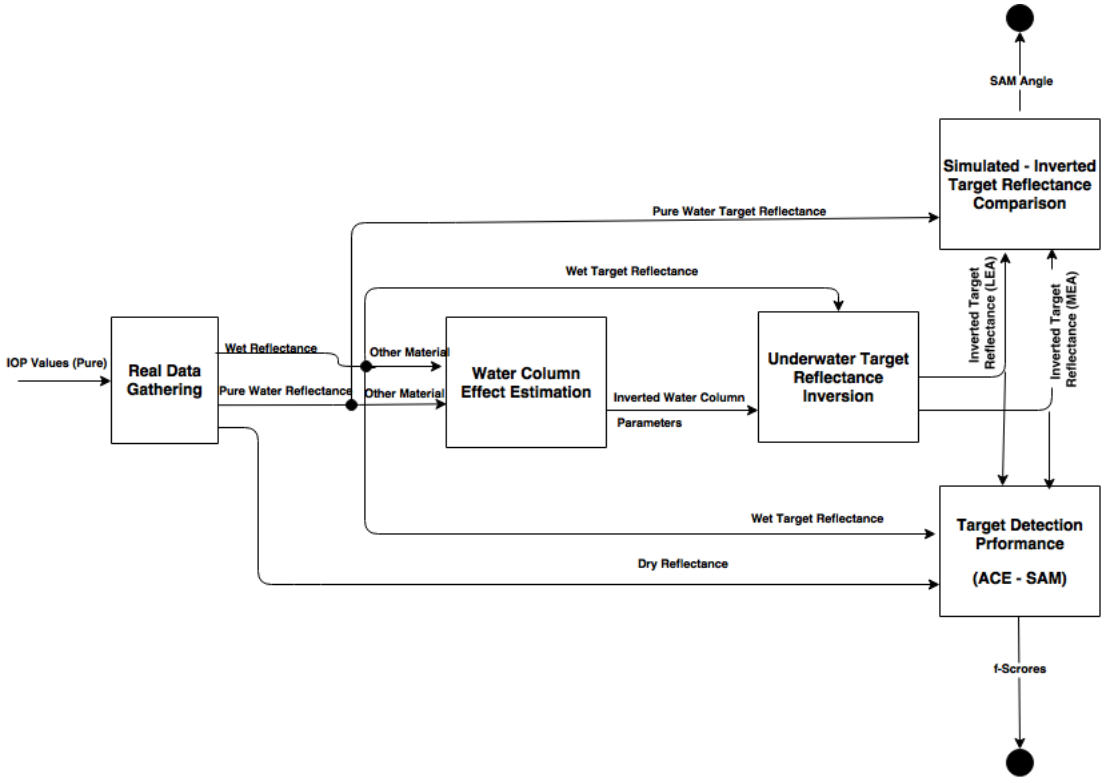

Figure 6: Flowchart of Target Detection with Real Data

As seen in Figure 6, real data detection of underwater objects is limited to 0.3 meter because of technical limitations. The real data is selected from possible materials that will be encountered in SAR missions like sheet metal, cotton fabric with different colors (red, green, blue, white, black) and denim. The other sections in the flowchart are same as the simulated data process. The real data experiment is applied to pure water type.

3.2. Choosing Water Column Correction and Target Detection Algorithms

As mentioned before, there are different algorithms for water column correction. The idea in this study is to simulate the bottom reflectance of searched materials by adding the water column effect to the wet (0 meter depth) material signature. The water column effect will be inverted from another material rather than target by its spectrum difference between underwater and wet signatures. To invert the water column effect, water column correction algorithm should give an output of underwater reflectance. Table 1 shows the output of the water column correction algorithms in (Zoffoli, Frouin, & Kampel, 2014).

As seen in Table 1, first algorithm type gives an output of linearised reflectance values of each band. The fourth algorithm type normalizes the reflectance of same materials in the same scene in different time periods. The fifth algorithm type divides the related scene into different geomorphologic zones to classify the area rather than giving a reflectance value for each pixel in the area.

On the other hand, second group of water column correction algorithm is directly interested in the bottom reflectance pixel by pixel. With this algorithm type water

Table 1: Outputs of the water column correction algorithms

Algorithm Number	Algorithm Type	Algorithm Output
1	Band Combination Algorithms	Bottom classification related to sequential bands
2	Model-Based Algebraic Algorithms	Bottom reflectance for each pixel
3	Optimization/Matching Algorithms	Bottom Map (Bottom materials must be known apriori)
4	Water Column Correction for Multi - Temporal Studies	Corrected reflectance of images of the same area
5	Geomorphologic Approach	Bottom map to differentiate the same reflectance of different bottoms

column correction can be obtained by inverting the algorithm parameters and adding these parameters to wet reflectance of the target material.

Two water column correction algorithms are selected for comparison: Models of (Lee, Carder, Mobley, Steward, & Patch, 1999)(further will be mentioned as LEA) and (Maritorena, Morel, & Gentili, 1994) (further will be mentioned as MEA). These models are selected to evaluate the difference between a complex (LEA) and a simpler method (MEA).

The third group of water column correction algorithms takes the models in second group and creates different reflectance outputs to be selected for the best fit. This group creates huge amount of spectral library with different water qualities to find the best match with the related target spectrum. Because the time required to execute this approach is much more than second group algorithm types, this approach is not followed.

The detection algorithms of spectral angle mapper (SAM) and signed adaptive coherence estimator (ACE) are selected for detection performance evaluation. Spectral angle mapper measures distance between the two vectors (x, y) by measuring the cosine of the angle between them as:

$$\angle(x, y) = \arccos\left(\frac{x^T y}{\|x\|\|y\|}\right) \tag{13}$$

$x^T y$ is the dot product of x and y vectors (Manolakis, Marden, & Shaw, 2003).

Adaptive coherence estimator adds the covariance matrix of the background to the target detection procedure as:

$$T_{ACE}(x) = \frac{(d^T \sum^{-1} x)^2}{(d^T \sum^{-1} d)\ (x^T \sum^{-1} x)} \tag{14}$$

where d is the target vector, x is the image pixel vector and $\sum$ is the covariance matrix of the background (Jin, Paswaters, & Cline, 2009). When the sign of the target vector and the pixel vector is taken into consideration, the ACE detector becomes (Truslow, 2012):

$$T_{ACE(Signed)}(x) = \frac{d^T \sum^{-1} x}{\sqrt{d^T \sum^{-1} d}\sqrt{x^T \sum^{-1} x}} \tag{15}$$

this derivation of the ACE will be used in this study.

The detection algorithms will be evaluated with F-measure technique:

$$F = \frac{2(PR)}{P+R} \tag{17}$$

where P is the precision and R is the recall of the related scene (Zhang & Zhang, 2009). The threshold for the F-measure technique will be calculated with the method of Otsu (Otsu, 1979).

CHAPTER 4

EXPERIMENTS AND RESULTS

4.1. Simulated and Real Data

Simulated Data: The reference reflectance of the materials are taken from USGS Spectral Library (Clark, et al., 2007). The reference signatures should represent the bottom reflectance of the simulation. Because the reference signatures are the dry material signatures, wet reflectance simulation is required. To solve this problem, the dry-wet transmissions of real data materials are measured and the mean transmission signature is obtained from those materials. Figure 7 shows the ratio signatures obtained from the materials sheet metal, concrete, sand and cotton fabric of colors white, black, blue, green and red. The dry reference spectra will be multiplied with the related dry-wet transmission ratio to obtain the bottom reflectance at zero depth (wet reflectance). The complexity of real data is simulated by applying each material ratio to related material rather than applying the mean ratio to all the materials.

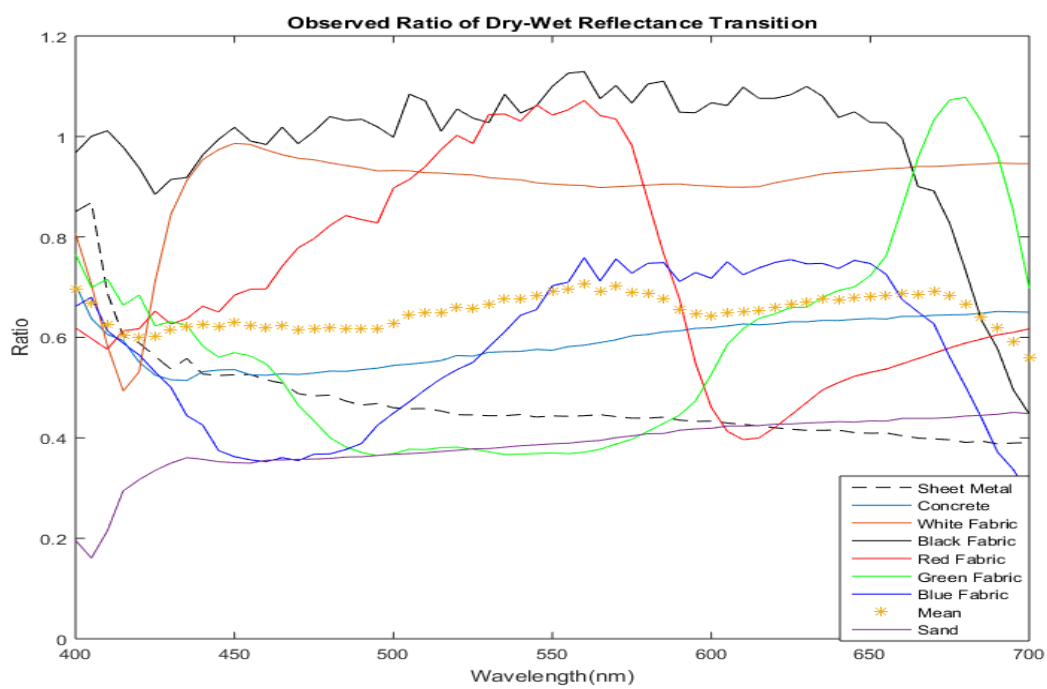

Figure 7: Observed Ratio of Dry-Wet Reflectance Transition

The water column simulation will be modeled with the algorithm of (Maritorena, Morel, & Gentili, 1994) and (Lee, Carder, Mobley, Steward, & Patch, 1999). The values of the active components in water are taken from (Brando, Anstee, Wettle, Dekker, Phinn, & Roelfsema, 2009) for turbid water. The values of the active components in water are set to zero for pure water simulation. Absorption and backscattering coefficients of pure water are taken from (Pope & Fry, 1997) and (Richardson & LeDrew, 2006) respectively. Figure 8 shows the wet, pure and turbid water simulation scene in 1 meter depth.

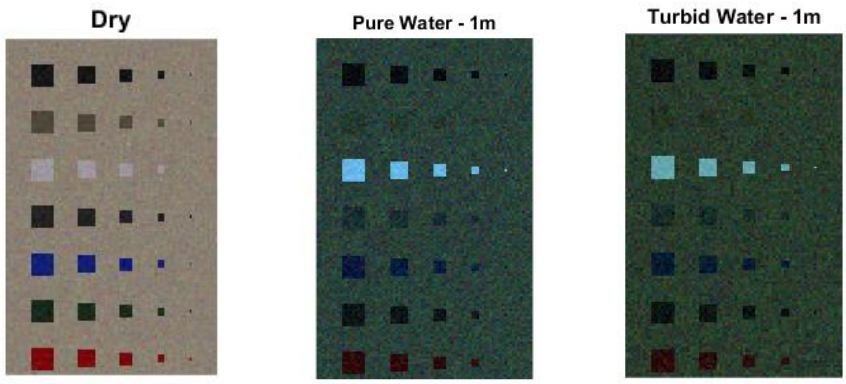

Figure 8: Simulation Scenes

As it is mentioned before the signatures are taken from USGS Spectral Library. The materials are, from top to down, sheet metal, concrete, white cotton fabric, black nylon fabric, blue nylon fabric, green nylon fabric and red nylon fabric. For natural variety of materials, white noise with a standard deviation 0.03 is added to simulation. For simulating noise through the bands of a pixel, a white noise with a standard deviation 0.001 again are added to simulation.

Real Data: As mentioned before, real data used in the experiment are the ones that can be encountered in a SAR operation such as metal, concrete (for background), cotton fabric with different colors and denim. The water used in the real data experiment is Ankara city water and the water quality parameters are set to zero as pure water parameters. The camera used in real data study is Headwall A Series Hyperspectral camera. Two different real data study is performed, one in laboratory environment and the other in outside. Light sources used in laboratory environment are tungsten light source for illumination and sun for outside.

Appendix A shows the spectrum of materials in different water depth in laboratory environment and outside. The first difference that can be seen in the figures is the common behavior of reflectance signatures in laboratory environment between 400 – 425 nm bands. The reflectance starts from a higher value and decreases until 425 nm

band. After this band, they give similar reflectance characteristics with outside environment. Because all the laboratory environment figures show this behavior, it is evaluated to be negligible. Another difference is that concrete and sheet metal reflectance is obtained until 20 cm depth in the outside environment because of the technical limitations. It can also be seen in the outside environment figures that there are some deviations in expected reflectance measures. For example in the black cotton reflectance of outside environment figure in page 48 (Figure 20), the 20 cm depth reflectance is greater than 10 cm depth reflectance although the opposite is expected. It is evaluated that in that kind of small reflectance values (0.01 – 0.02) these deviations might be observed. Beside these differences, because laboratory environment is better for eliminating other effects like clouds, change of illumination angle, change of illumination volume and sun glint, laboratory study will be discussed in this thesis.

The studied hyperspectral camera creates 204 bands between 400 – 700 nm. This much band coverage might help to detect differences between material spectra but it also increases computation time. Because detecting remnants of an incident fast is important in SAR missions, band reduction is needed. In order to reduce the band number without losing the effect of reduced bands, 61 bands with 5 nm sequence data cube is prepared by obtaining the mean spectra of 5 bands in the related 5 nm width. Appendix B shows the spectrum of materials with 210 and 61 band coverage. Except the minor differences specified in the appendix, arithmetic mean approach for reducing band number makes nearly no changes in the spectrum of materials. Because of this observation, 61 band data cubes are studied.

4.2. Evaluating the Performance of Water Column Correction Algorithms in Spectral Signatures

In this part of the study, MEA and LEA will be compared in various depths with simulated and real data. In simulated data, the water column effect will be inverted from these models by using wet and underwater background (sand) reflectance as input and output respectively. In real data, the water column effect will be inverted from another material beside the target in the scene. Related parameters of the algorithms will be inverted for MEA and LEA. These parameters are assumed to be constant in the whole image as it is assumed that the water is homogenous.

After the parameters are inverted from background and other materials, the wet target spectrum and these parameters are used as input in MEA and LEA to obtain the inverted target spectrum, and the outputs of MEA and LEA will be compared with each other and the actual underwater target spectra.

4.2.1 Simulation Comparison

Figure 9 shows the reflectance of sheet metal, concrete, white cotton fabric, black nylon fabric, blue nylon fabric, green nylon fabric and red nylon fabric in dry, wet, pure 1

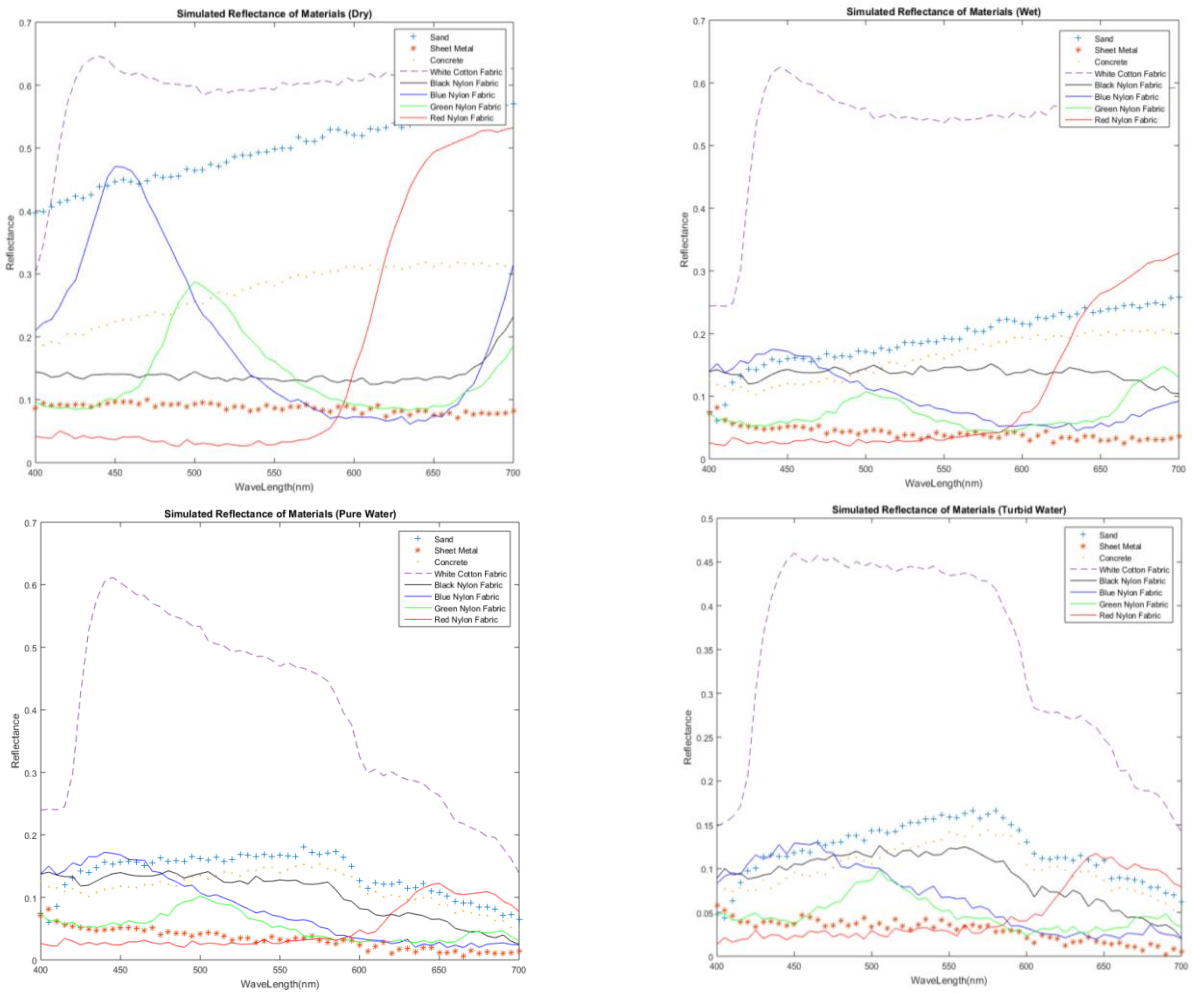

Figure 9: ReflectanceChanges of Materials in Dry, PureandTurbidWater (Depth = 1 meter)

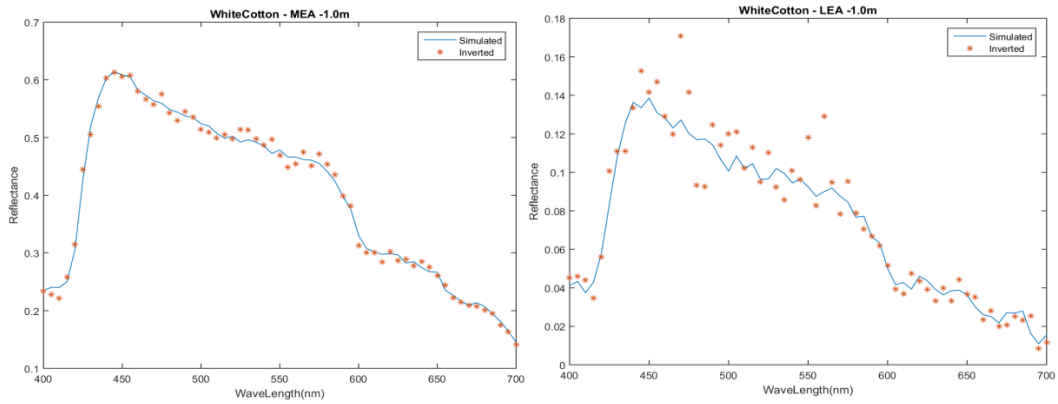

Figure 10: Simulated and Inverted Reflectance of Sheet Metal with MEA and LEA Algorithms in 1 meter depth

meter and turbid 1 meter depth. The wet reflectance is obtained with the dry/wet ratio of each material plotted in Figure 7.

As it is seen in Figure 9, the reflectance of materials reduce from red bands in pure water, from blue and red bands in turbid water. As a result of this observation, it can be inferred that the difference between the reflectance of two materials can be detected better in blue bands and green bands for pure and turbid water respectively.

Figure 10 shows the inverted reflectance of white cotton fabric in 1 meter depth with MEA and LEA according to the procedure discussed above. As seen in Figure 10, by applying the inverted parameters to the wet reflectance of sheet metal, very close signatures obtained by both models. The similarity of two spectra can be measured by Spectral Angle Mapper (SAM). With SAM, reflectance obtained by MEA has an angle (0.0242rad) smaller than the reflectance obtained by LEA (0.1400rad).

Appendix C shows the inverted reflectance of all related materials in various depths with MEA and LEA. The angles between the simulated and the corresponding inverted reflectance are summed up in Table 2. When Table 2 is examined, it is seen that the reflectance obtained with the parameters inverted by the MEA algorithm creates smaller angles between simulated and inverted signatures compared to the ones with LEA algorithm. It is also expected that when the depth increases, the angles should also increase. But there are some angle values in contrast with this assumption in most of the materials. Some angle values are smaller than the shallower depths, and some are larger than deeper values. The performance evaluation for detection will be investigated in further parts of this chapter.

4.2.2 Real Data Comparison

Figure 11 shows the inverted reflectance of sheet metal and concrete in various depths.

Table 2: Angles between simulated and obtained signatures with inverted parametersin simulated data

ANGLE BETWEEN SIMULATED AND INVERTED SIGNATURES									
MAT. NO	**MAT. TYPE**	**ALGORITHM TYPE**	**DEPTH**						
			0.1	**0.2**	**0.3**	**1**	**2**	**5**	**10**
1	Sheet Metal	MEA	**0.0739**	**0.0727**	**0.0527**	**0.0762**	**0.0729**	**0.1024**	**0.1083**
		LEA	0.5693	0.4901	0.5188	0.5359	0.5308	0.6034	0.7938
2	Concrete	MEA	**0.0270**	**0.0305**	**0.0260**	**0.0355**	**0.0421**	**0.0498**	**0.0605**
		LEA	0.1356	0.1538	0.1644	0.2813	0.2667	0.2706	0.3765
3	White Cotton Fabric	MEA	**0.0194**	**0.0235**	**0.0258**	**0.0242**	**0.0332**	**0.0334**	**0.0404**
		LEA	0.0701	0.0870	0.1073	0.1400	0.1495	0.2572	0.2866
4	Black Nylon Fabric	MEA	**0.0316**	**0.0353**	**0.0303**	**0.0372**	**0.0416**	**0.0471**	**0.0647**
		LEA	0.1743	0.1821	0.2057	0.2357	0.2642	0.2795	0.4144
5	Blue Nylon Fabric	MEA	**0.0368**	**0.0441**	**0.0378**	**0.0384**	**0.0425**	**0.0460**	**0.0567**
		LEA	0.2277	0.2107	0.2273	0.2646	0.2489	0.2396	0.3620
6	Green Nylon Fabric	MEA	**0.0446**	**0.0466**	**0.0362**	**0.0497**	**0.0582**	**0.0597**	**0.0950**
		LEA	0.2799	0.2762	0.3344	0.5165	0.4707	0.5851	0.5766
7	Red Nylon Fabric	MEA	**0.0261**	**0.0253**	**0.0195**	**0.0452**	**0.0759**	**0.1421**	**0.1951**
		LEA	0.1511	0.1867	0.2352	0.5706	0.9581	1.1487	1.1422

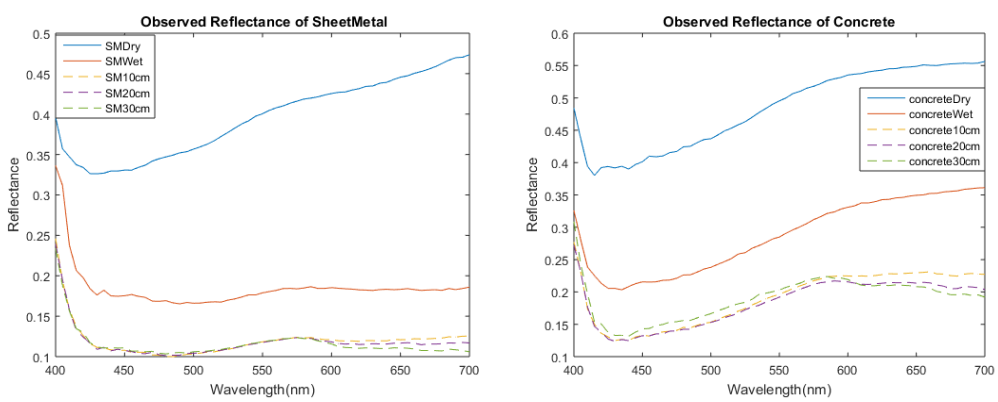

Figure 11: Observed Reflectance Changes of Sheet Metal and Concrete in different depths

As seen in Figure 11, the reflectance of materials start to attenuate from red bands as the water is clear. There might be differences between the reference signatures from USGS Spectral library and the real data obtained by the author. The reason is assumed to be in the natural variety among materials and data collection environment. Nevertheless the expected reflectance changes can be observed in the data.

Figure 12 shows the inverted reflectance of sheet metal and concrete in 0.3 meter depth with MEA and LEA.

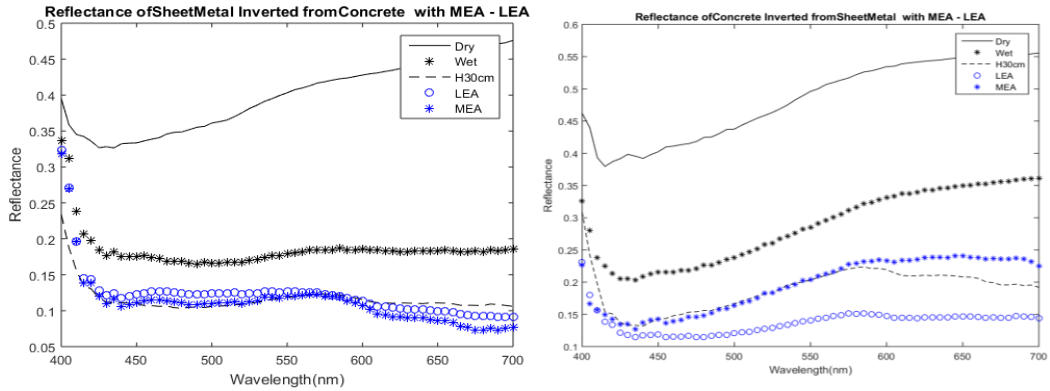

Figure 12: Observed Reflectance Changes of Sheet Metal and Concrete in different depths

As seen in Figure 12, by using SAM method, LEA has smaller angle in both materials (Sheet Metal = 0.1446 rad, Concrete = 0.0718 rad) than MEA (Sheet Metal = 0.1865 rad, Concrete = 0.1173 rad).

Appendix D shows the inverted reflectance of other materials in 0.3 meter depth with MEA and LEA. The angles between the simulated and the corresponding inverted reflectance are summed up in Table 3. When Table 3 is examined, some materials have

Table 3: Angles between simulated and obtained signatures with inverted parameters in real data

ANGLES BETWEEN OBSERVED AND INVERTED SIGNATURES				
MATERIAL NO	**MATERIAL TYPE**	**INVERT FROM**	**ALGORITHM TYPE**	
			MEA	**LEA**
1	Sheet Metal	Concrete	0.1865	**0.1446**
2	Concrete	Sheet Metal	0.1173	**0,0718**
3	White Cotton Fabric	Black Cotton Fabric	**0.0587**	0.1778
4	Black Cotton Fabric	White Cotton Fabric	0.4862	**0.3749**
5	Blue Cotton Fabric	Red Cotton Fabric	0.2763	**0.2680**
		Green Cotton Fabric	**0.1827**	0.2184
6	Green Cotton Fabric	Red Cotton Fabric	**0.1212**	0.4141
		Blue Cotton Fabric	**0.0871**	0.3307
7	Red Cotton Fabric	Blue Cotton Fabric	**0.0881**	0.4361
		Green Cotton Fabric	**0.0916**	0.5086
8	Blue Denim	Blue Cotton Fabric	**0.0550**	0.0889

smaller angles with, MEA and some with LEA. For example, sheet metal, concrete and black cotton fabric has smaller angles in LEA.

Cotton fabric in colors white, red and green has smaller angle with MEA. Blue cotton fabric has smaller angle with LEA when the required parameters are inverted with red cotton fabric. When the parameters are inverted with green cotton fabric, it creates a smaller angle with MEA algorithm. The performance evaluation for detection will be investigated in further parts of this chapter.

4.3. Evaluating the Performance of Water Column Correction Algorithms in Target Detection

In this part of the study, MEA and LEA is compared on simulated and real data with two detection algorithms mentioned above. The purpose is to obtain the best combination of material - water column correction - detection algorithms for SAR missions.

4.3.1 Simulation Comparison

Figure 13 shows the detection results of white cotton fabric (the third target from the top of the scene) with dry-wet-MEA inverted and LEA inverted reflectance with SAM and ACE detection algorithms in 1 meter depth. The first column of the Figure 13 is the simulation scene in 1 meter depth. The other columns show the detection results. For both detection algorithms (ACE, SAM), the colors ranging from black to white in detection results indicate the similarity of the materials to target reflectance from least similarity (zero, black) to most similarity (one, white) respectively. To examine Figure 13 by visual inspection, in both detection algorithms, target detection performance enhances with the use of water column correction. In both detection algorithms (ACE and SAM) the dry material reflectance is the least detectable target. In ACE detection, there is also false detection that red cotton fabric is detected with a greater contrast compared to white cotton fabric. The wet reflectance target is not so effective in that scenario too. It has also false detection in ACE detection, and it is mixed with background in SAM detection.

The MEA and LEA algorithms did quite good in ACE detection. The contrast between both algorithms and the background seems closely same, just a nuance for MEA that it contrasts with other materials little better than LEA. When the algorithms are compared in SAM detection, MEA again has a slightly better performance than LEA. The contrast of MEA is lesser than ACE in SAM detection, but it still does better performance when compared to other targets (dry, wet, LEA).

When the detection performances are measured by f-measure, the result for Figure 13 is summarized in Table 4.

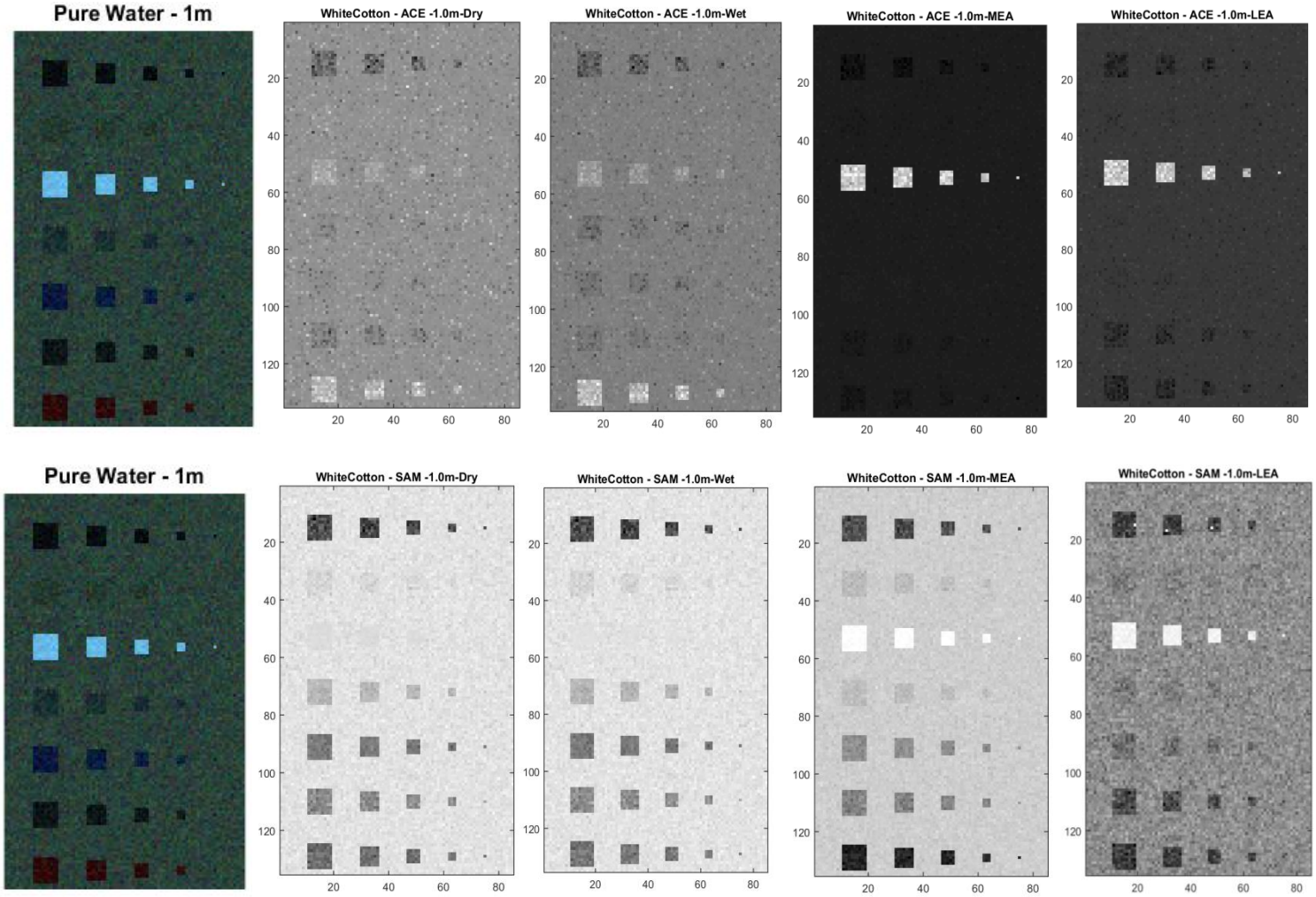

Figure 13: Detection Results of White Cotton Fabric with Different Target Reflectance

Table 4: Performance Evaluation of White Cotton Fabric in 1 meter Depth

DETECTION PERFORMANCE EVALUATION WITH F-MEASURE			
MATERIAL TYPE	**TARGET TYPE**	**DETECTION TYPE**	
		ACE	**SAM**
WHITE COTTON FABRIC	**DRY**	0.0311	0.0003
	WET	0.3722	0.0131
	MEA	**1.0000**	**1.0000**
	LEA	**1.0000**	**0.9910**

Performance evaluation with f-measure gave similar results as visual inspection. Because both MEA and LEA algorithms in ACE and SAM detection gave good contrast among other materials and background, f-measure had a score of 1 except LEA algorithm with SAM detection. It still has a good result of 0.99.

Appendix E shows the result of all materials in 0.1 – 10 meter depth. The f-measure performances of the related data are summed up in the Table 5 (for ACE) and Table 6 (for SAM). As it is seen in the tables, the detection performances enhance with the water column correction algorithms especially in deeper situations. It is also seen that ACE makes better performance than SAM method, and MEA has better performance results than LEA.

The "NAN" values in the tables occur from the misdetection of another material. Because of the f-measure formula, when other material pixels are fully above the threshold value as the target pixels, or in any other scenarios which has the same result, the number of true positive and false positive pixels become even and the formula tries to divide a number by zero. Thus it cannot create a number. In the following the materials will be examined.

Sheet metal detection performance is in the expected path with an exception in the 0.1 meter and 0.2 meter between wet and MEA signature. It is expected that MEA should pass wet reflectance in all depths. This exception is assumed to occur from the shallow depth. After 0.2 meter depth, the detection performance between wet and MEA reflectance rises positively on the MEA side as the depth increases. In SAM detection, the performance of all the targets is negligible.

Concrete detection performance is also in the expected path with an exception in again shallow waters of 0.1 - 0.3 meters. MEA signature performance increases until 0.3 meters while the opposite is expected. After that depth performance drops as the depth increases. The wet reflectance exception explained above occurs in 0.1 meter. In SAM detection all signature performances are negligible again.

Table 5: Detection performance of simulated materials with ACE

DETECTION PERFORMANCE WITH F-MEASURE - ACE								
MATERIAL TYPE	TARGET TYPE	DEPTH						
		0.1	**0.2**	**0.3**	**1**	**2**	**5**	**10**
Sheet Metal	DRY	0.5641	0.5967	0.5749	0.0498	0.0112	0.0243	0.0263
	WET	**0.6483**	**0.6383**	0.6310	0.5223	0.3187	0.1186	0.0737
	MEA	0.6286	0.6298	**0.6445**	**0.5612**	**0.5205**	**0.4366**	**0.4378**
	LEA	0.0500	0.0035	0.0035	0.0389	0.0212	0.0210	0.0223
Concrete	DRY	0.1888	0.0318	0.0319	0.1115	0.0657	0.0321	0.0409
	WET	**0.3858**	0.2891	0.2284	0.0995	0.0721	0.0548	0.0440
	MEA	0.3647	**0.3949**	**0.4047**	**0.3688**	**0.3545**	**0.2782**	**0.2511**
	LEA	0.0303	0.0305	0.0312	0.0305	0.0310	0.0308	0.0296
White Cotton Fabric	DRY	0.4110	0.3839	0.0306	0.0311	0.0327	0.0326	0.0421
	WET	1.0000	1.0000	1.0000	0.3722	0.0788	0.0325	0.0416
	MEA	**1.0000**	**1.0000**	**1.0000**	**1.0000**	**1.0000**	**1.0000**	**1.0000**
	LEA	**1.0000**	**1.0000**	**1.0000**	**1.0000**	**1.0000**	**0.9908**	**0.9816**
Black Nylon Fabric	DRY	0.1055	0.0681	0.0605	0.0115	0.0256	0.0304	0.0360
	WET	**0.5670**	**0.5826**	**0.6030**	0.0678	0.0361	0.0300	0.0304
	MEA	0.5596	0.5704	0.5760	**0.5196**	**0.5009**	**0.4918**	**0.3786**
	LEA	0.2230	0.1703	0.1452	0.0744	0.0320	0.0600	0.0440
Blue Nylon Fabric	DRY	0.9532	0.9132	0.9298	0.5307	0.2325	0.1224	0.0358
	WET	**1.0000**	**0.9940**	**0.9970**	0.9524	0.2881	0.0334	0.0249
	MEA	**1.0000**	0.9910	0.9851	**0.9821**	**0.9940**	**0.9617**	**0.8533**
	LEA	0.4629	0.4641	0.3828	0.1757	0.1342	0.0849	0.0318
Green Nylon Fabric	DRY	0.8983	0.8021	0.8403	0.2565	0.1121	0.0317	0.0294
	WET	0.9879	**0.9910**	**0.9728**	0.3629	0.0697	0.0446	0.0396
	MEA	**0.9880**	0.9706	0.9674	**0.8787**	**0.7603**	**0.6175**	**0.4183**
	LEA	0.0287	0.0287	0.0287	0.0288	0.0287	0.0288	0.0287
Red Nylon Fabric	DRY	1.0000	1.0000	1.0000	1.0000	0.2911	0.0314	0.0266
	WET	1.0000	1.0000	1.0000	0.9939	0.3013	0.0318	0.0282
	MEA	**1.0000**	**1.0000**	**1.0000**	**1.0000**	**0.9879**	**0.6245**	**0.6488**
	LEA	0.7617	0.5866	0.0289	0.0287	0.0288	0.0288	0.0287

White cotton fabric detection performance shows that water column correction enhances the detection performance in both ACE and SAM detection. MEA performs better than LEA.

Table 6: Detection performance of simulated materials with SAM

DETECTION PERFORMANCE WITH F MEASURE - SAM								
MATERIAL TYPE	**TARGET TYPE**	**DEPTH**						
		0.1	**0.2**	**0.3**	**1**	**2**	**5**	**10**
Sheet Metal	DRY	NaN	NaN	NaN	NaN	NaN	0.0009	0.0014
	WET	0.0034	0.0020	0.0023	0.0002	0.0004	0.0020	0.0016
	MEA	0.0048	0.0060	0.0059	0.0034	0.0016	0.0032	0.0011
	LEA	0.0025	0.0026	0.0034	0.0327	0.0248	0.0276	0.0326
Concrete	DRY	0.0119	0.0082	0.0136	0.0226	0.0236	0.0252	0.0217
	WET	0.0232	0.0296	0.0290	0.0303	0.0310	0.0295	0.0245
	MEA	0.0262	0.0262	0.0299	0.0239	0.0249	0.0189	0.0206
	LEA	0.0139	0.0134	0.0154	0.0144	0.0172	0.0198	0.0186
White Cotton Fabric	DRY	0.9456	0.5008	0.1465	0.0003	0.0031	0.0491	0.0535
	WET	1.0000	1.0000	0.4860	0.0131	0.0243	0.0549	0.0636
	MEA	**1.0000**	**1.0000**	**1.0000**	**1.0000**	**1.0000**	**1.0000**	**1.0000**
	LEA	**0.9910**	**0.9910**	**0.9910**	**0.9910**	**0.9880**	**0.8967**	**0.8376**
Black Nylon Fabric	DRY	0.0090	0.0041	0.0031	0.0017	0.0059	0.0158	0.0176
	WET	0.1498	0.0486	0.0225	0.0013	0.0040	0.0114	0.0189
	MEA	**0.3806**	**0.2915**	**0.2775**	0.0828	0.0556	0.0486	0.0479
	LEA	0.0065	0.0100	0.0118	0.0135	0.0224	0.0233	0.0234
Blue Nylon Fabric	DRY	**0.9792**	**0.9375**	**0.7253**	**0.6371**	0.3469	0.0410	0.0116
	WET	0.8354	0.7383	0.5631	0.4467	0.0497	0.0233	0.0090
	MEA	0.8777	0.9066	0.6804	0.5631	**0.5612**	**0.3557**	**0.1133**
	LEA	0.0104	0.0192	0.0184	0.0222	0.0237	0.0302	0.0334
Green Nylon Fabric	DRY	0.0255	0.0173	0.0190	0.0062	0.0029	0.0048	0.0075
	WET	0.0456	0.0279	0.0226	0.0082	0.0048	0.0072	0.0090
	MEA	0.0491	0.0282	0.0210	0.0078	0.0056	0.0031	0.0013
	LEA	0.0026	0.0020	0.0019	0.0036	0.0042	0.0042	0.0122
Red Nylon Fabric	DRY	**1.0000**	**1.0000**	**1.0000**	**1.0000**	**0.9908**	0.0229	0.0174
	WET	1.0000	1.0000	1.0000	1.0000	0.9846	0.0180	0.0146
	MEA	1.0000	1.0000	1.0000	1.0000	0.0140	NaN	NaN
	LEA	0.0553	0.0374	0.0268	0.0091	0.0034	0.0050	0.0072

Black nylon fabric performance has shown that water column correction algorithms enhance the detection process in both ACE and SAM detection. The wet reflectance exception occurs in ACE detection between 0.1 – 0.3 meters. In SAM detection, good detection performance of MEA algorithm is observed between 0.1 – 0.3 meters.

Blue nylon fabric has the second highest detection performance after white cotton fabric in both ACE and SAM detection. It has wet reflectance exception in ACE detection between 0.1 – 0.3 meters. In SAM detection, dry reflectance performs better than MEA between 0.1 – 1 meters. The reason is again assumed to occur from shallow depth. After 1 meter, MEA outperforms other reflectance.

Green nylon fabric has also good detection performance in ACE detection. There are again some nuance in wet and MEA signature 0.2 and 0.3 meters. In SAM detection all signature performances are negligible.

Red nylon fabric detection performance has good detection performance in ACE detection. In SAM detection, good detection performance is observed between 0.1 – 1 meters.

4.3.2 Real Data Comparison

Figure 14 shows the detection results of white cotton fabric with dry-wet-MEA inverted and LEA inverted reflectance with SAM and ACE detection algorithms in 0.3 meter depth. For both algorithms (ACE, SAM), the colors ranging from black to white indicate the similarity of the materials to target reflectance from least similarity (zero, black) to most similarity (one, white) respectively. When it is inspected visually, it can be seen that MEA water column correction with ACE detection gives the best contrast among the target-algorithm combinations. The dry and wet reflectance seems to give same results in ACE. LEA also enhances detection performance compared to dry and wet reflectance, but its contrast is smaller than MEA, and this might create false positives in detection evaluation. SAM seems to have similar detection performance for all the target reflectance, a little performance degradation in LEA because of the contrast degradation with background. Table 7 shows the f-measure result of white cotton fabric detection performance.

The f-measure evaluation area is the water related part of the scene. When the f-measure results of Table 7 are examined, MEA has both enhancements in ACE and SAM detection. The dry target f-measure score in ACE has the highest f-measure score in ACE because each image obtains a threshold from Otsu's method separately. In this case, the threshold of the dry target image (0.3215) is smaller than the threshold of MEA (0.5568) or LEA (0.5216). This creates an f-measure score according to these thresholds. If same threshold is given to each image, the MEA and LEA algorithms would outperform other target spectra. With this fact in mind, it would not be false to inspect the targets visually. When the visual inspection is performed, it can be seen that MEA enhances detection performance quite well.

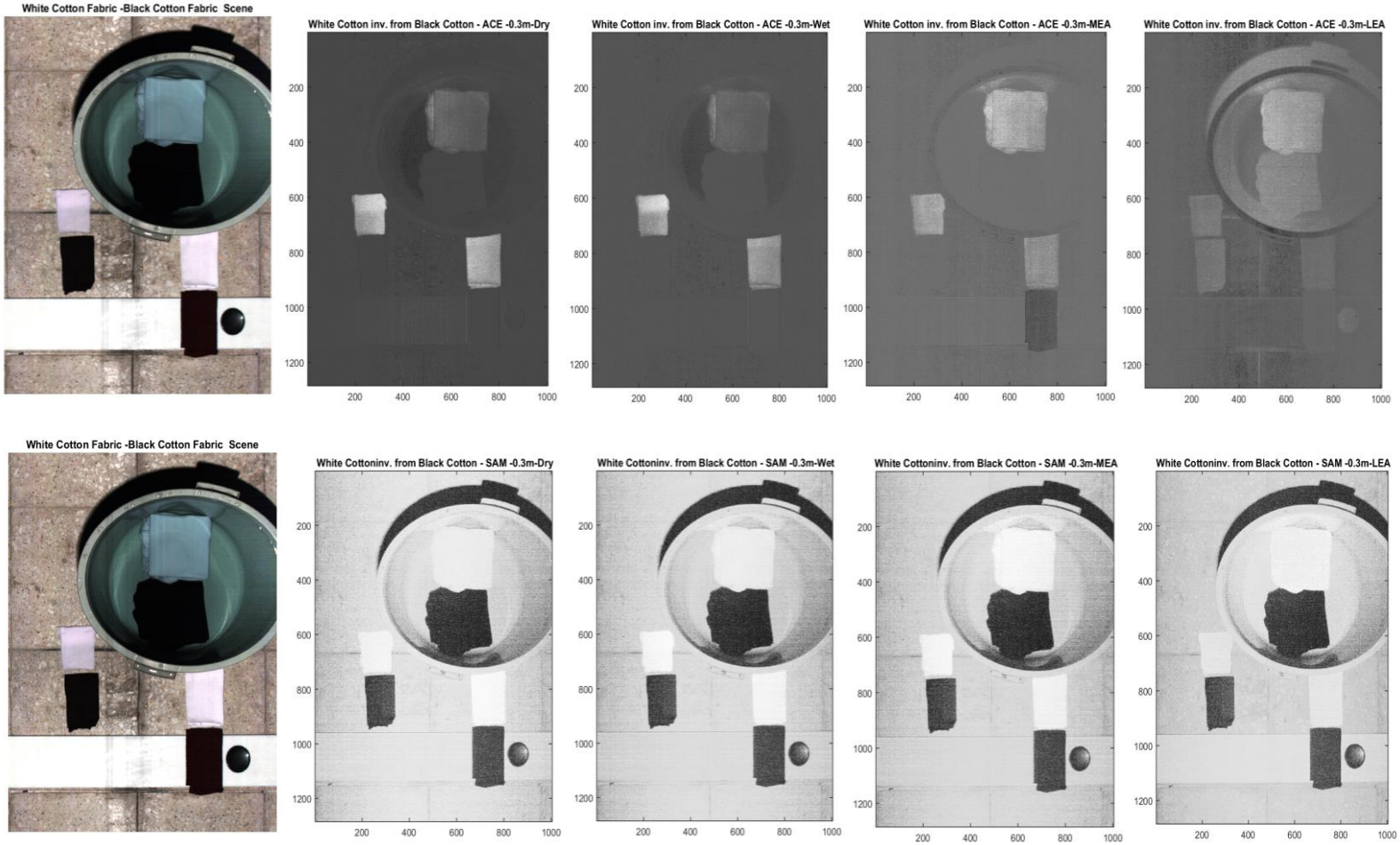

Figure 14: Detection Results of White Cotton Fabric with Different Target Reflectance (Real Data)

Table 7: Detection performance of white cotton fabric with F-measure

DETECTION PERFORMANCE OF WHITE COTTON FABRIC WITH F-MEASURE			
MATERIAL TYPE	TARGET TYPE	DETECTION TYPE	
		ACE	SAM
WHITE COTTON FABRIC	DRY	0.9259	0.4485
	WET	0.8585	0.4487
	MEA	0.9076	0.4495
	LEA	0.6735	0.4465

LEA also increases performance but the contrast with background is lesser compared to MEA. In SAM a clear difference between target spectra cannot be seen, except the fact that LEA has lower performance on the contrast with background again. Another cause of this issue is assumed that the water column correction algorithms will pass dry and wet signatures in deeper scenarios. As it is seen in the simulation, some situations like this occur in shallower waters.

Appendix F shows the result figures of other materials in 0.3 meter depth. The f-measure performances of the related data are summed up in the Table 8 (for ACE) and Table 9 (for SAM). It can be seen that in Table 8, f-measure score of dry reflectance is again higher in some of materials. Because the threshold issue is explained before, the inspection will be conducted both visually and f-measurably for ACE. In Table 9, it can be seen that SAM method shows the effect of water column correction algorithms (MEA and LEA) better because different materials has close thresholds obtained by Otsu's method. In the following the materials will be evaluated with both f-measure scores and visual inspection.

Sheet metal has a better detection performance in ACE with wet reflectance target. In ACE, false positives of MEA have dropped the f-measure score even it has more true positives in higher thresholds. The contrast with background is lowered the MEA score both in ACE and SAM detection. In SAM, LEA has better detection performance compared to any other target reflectance.

Concrete has a good detection performance with MEA in both ACE and SAM detection compared to other target spectra. LEA has some enhancement in SAM detection but it is detected sheet metal rather than concrete in ACE detection.

As white cotton fabric is explained before, it can only be said that MEA has the best detection performance both in ACE and SAM detection.

In black cotton fabric, wet and LEA target spectra have nearly same performance in ACE detection. In SAM, MEA and LEA has shown the enhancement of water column correction algorithms. Among them MEA has better performance.

Blue cotton fabric has two scenarios for detection, inverted from green cotton fabric and red cotton fabric. In the green cotton fabric scenario, wet and MEA target spectra has similar performance in ACE detection, whereas LEA has created false positives as detecting green cotton fabric with a higher rate. In SAM detection MEA algorithm have better performance over other targets. In red cotton fabric scenario, even though MEA has a good performance, wet target spectra has the best performance in ACE detection. In SAM, MEA has better performance than other target spectra.

Green cotton fabric has two scenarios. In blue cotton fabric scenario, MEA and wet target spectra has similar performance in ACE detection. In SAM, MEA has better performance compared to other targets. In red cotton fabric scenario, wet target reflectance has a slight better performance compared to MEA in ACE detection as MEA has a lesser contrast with background. But in SAM detection MEA has the best performance.

Table 8: Detection performance of real materials with ACE

DETECTION PERFORMANCE WITH F MEASURE - ACE					
MATERIAL TYPE	**INVERTED FROM**	**TARGET TYPE**			
		DRY	**WET**	**MEA**	**LEA**
Sheet Metal	Concrete	0.2921	**0.7008**	0.5307	0.4234
Concrete	Sheet Metal	0.3481	0.3348	**0.6587**	0.0687
White Cotton Fabric	Black Cotton Fabric	0.9259	0.8585	**0.9076**	0.6735
Black Cotton Fabric	White Cotton Fabric	0.8619	**0.8779**	0.7623	**0.8716**
Blue Cotton Fabric	Red Cotton Fabric	0.7741	**0.8192**	**0.7964**	0.6558
	Green Cotton Fabric	0.8256	**0.9045**	**0.8859**	0.5581
Green Cotton Fabric	Red Cotton Fabric	0.8431	**0.9226**	**0.8688**	0.3699
	Blue Cotton Fabric	0.8819	**0.9350**	**0.9344**	0.3487
Red Cotton Fabric	Blue Cotton Fabric	**0.9300**	0.8428	**0.8939**	0.1661
	Green Cotton Fabric	**0.9732**	0.8650	**0.9457**	0.1146
Denim	Blue Cotton Fabric	**0.8602**	0.8167	0.8238	0.8356

Table 9: Detection performance of real materials with SAM

DETECTION PERFORMANCE WITH OTSU F MEASURE -SAM					
MATERIAL TYPE	**INVERTED FROM**	**TARGET TYPE**			
		DRY	**WET**	**MEA**	**LEA**
Sheet Metal	Concrete	0.1894	0.2120	0.2089	**0.2140**
Concrete	Sheet Metal	0.2641	0.2660	**0.2671**	0.2537
White Cotton Fabric	Black Cotton Fabric	0.4485	0.4487	**0.4495**	0.4465
Black Cotton Fabric	White Cotton Fabric	0.0015	0.0015	**0.8709**	0.3166
Blue Cotton Fabric	Red Cotton Fabric	0.4730	0.5252	**0.7120**	0.0000
	Green Cotton Fabric	0.2781	0.4218	**0.5590**	0.3965
Green Cotton Fabric	Red Cotton Fabric	0.4397	0.3386	**0.4668**	0.4234
	Blue Cotton Fabric	0.3233	0.2970	**0.3760**	0.0747
Red Cotton Fabric	Blue Cotton Fabric	0.9142	0.9137	**0.9170**	0.2730
	Green Cotton Fabric	0.9609	0.9614	**0.9690**	0.4413
Denim	Blue Cotton Fabric	0.1207	0.3318	0.5032	**0.5385**

Red cotton fabric has two scenarios. In both blue cotton fabric and green cotton fabric scenarios, MEA has better performance than other materials except dry material target in ACE detection. In SAM detection, dry, wet and MEA has similar detection performance. LEA did not have an effective performance in both detection algorithms.

Blue denim has similar detection performance for all targets in ACE detection, but water column correction algorithms increase detection performance in SAM detection. In between them, LEA has a slight better performance than MEA.

CHAPTER 5

CONCLUSION AND FUTURE WORK

5.1. Results of the Study

In this study, the underwater target detection with hyperspectral imagery for SAR missions is examined. To increase the detection performance, the effect of water to material signatures is examined. As it is mentioned above, it has a nonlinear exponential effect in spectral signatures, and it suppresses the whole signature of the visible spectrum starting from the red bands (pure water) as the depth increases.

To reduce the effect of water for underwater targets, two water column correction algorithms are used. The inversion phase is set between wet and underwater background (for simulation) – other material (for real data) spectra. The inverted input parameters for the water column correction algorithms are applied to the wet reflectance target spectra. The reason for applying to wet reflectance rather than dry reflectance is that these water column correction algorithms take the bottom reflectance into consideration and bottom reflectance with zero depth will be a wet reflectance rather than a dry one. With this phase, inverted reflectance of target materials are obtained.

After the inversion of the target reflectance, the difference between the underwater target signature and the inverted signature is measured with SAM method. As it is mentioned above, the inverted reflectance with MEA generally creates smaller angles compared to the ones with LEA with some exceptions in real data. The reason is assumed to be positive effect of the simplicity of the algorithm in inversion techniques.

These models are compared with two detection algorithms, ACE and SAM. When these models compared in these detection algorithms, MEA has generally better detection performance than LEA. When comparing ACE and SAM, ACE has a better performance in scenarios. But it is not true that just ACE and MEA is the best combination for every material. Each target should be inverted with both water column correction algorithms and should be detected with both target detection algorithms. Table 10 shows the detection performance of algorithms with real data materials.

Table 10: Overall Evaluation of Real Data

OVERALL EVALUATION OF REAL DATA					
MATERIAL TYPE	**INVERTED FROM**	**ACE**		**SAM**	
		MEA	**LEA**	**MEA**	**LEA**
Sheet Metal	Concrete	**0.5307**	0.4234	0.2089	0.2140
Concrete	Sheet Metal	**0.6587**	0.0687	0.2671	0.2537
White Cotton Fabric	Black Cotton Fabric	**0.9076**	0.6735	0.4495	0.4465
Black Cotton Fabric	White Cotton Fabric	0.7623	**0.8716**	0.8709	0.3166
Blue Cotton Fabric	Red Cotton Fabric	**0.7964**	0.6558	0.7120	0.0000
	Green Cotton Fabric	**0.8859**	0.5581	0.5590	0.3965
Green Cotton Fabric	Red Cotton Fabric	**0.8688**	0.3699	0.4668	0.4234
	Blue Cotton Fabric	**0.9344**	0.3487	0.3760	0.0747
Red Cotton Fabric	Blue Cotton Fabric	0.8939	0.1661	**0.9170**	0.2730
	Green Cotton Fabric	0.9457	0.1146	**0.9690**	0.4413
Denim	Blue Cotton Fabric	0.8238	**0.8356**	0.5032	0.5385

First of all it can be seen that when inverting the parameters from different materials, the better performance comes from the materials that are close in waveband reflectance. For example the detection performance of blue cotton, green cotton and red cotton fabric is higher with the inversion process with green, blue and green cotton fabric respectively.

The highlighted cells of Table 10 are the best water column correction – detection algorithms for related materials. As it is seen in the table, MEA algorithm gives much better performance compared to LEA as it is generally chosen for better detection performance. Moreover ACE detection has a better performance than SAM as it is selected more often. ACE is chosen for 9 times whereas SAM is chosen for 2 times.

Table 11 shows the detection and inversion performance of algorithms with simulated data materials. As seen on Table 11, ACE detection with MEA water column correction algorithm gives better performance compared to other combinations. As in the previous table, some materials have same detection performance with different algorithms. That is the reason some materials are highlighted with different algorithms. When evaluating the materials in order to select the best detectable objects, both simulation and real data performance are inspected. The simulation results show that white, blue and red nylon fabric is detected successfully with different combinations that are highlighted. When real data equivalents of these materials are inspected, it can be seen that red and blue

Table 11: Overall Evaluation of Simulated Data

OVERALL EVALUATION OF SIMULATED DATA									
MAT. TYPE	**DET. TYPE**	**WCC MODEL**	**DEPTH**						
			0.1	**0.2**	**0.3**	**1**	**2**	**5**	**10**
Sheet Metal	ACE	MEA	**0.6286**	**0.6298**	**0.6445**	**0.5612**	**0.5205**	**0.4366**	**0.4378**
		LEA	0.0500	0.0035	0.0035	0.0389	0.0212	0.0210	0.0223
	SAM	MEA	0.0048	0.0060	0.0059	0.0034	0.0016	0.0032	0.0011
		LEA	0.0025	0.0026	0.0034	0.0327	0.0248	0.0276	0.0326
Concrete	ACE	MEA	**0.3647**	**0.3949**	**0.4047**	**0.3688**	**0.3545**	**0.2782**	**0.2511**
		LEA	0.0303	0.0305	0.0312	0.0305	0.0310	0.0308	0.0296
	SAM	MEA	0.0262	0.0262	0.0299	0.0239	0.0249	0.0189	0.0206
		LEA	0.0139	0.0134	0.0154	0.0144	0.0172	0.0198	0.0186
White Cotton Fabric	ACE	MEA	**1.0000**	**1.0000**	**1.0000**	**1.0000**	**1.0000**	**1.0000**	**1.0000**
		LEA	**1.0000**	**1.0000**	**1.0000**	**1.0000**	**1.0000**	**0.9908**	**0.9816**
	SAM	MEA	**1.0000**	**1.0000**	**1.0000**	**1.0000**	**1.0000**	**1.0000**	**1.0000**
		LEA	**0.9910**	**0.9910**	**0.9910**	**0.9910**	**0.9880**	**0.8967**	**0.8376**
Black Nylon Fabric	ACE	MEA	**0.5596**	**0.5704**	**0.5760**	**0.5196**	**0.5009**	**0.4918**	**0.3786**
		LEA	0.2230	0.1703	0.1452	0.0744	0.0320	0.0600	0.0440
	SAM	MEA	0.3806	0.2915	0.2775	0.0828	0.0556	0.0486	0.0479
		LEA	0.0065	0.0100	0.0118	0.0135	0.0224	0.0233	0.0234
Blue Nylon Fabric	ACE	MEA	**1.0000**	**0.9910**	**0.9851**	**0.9821**	**0.9940**	**0.9617**	**0.8533**
		LEA	0.4629	0.4641	0.3828	0.1757	0.1342	0.0849	0.0318
	SAM	MEA	**0.8777**	**0.9066**	**0.6804**	**0.5631**	**0.5612**	**0.3557**	0.1133
		LEA	0.0104	0.0192	0.0184	0.0222	0.0237	0.0302	0.0334
Green Nylon Fabric	ACE	MEA	**0.9880**	**0.9706**	**0.9674**	**0.8787**	**0.7603**	**0.6175**	**0.4183**
		LEA	0.0287	0.0287	0.0287	0.0288	0.0287	0.0288	0.0287
	SAM	MEA	0.0491	0.0282	0.0210	0.0078	0.0056	0.0031	0.0013
		LEA	0.0026	0.0020	0.0019	0.0036	0.0042	0.0042	0.0122
Red Nylon Fabric	ACE	MEA	**1.0000**	**1.0000**	**1.0000**	**1.0000**	**0.9879**	**0.6245**	**0.6488**
		LEA	**0.7617**	**0.5866**	0.0289	0.0287	0.0288	0.0288	0.0287
	SAM	MEA	**1.0000**	**1.0000**	**1.0000**	**1.0000**	0.0140	NaN	NaN
		LEA	0.0553	0.0374	0.0268	0.0091	0.0034	0.0050	0.0072

cotton fabric has detected with a good performance in two different algorithm combinations. White and Green cotton fabric is also detected with a good performance.

When the f-score measures and visual inspection of both data types are evaluated, it can be said that white cotton, blue cotton and red cotton fabric are the most detectable materials for search and rescue operations. It should be noted that the detection performance of red cotton fabric decreases more than other materials in simulated data. The detection performance evaluation of red cotton in deeper depths should be investigated in real data to get more accurate results.

For the three most detectable objects, naming white cotton, blue cotton and red cotton fabric, MEA algorithm with ACE detection is the most suited water column correction – target detection algorithm combination. There is only one exception for better performance. In red cotton fabric object, MEA algorithm with SAM detection brings a higher f-measure score in real data. Other combinations for those three most detectable objects are not better than MEA-ACE as it is mentioned above.

5.2. Future Work

Future study will be taken on increasing the number of material types to be evaluated for SAR missions. The real data depth will be increased to analyze the model with a broader perspective in real world. Study in different water quality types (salt water, turbid water) will also be investigated in future studies. As mentioned before, the goal of the thesis is to investigate the enhancement of underwater target detection for search and rescue missions. In future studies underwater target detection will also be investigated for other applications like archeological remain search and sea-mine detection. To perform effectively with these new concepts, the need for fast processing might arise. For this reason, performance enhancing studies like parallel programming will also be taken into consideration in future studies.

REFERENCES

A physics based retrieval and quality assessment of bathymetry from suboptimal hyperspectral data2009*Remote Sensing of Environment* 755 - 770

Bierwirth, P., Lee, T., & Burne, R. (1993). Shallow sea floor reflectance and water depth derived by unmixing multispectral imagery. *Photogrammetric Engineering & Remote Sensing* , 331 - 338.

Burt, C. (2012). Detection of spatially unresolved (nominally sub-pixel) submerged and surface targets using hyperspectral data. *Master's Thesis* . Naval Postgraduate School.

Clark, R. N., Swayze, G. A., Wise, R., Livo, K. E., Hoefen, T. M., Kokaly, R. F., et al. (2007). *USGS Digital Spectral Library splib06a*. Retrieved from U.S. Geological Survey, Data Series 231: https://speclab.cr.usgs.gov/spectral.lib06/ds231/datatable.html

Detection of underwater objects in hyperspectral imagery2016*Proc. SPIE 9840, Algorithms and Technologies for Multispectral, Hyperspectral, and Ultraspectral Imagery XXII*

Efficient radiative transfer model inversion for remote sensing applications2009*Remote Sensing of Environment* 2527 - 2532

*Hydrologic Optics Volume 1: Introduction*1976National Texchnical Information Service

Influence of bottom depth and albedo on the diffuse reflectance of a flat homogeneous ocean1974*Applied Optics* 2153 - 2159

Interpretation of hyperspectral remote-sensing imagery by spectrum matching and look-up tables2005*Applied Optics* 3576 - 3592

Jay, S., & Guillaume, M. (2010). Underwater target detection with hyperspectral remote-sensing imagery. *IGARSS*, (pp. 2820, 2823).

Jin, X., Paswaters, S., & Cline, H. (2009). A comparative study of target detection algorithms for hyperspectral imagery. *SPIE Defense, Security, and Sensing.* Orlando, Florida, United States.

Lee, Z., Carder, K. L., Mobley, C. D., Steward, R. G., & Patch, J. S. (1999). Hyperspectral remote sensing for shallow waters: 2. Deriving bottom depths and water properties by optimization. *Applied Optics* , 3831-3843.

Lyzenga, D. R. (1981). Remote sensing of bottom reflectance and water attenuation parameters in shallo water using aircraft and landsat data. *International Journal of Remote Sensing* , 71 - 82.

Manolakis, D., Marden, D., & Shaw, G. A. (2003). Hyperspectral Image Processing for Automatic Target Detection Applications. *Lincoln Laboratory Journal* , 79 - 116.

Mapping of coral reefs using hyperspectral CASI data; a case study: Fordata, Tanimbar, Indonesia2008*International Journal of Remote Sensing* 2359 - 2391

Maritorena, S., Morel, A., & Gentili, B. (1994). Diffuse reflectance of oceanic shallow waters: Influence of water depth and bottom albedo. *Limnology and Oceanography* , 1689 - 1702.

Michalek, J. L., Wagner, T. W., Luczkovich, J. J., & Staffle, R. W. (1993). Multispectral change vector analysis for monitoring coastal marine environments. *Photogramm. Eng. Remote Sens.* , 381 - 384.

Mobley, C. (1994). *Light and Water, Radiative Transfer in Natural Waters.* Academic Press.

Optical remote sensing of benthic habitats and bathymetry in coastal environments at Lee Stocking Island, Bahamas: A comparative spectral classification approach2003*Limnol. Oceanogr.* 511 - 521

Otsu, N. (1979). A treshold selection method from gray-level histograms. *IEEE Transactions on Systems, Man, and Cybernetics* , 62 - 66.

Passive remote sensing techniques for mapping water depth and bottom features1978*Applied Optics* 379 - 383

Performance evaluationof the adaptive cosine estimator detector for hyperspectral imaging applications*Master's Thesis* Boston, MassachusettsNortheastern University

Polder, G., & Pekkeriet, E. (2013). A Spectral Imaging System for Detection of Botrytis in Greenhouses. *EFITA-WCCA-CIGR Conference.*

Pope, R. M., & Fry, E. S. (1997). Absorption spectrum (380–700 nm) of pure water. II. Integrating cavity measurements. *Applied Optics* , 8710 - 8723.

Pour, A., & Hashim, M. (2014, March). ASTER, ALI and Hyperion sensors data for lithological mapping and ore minerals exploration. *Springer Plus , 21* (4), pp. 503-546.

Retrieving key benthic cover types and bathymetry from hyperspectral imagery2007*Journal of Applied Remote Sensing*

Richardson, L. L., & LeDrew, E. F. (2006). *Remote Sensing of Aquatic Coastal Ecosystem Processes.* Springer Netherlands.

Schott, J. R., Salvaggio, C., & Volchok, W. J. (1988). Radiometric scene normalization using pseudoinvariant features. *Remote Sensing of Environment* , 1 - 16.

Using bottom surface reflectance to map coastal marine areas: a new application method for Lyzenga's model2010*International Journal of Remote Sensing* 3051 - 3064

Zhang, E., & Zhang, Y. (2009). F-Measure. In L. LIU, & M. ÖZSU, *Encyclopedia of Database Systems* (pp. 1147 - 1147). Boston, MA: Springer US.

Zoffoli, M. L., Frouin, R., & Kampel, M. (2014). Water Column Correction for Coral Reef Studies by Remote Sensing. *Sensors* , 16881 - 16931.

APPENDICES

APPENDIX A

LABORATORY AND OUTSIDE DATA COMPARISON

The following figures are the comparison of data collection from laboratory and outside environment.

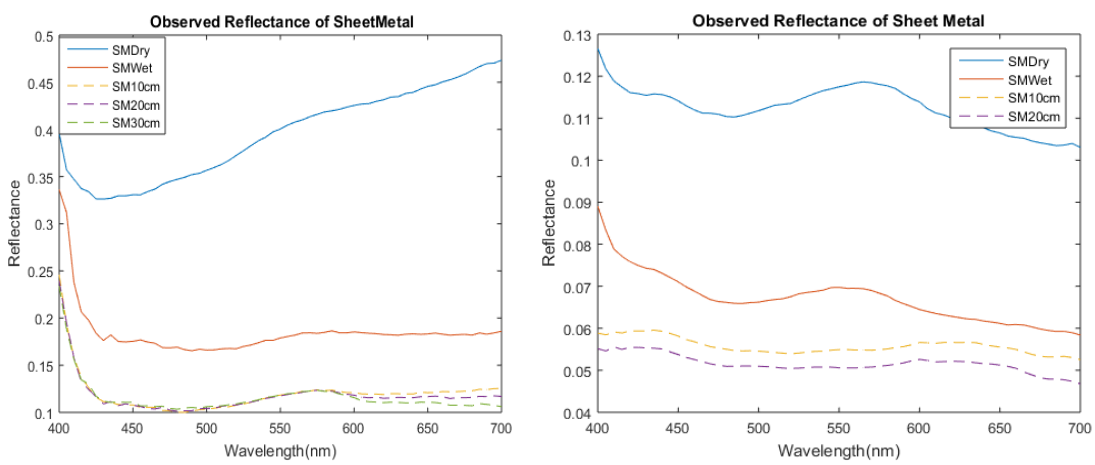

Figure 15: Signature comparison of sheet metal from laboratory and outside environments (Left: Lab, Right: Outside)

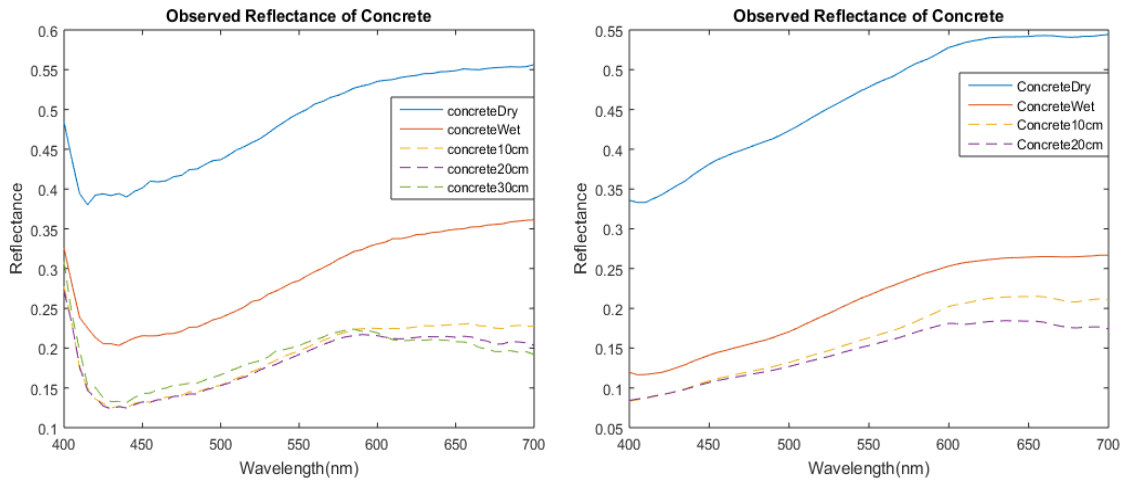

Figure 16: Signature comparison of concrete from laboratory and outside environments
(Left: Lab, Right: Outside)

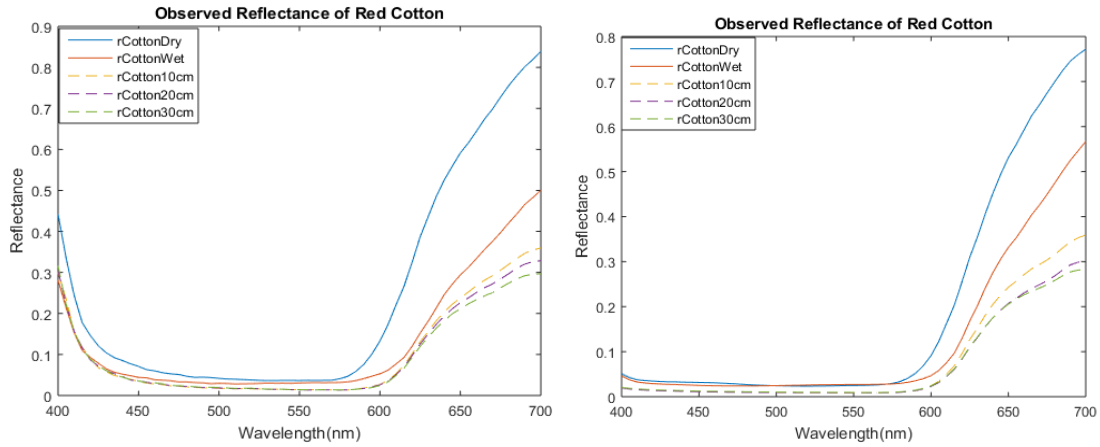

Figure 17: Signature comparison of red cotton fabric from laboratory and outside environments
(Left: Lab, Right: Outside)

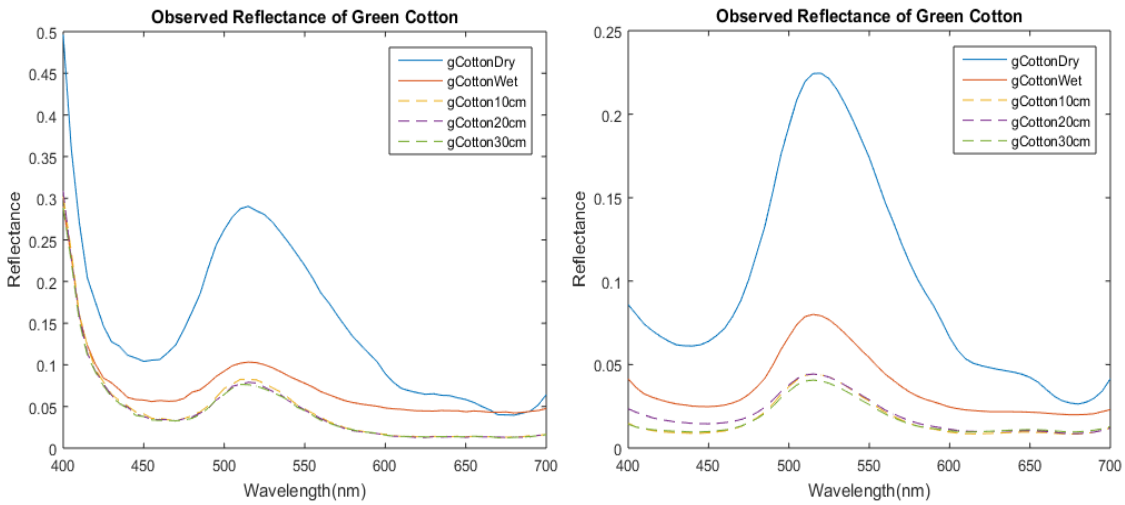

Figure 18: Signature comparison of green cotton fabric from laboratory and outside environments (Left: Lab, Right: Outside)

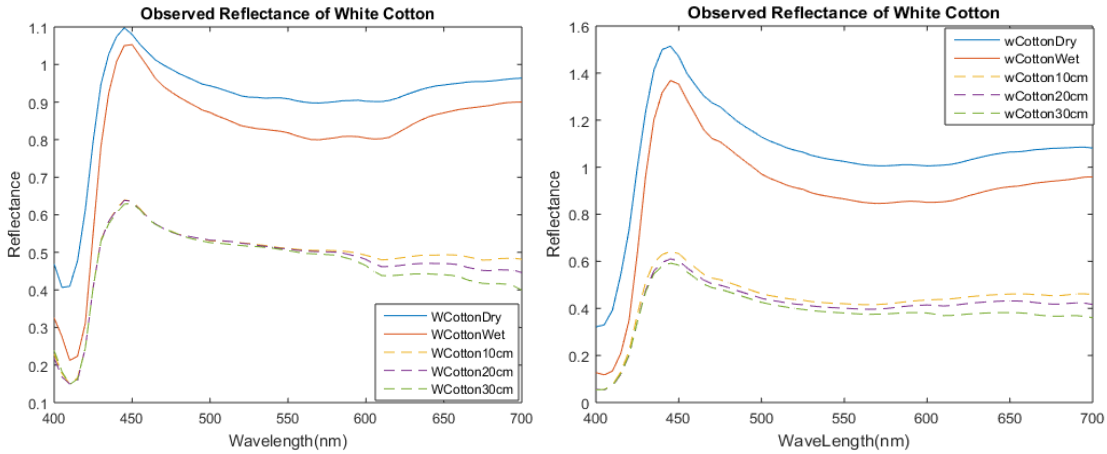

Figure 19: Signature comparison of white cotton fabric from laboratory and outside environments (Left: Lab, Right: Outside)

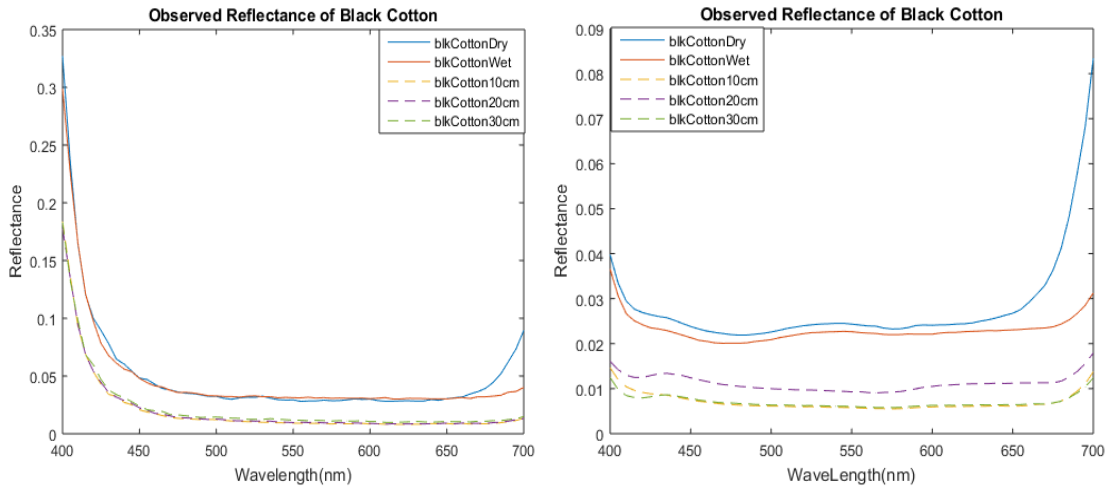

Figure 20: Signature comparison of black cotton fabric from laboratory and outside environments (Left: Lab, Right: Outside)

APPENDIX B

61 – 204 BAND DATA COMPARISON

The following figures are the comparison of same material signatures with 61 and 204 band data. The comparison is performed withoutside environment data. Because no difference is detected by visual inspection among all materials in outside environment data, the lab environment data is not investigated.

In the following figures, dry-wet reflectance of materials and white reference material are plotted. Data collection is performed for several times. Each material signature in those collections are plotted in these figures to observe consistency. In these figures, sheet metal Dry1 reflectance is dropped about 0.001 reflectance value in the whole spectrum. Beside this, reference material reflectance of the red cotton and green cotton is smoothed in 61 band data when compared to 204 band data. Except these minor changes, no difference is detected by visual inspection.

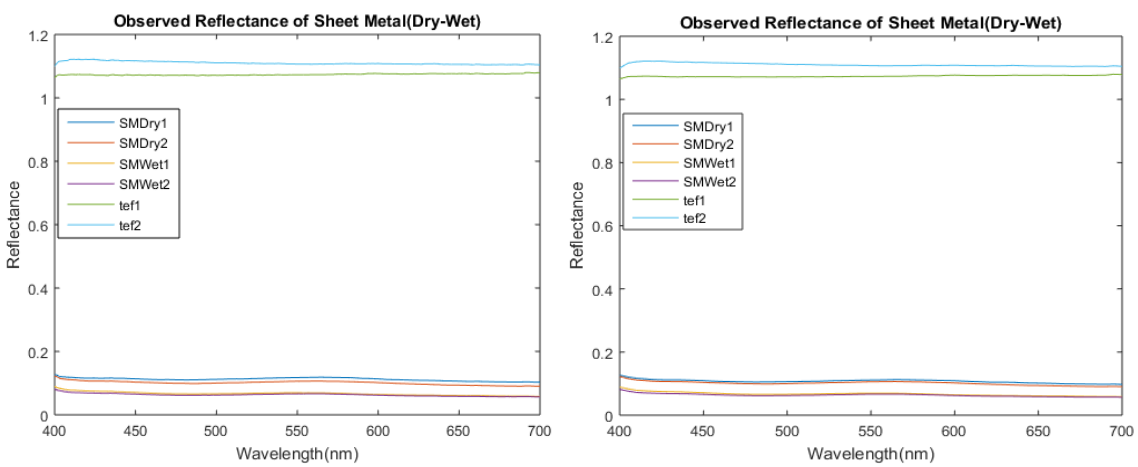

Figure 21: Signature comparison of sheet metal (Dry-Wet)

(Left: 204 band data, Right: 61 band data)

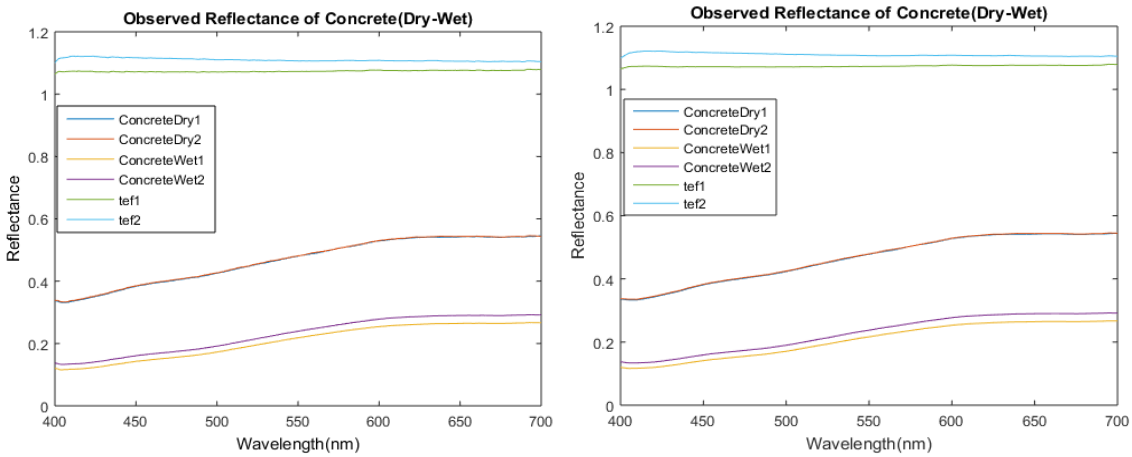

Figure 22: Signature comparison of concrete (Dry-Wet)

(Left: 204 band data, Right: 61 band data)

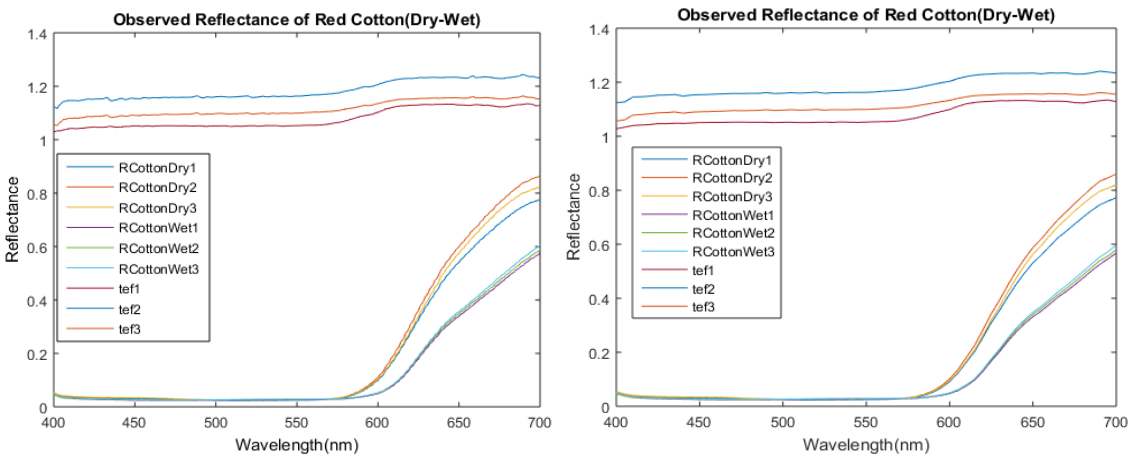

Figure 23: Signature comparison of red cotton fabric (Dry-Wet)

(Left: 204 band data, Right: 61 band data)

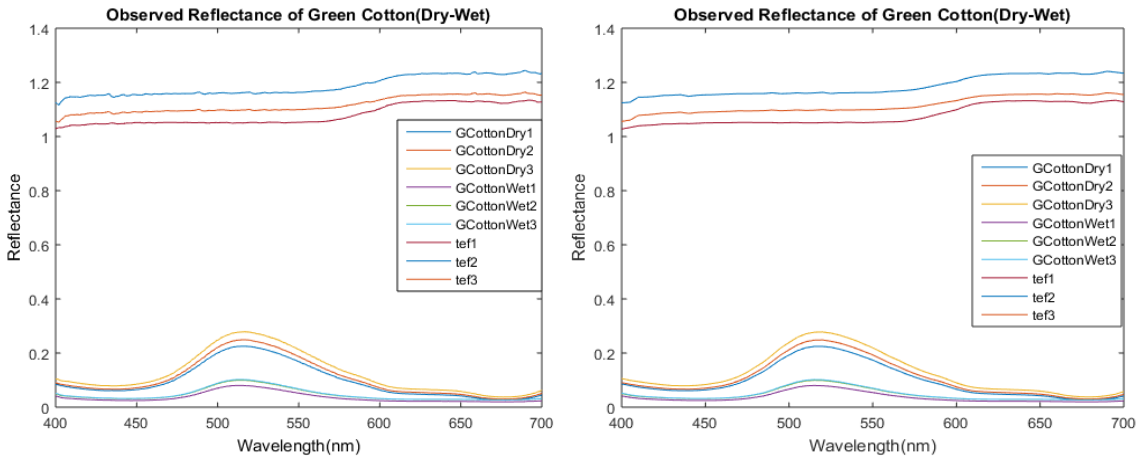

Figure 24: Signature comparison of green cotton fabric (Dry-Wet)

(Left: 204 band data, Right: 61 band data)

In the following figures, dry-wet-underwater reflectance of materials with different depths are plotted. In these figures, the sheet metal reflectance is smoothed in 61 band data when compared to 204 band data. Except this minor change, no difference is detected by visual inspection.

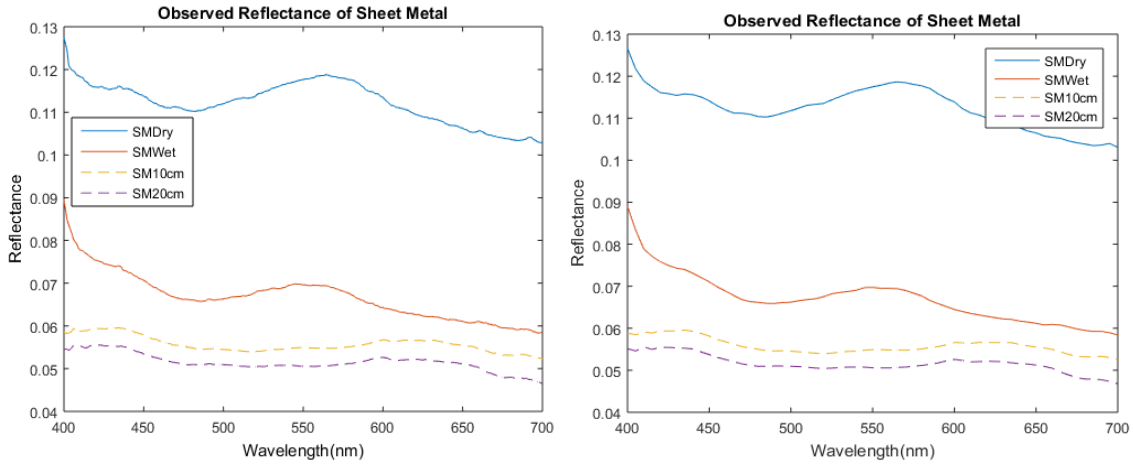

Figure 25: Signature comparison of sheet metal (Dry-Wet-Underwater)

(Left: 204 band data, Right: 61 band data)

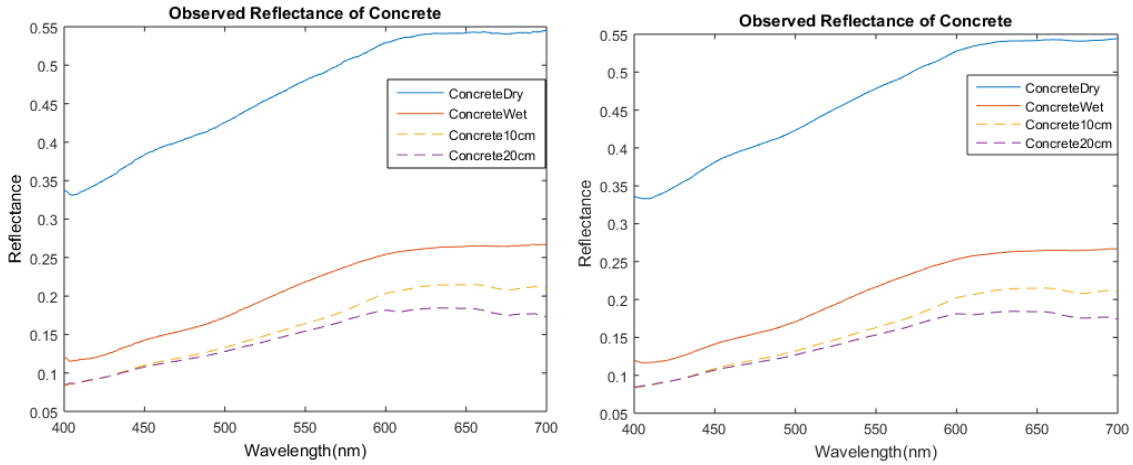

Figure 26: Signature comparison of concrete (Dry-Wet-Underwater)

(Left: 204 band data, Right: 61 band data)

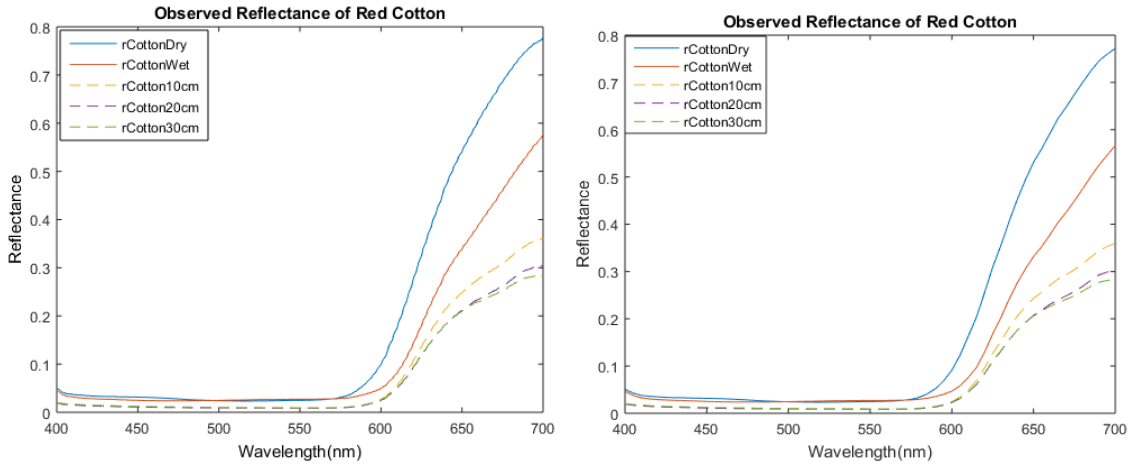

Figure 27: Signature comparison of red cotton fabric (Dry-Wet-Underwater)

(Left: 204 band data, Right: 61 band data)

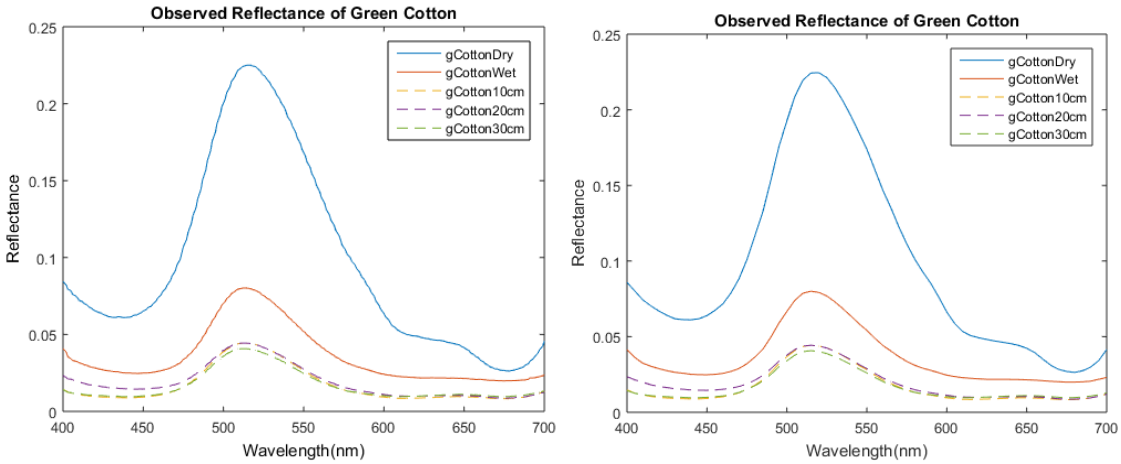

Figure 28: Signature comparison of green cotton fabric (Dry-Wet-Underwater)

(Left: 204 band data, Right: 61 band data)

APPENDIX C

SIMULATED AND INVERTED REFLECTANCE OF MATERIALS

(SIMULATED DATA)

The following figures shows the comparison of reflectance between the simulated material and obtained reflectance by inverting the model parameters in the depths 0.1, 0.2, 0.3, 1, 2, 5 and 10 meters. In figures, the blue lines indicate the simulated reflectance of the related material. The brown star lines indicate the obtained reflectance by inverting the model parameters in related depths. The first and the third rows show the figures of the MEA algorithm. The second and the fourth rows show the figures of the LEA algorithm.

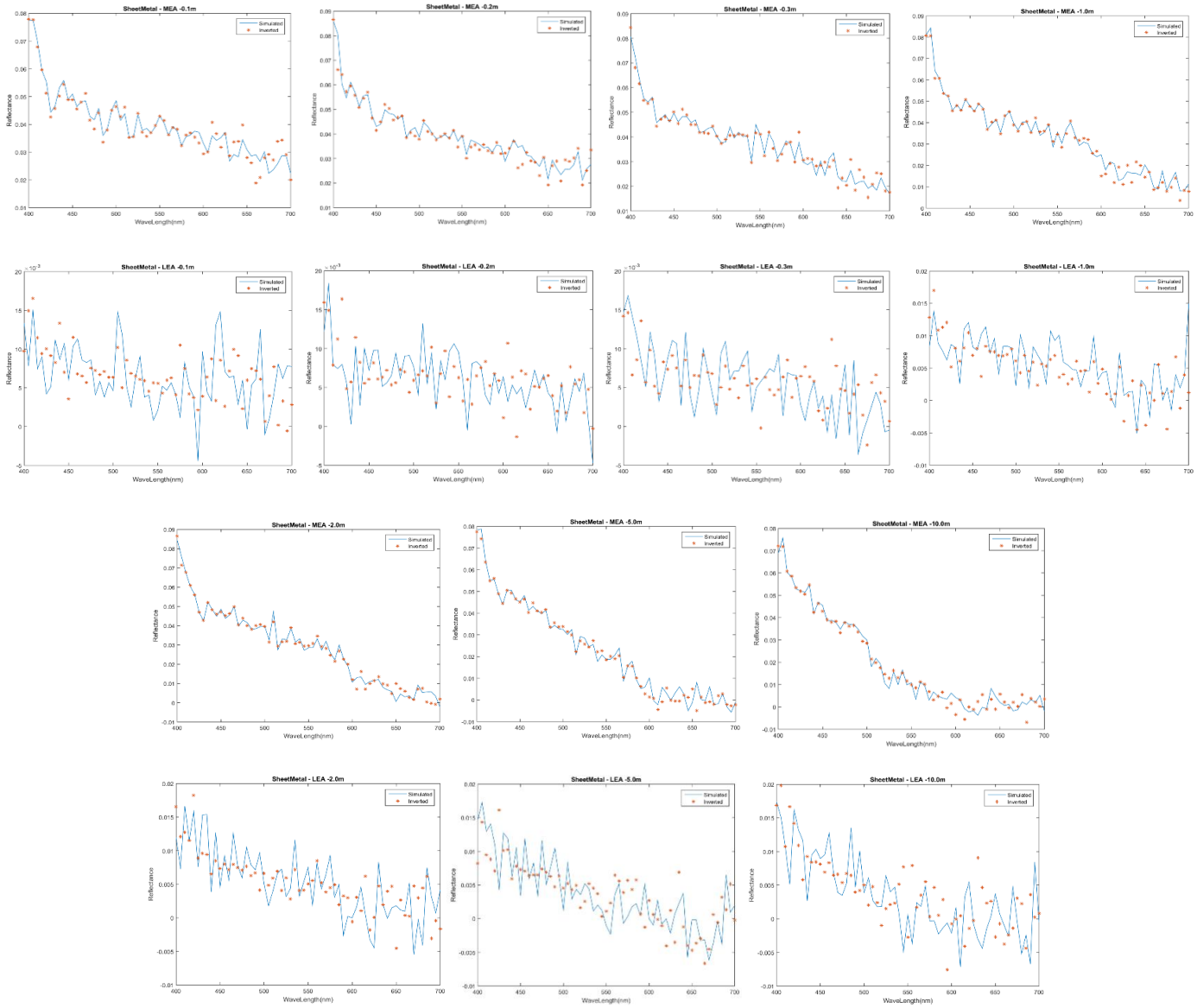

Figure 29: Simulated and Inverted Reflectance of Sheet Metal in Various Depths

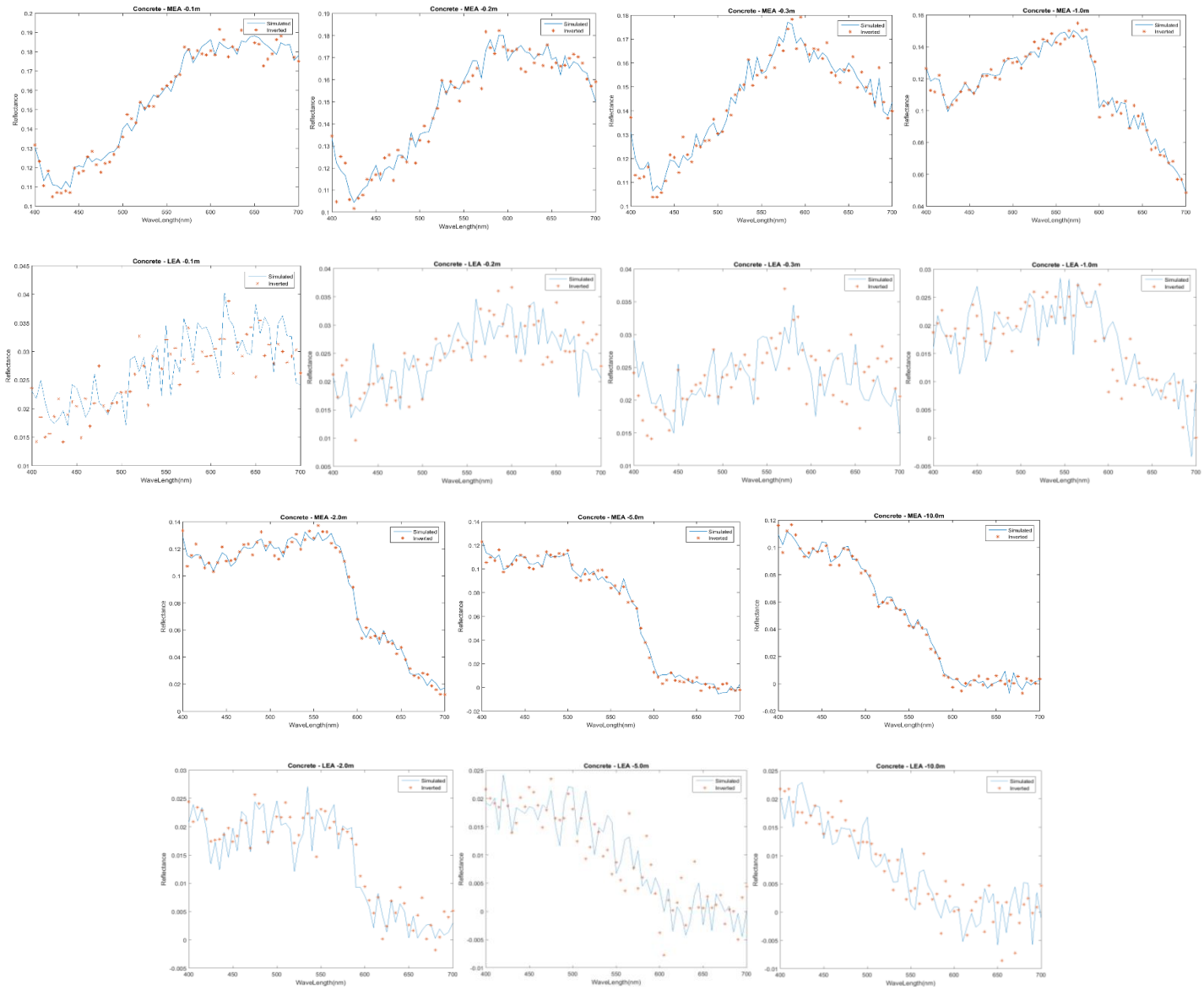

Figure 30: Simulated and Inverted Reflectance of Concrete in Various Depths

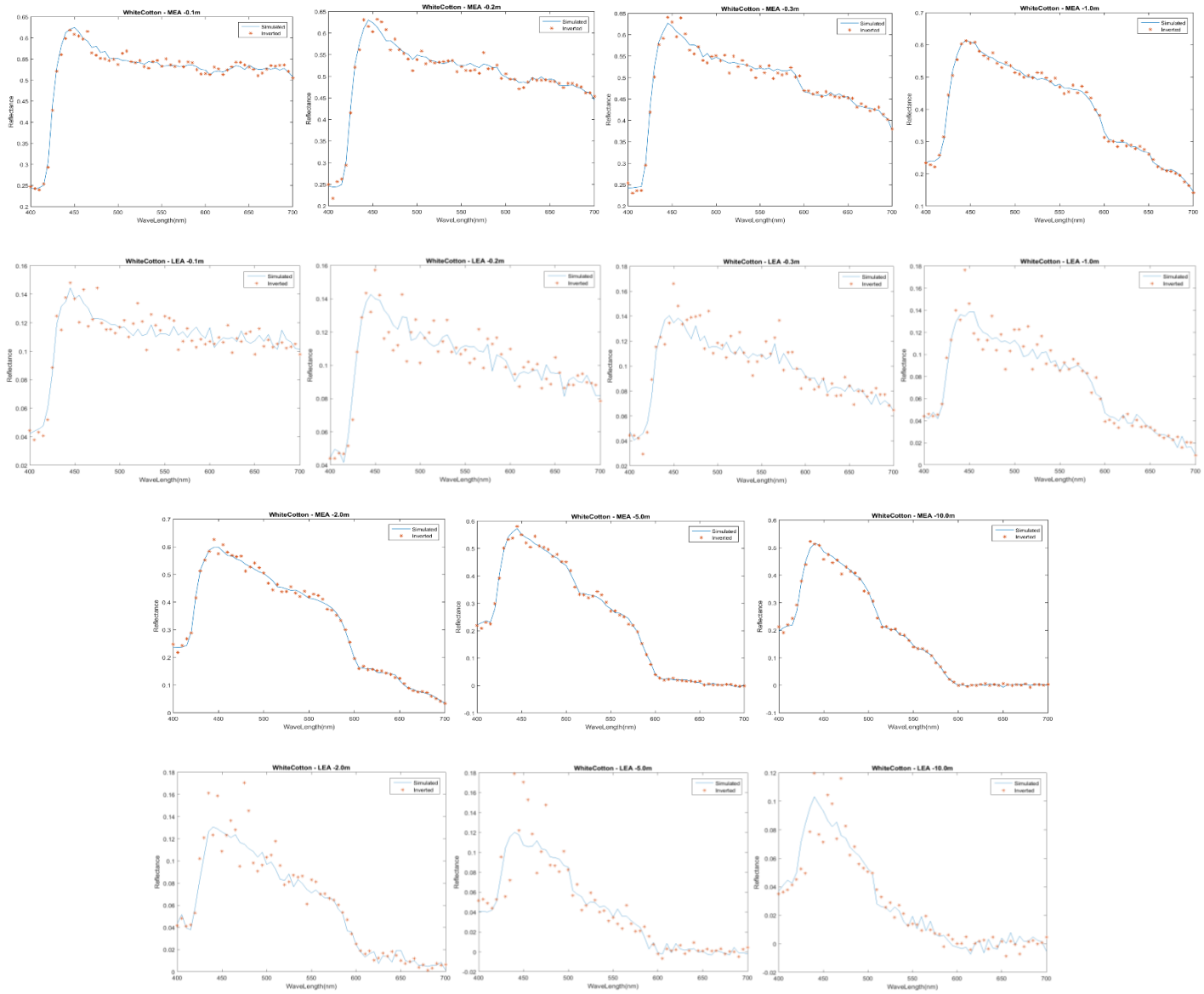

Figure 31: Simulated and Inverted Reflectance of White Cotton Fabric in Various Depths

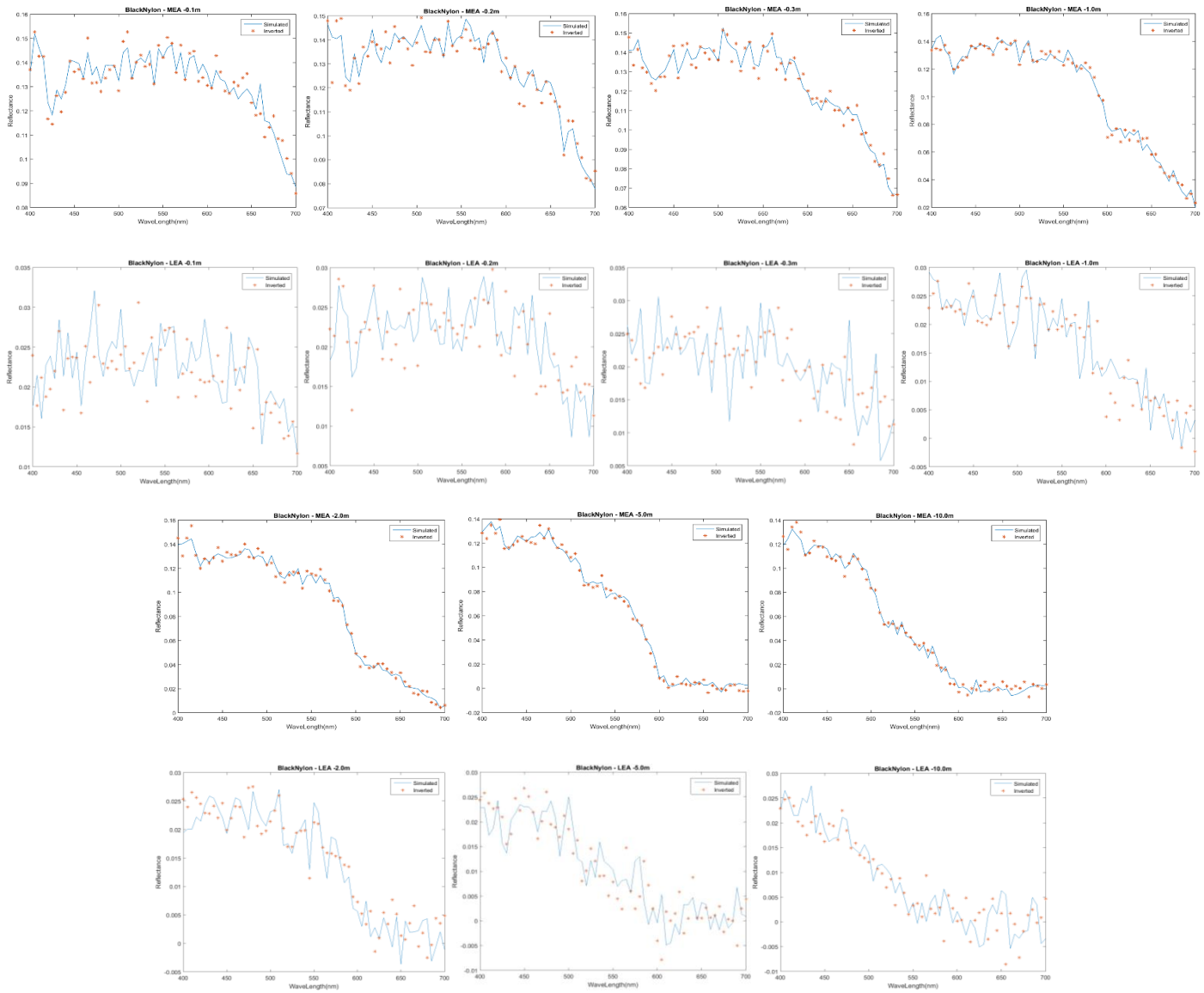

Figure 32: Simulated and Inverted Reflectance of Black Nylon Fabric in Various Depths

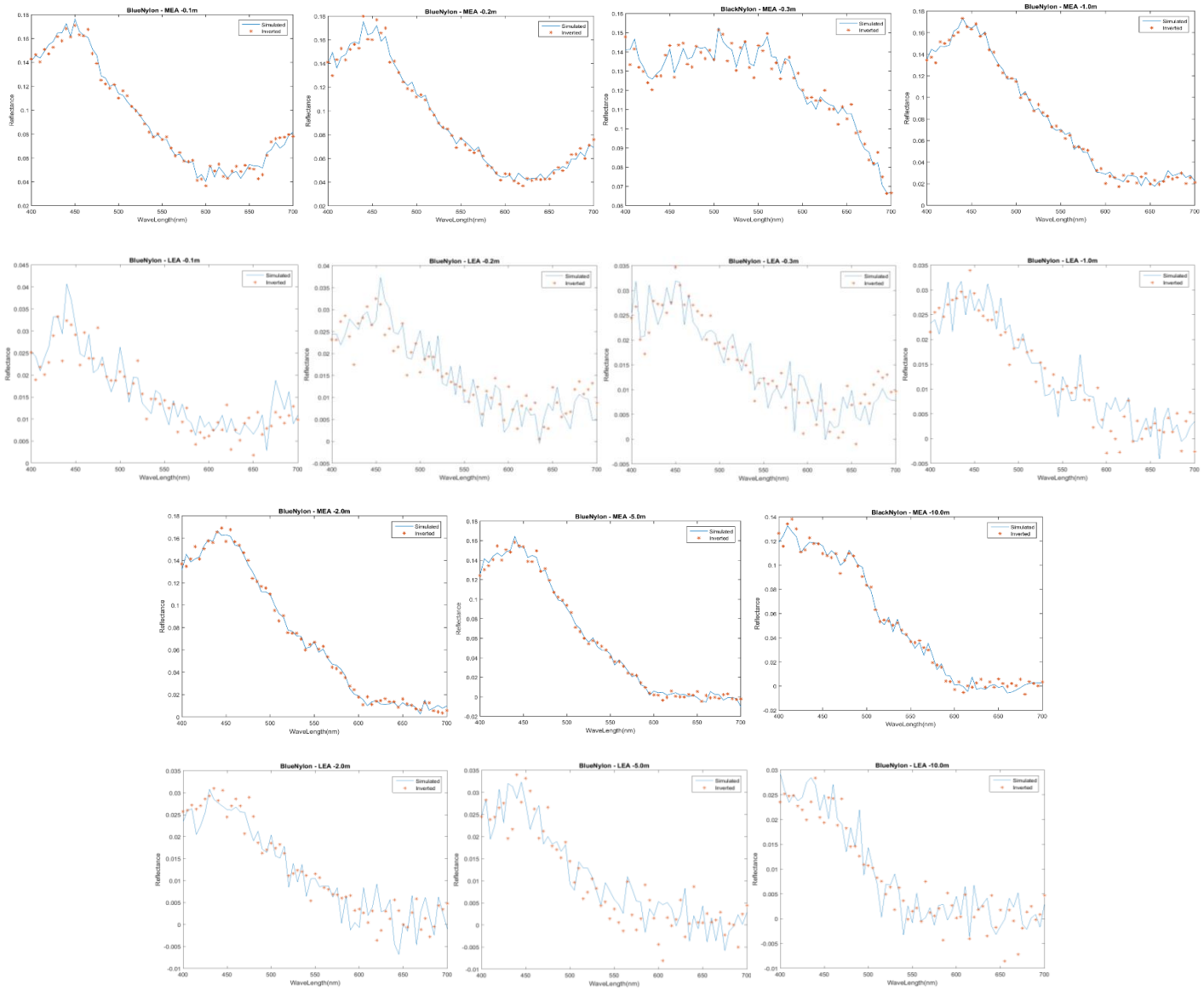

Figure 33: Simulated and Inverted Reflectance of Blue Nylon Fabric in Various Depths

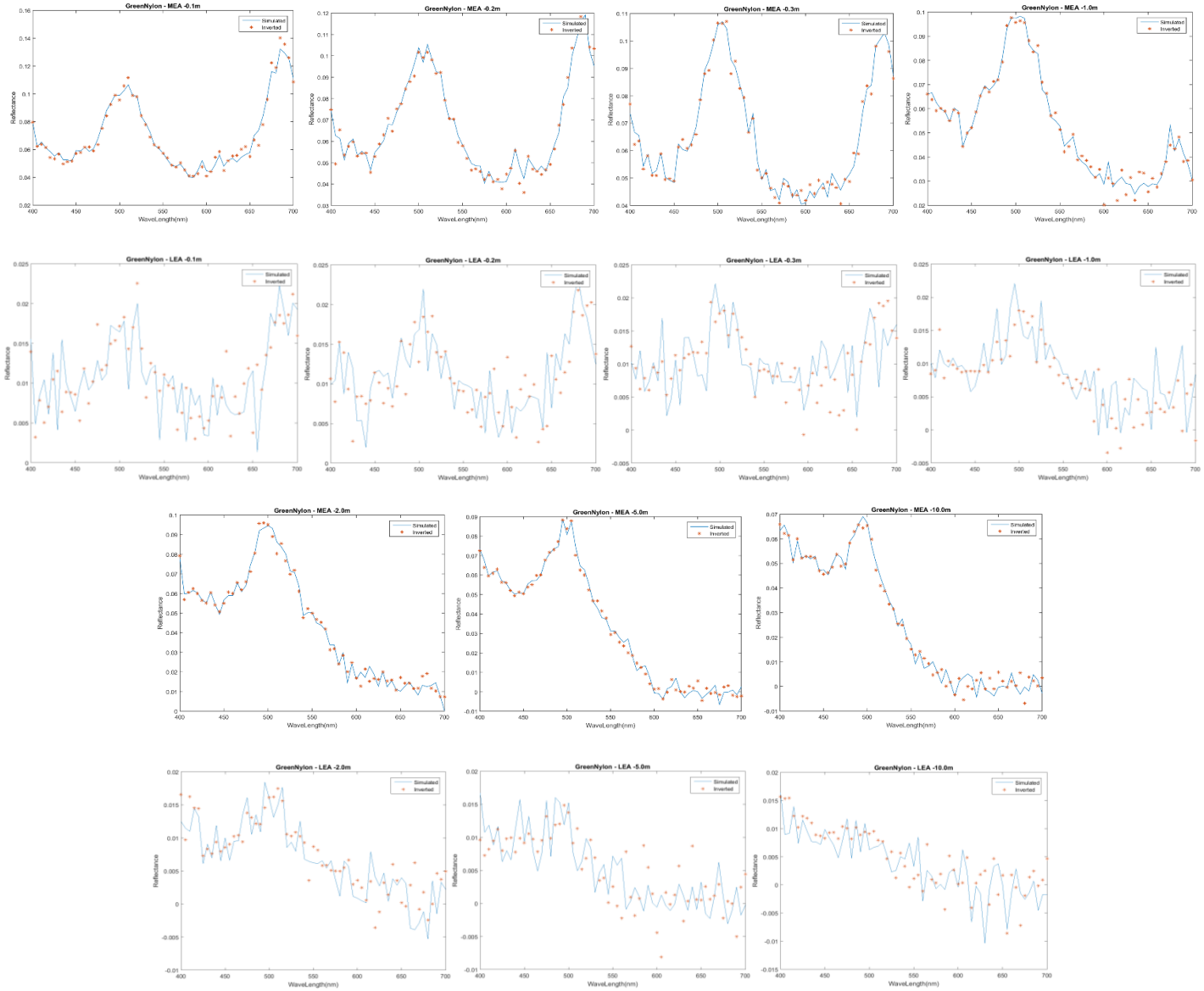

Figure 34: Simulated and Inverted Reflectance of Green Nylon Fabric in Various Depths

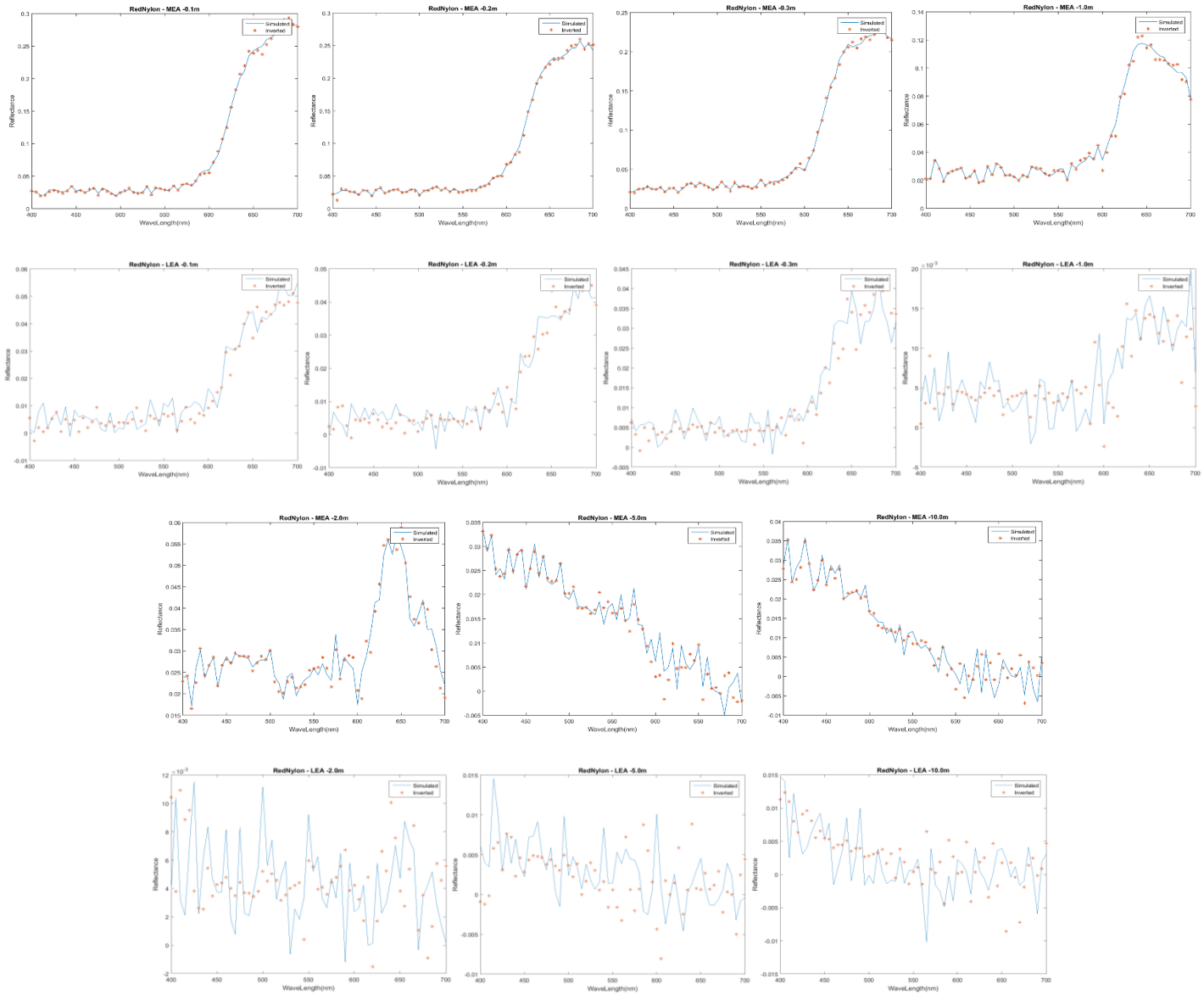

Figure 35: Simulated and Inverted Reflectance of Red Nylon Fabric in Various Depths

APPENDIX D

SIMULATED AND INVERTED REFLECTANCE OF MATERIALS (REAL DATA)

The following figures show the comparison of reflectance between the simulated material and obtained reflectance by inverting the model parameters in the depths 0.3 meter in real data.

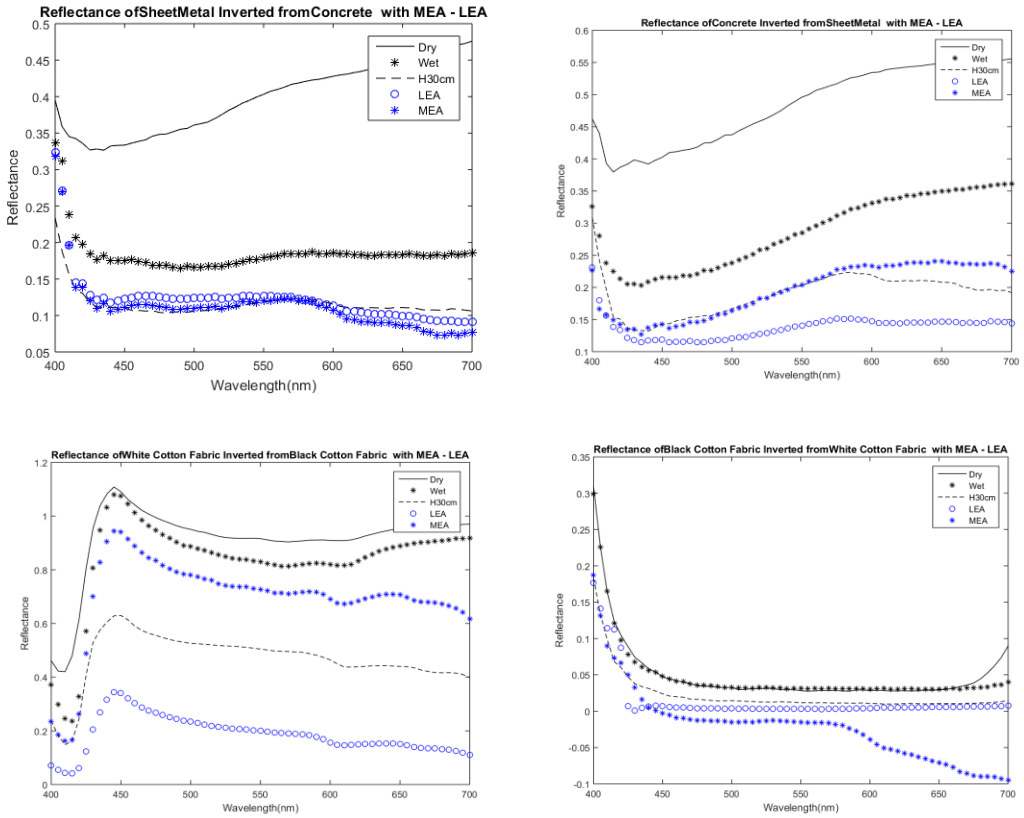

Figure 36: Simulated and Inverted Reflectance of Sheet Metal, Concrete, White and Black Cotton Fabric (0.3m depth)

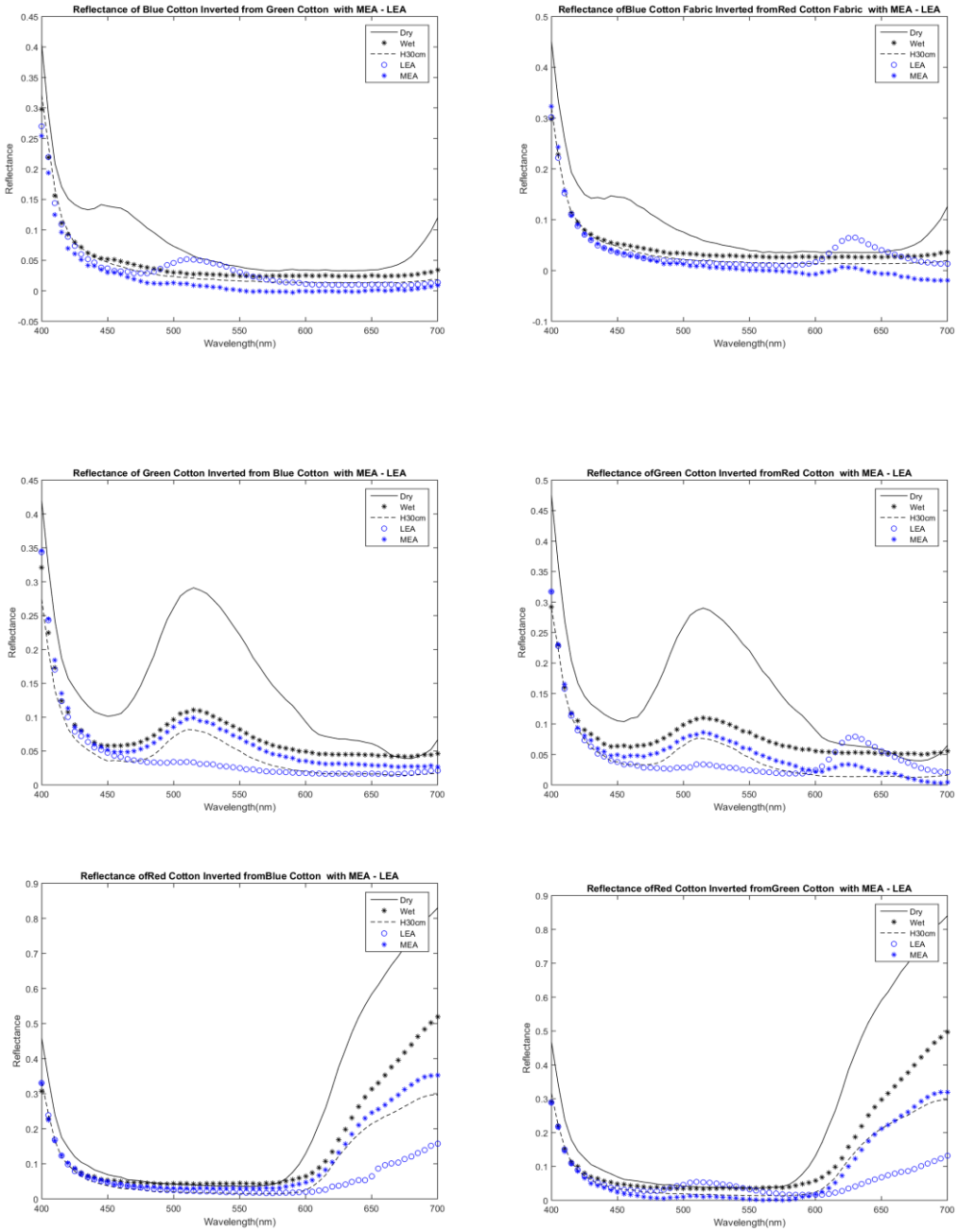

Figure 37: Simulated and Inverted Reflectance of Cotton Fabric with Colors of Red, Green, Blue(0.3m depth)

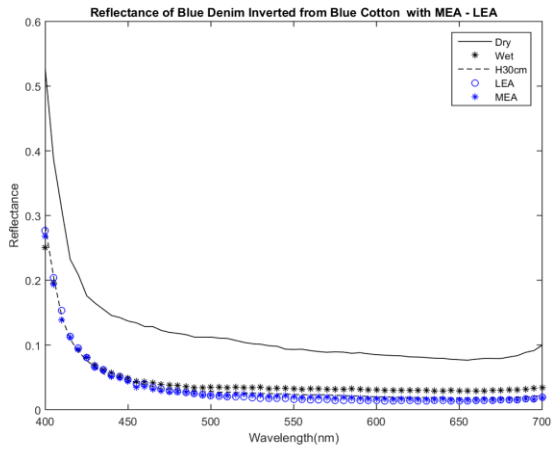

Figure 38: Simulated and Inverted Reflectance of Blue Denim (0.3m depth)

APPENDIX E

DETECTION RESULTS OF MATERIALS

(SIMULATED DATA)

The following figures show the comparison of detection results of all materials with different target signatures in depths of 0.1 – 0.2 – 0.3 – 1 – 2 – 5 – 10 meters. The materials are, from top to down, sheet metal, concrete, white cotton fabric, black nylon fabric, blue nylon fabric, green nylon fabric and red nylon fabric. The first columns of the figures are the simulation scenes in the related depth. The other columns show the detection results. For both detection algorithms (ACE, SAM), the colors ranging from black to white in detection results indicate the similarity of the materials to target reflectance from least similarity (zero, black) to most similarity (one, white) respectively.

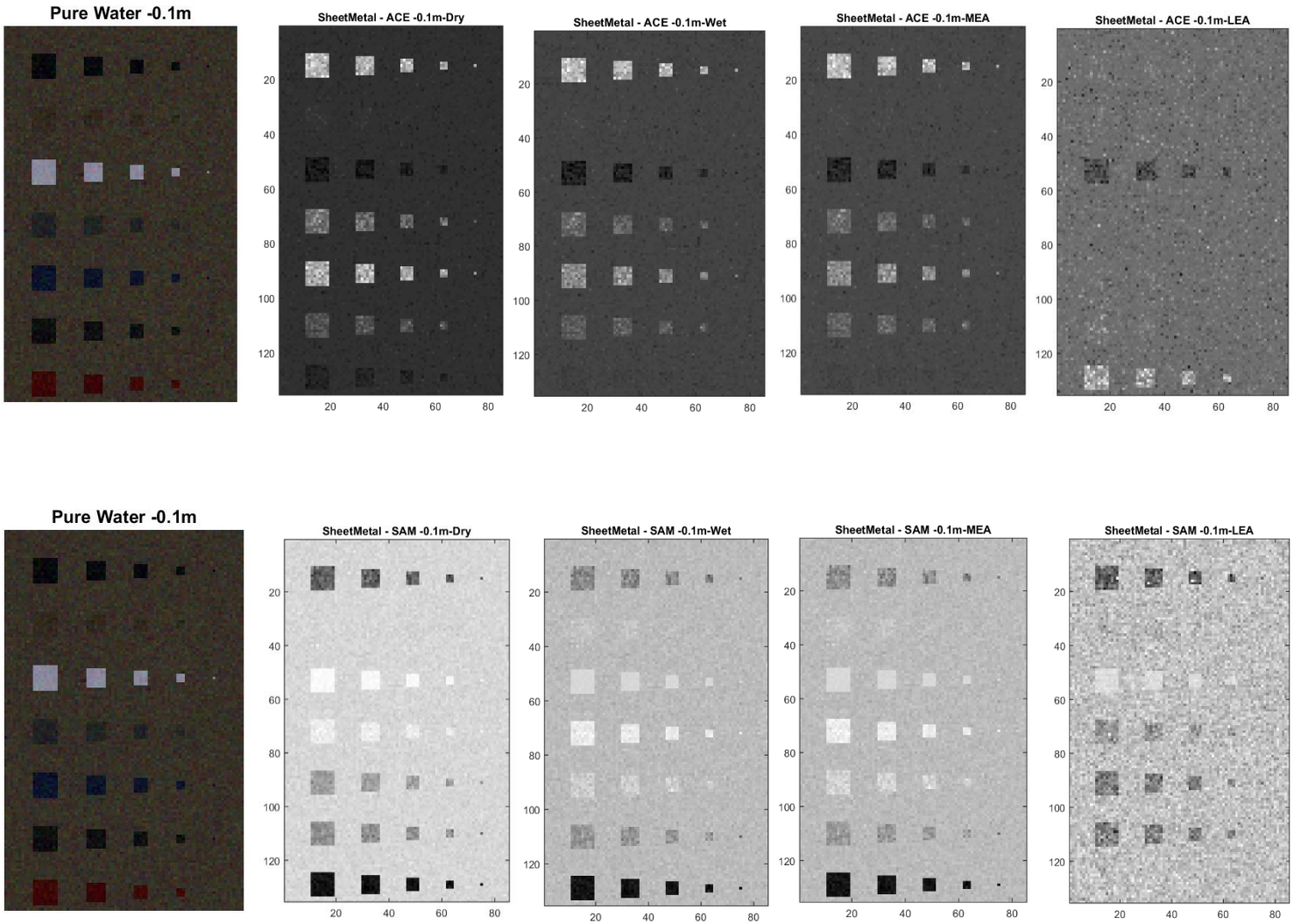

Figure 39: Detection Results of Sheet Metal with Different Target Reflectance(0.1m depth)

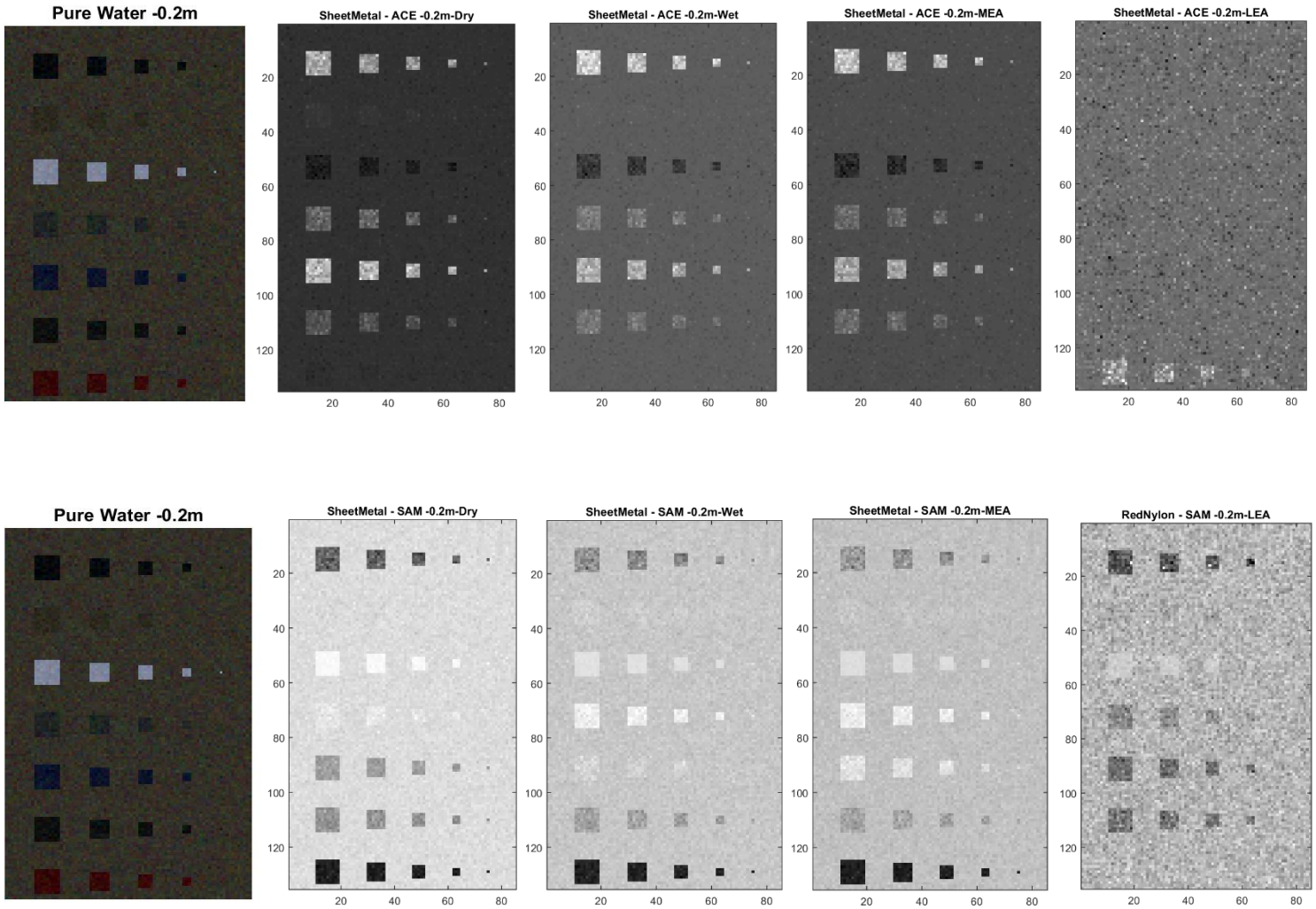

Figure 40: Detection Results of Sheet Metal with Different Target Reflectance (0.2m depth)

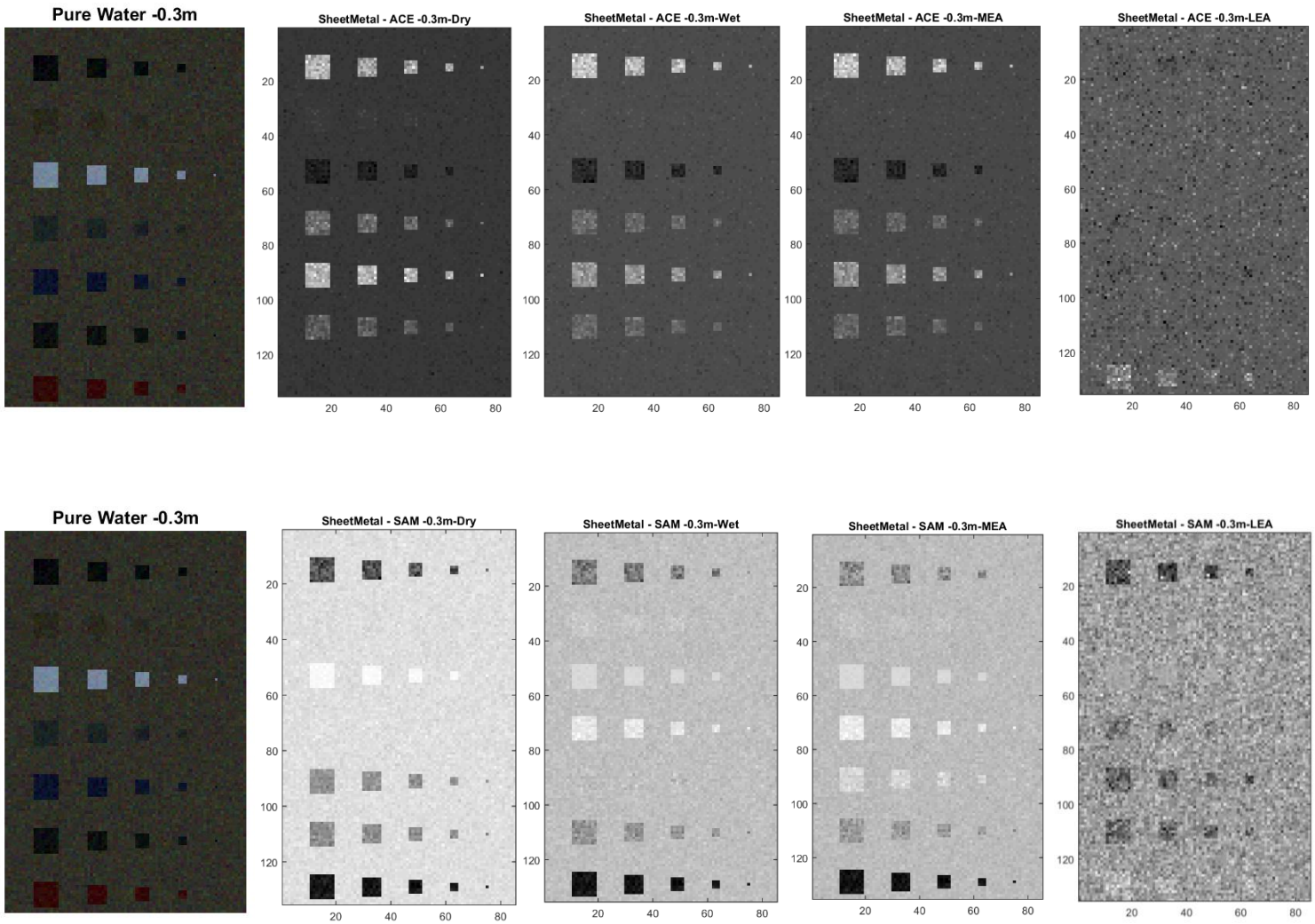

Figure 41: Detection Results of Sheet Metal with Different Target Reflectance (0.3m depth)

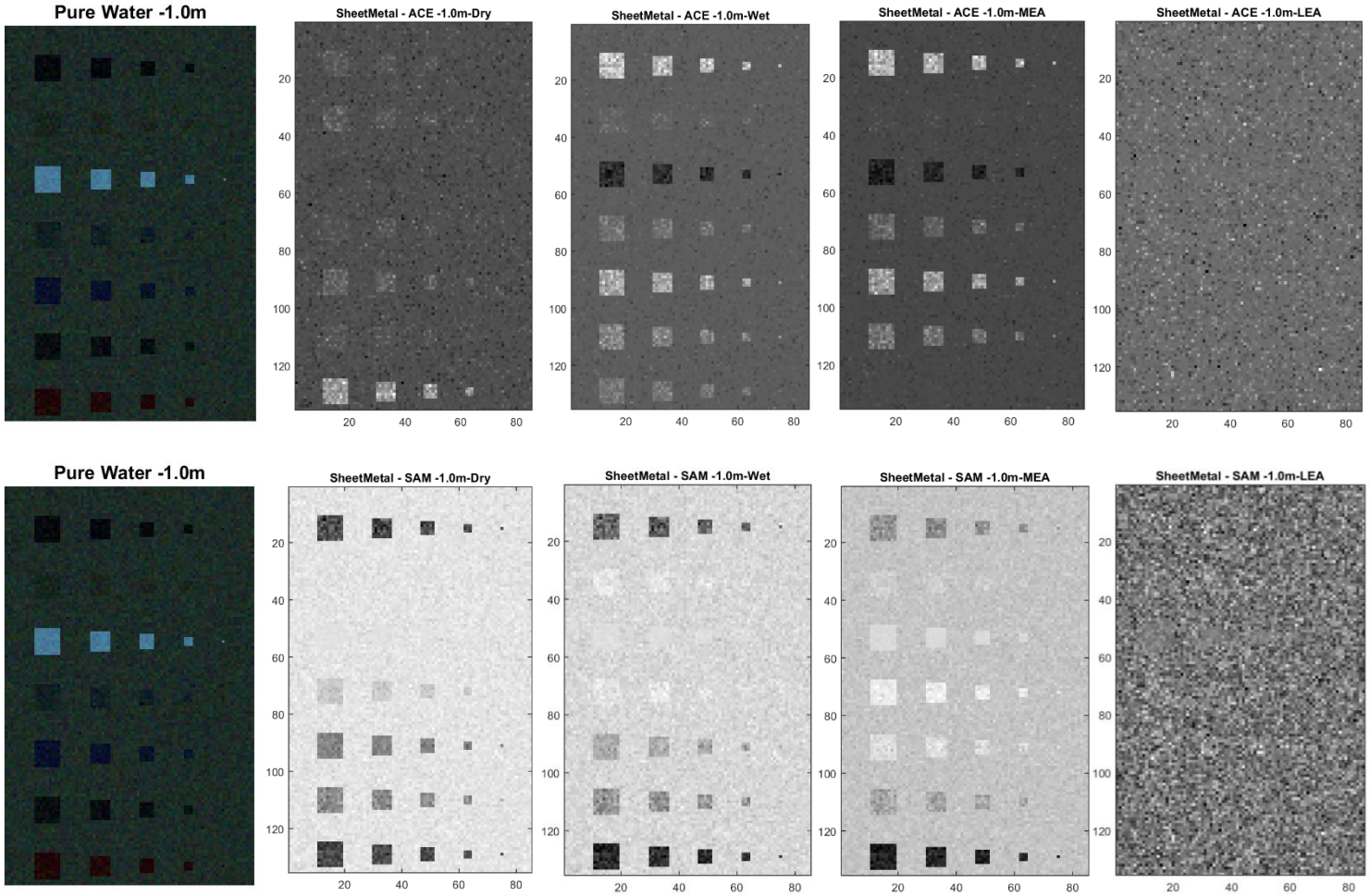

Figure 42: Detection Results of Sheet Metal with Different Target Reflectance (1m depth)

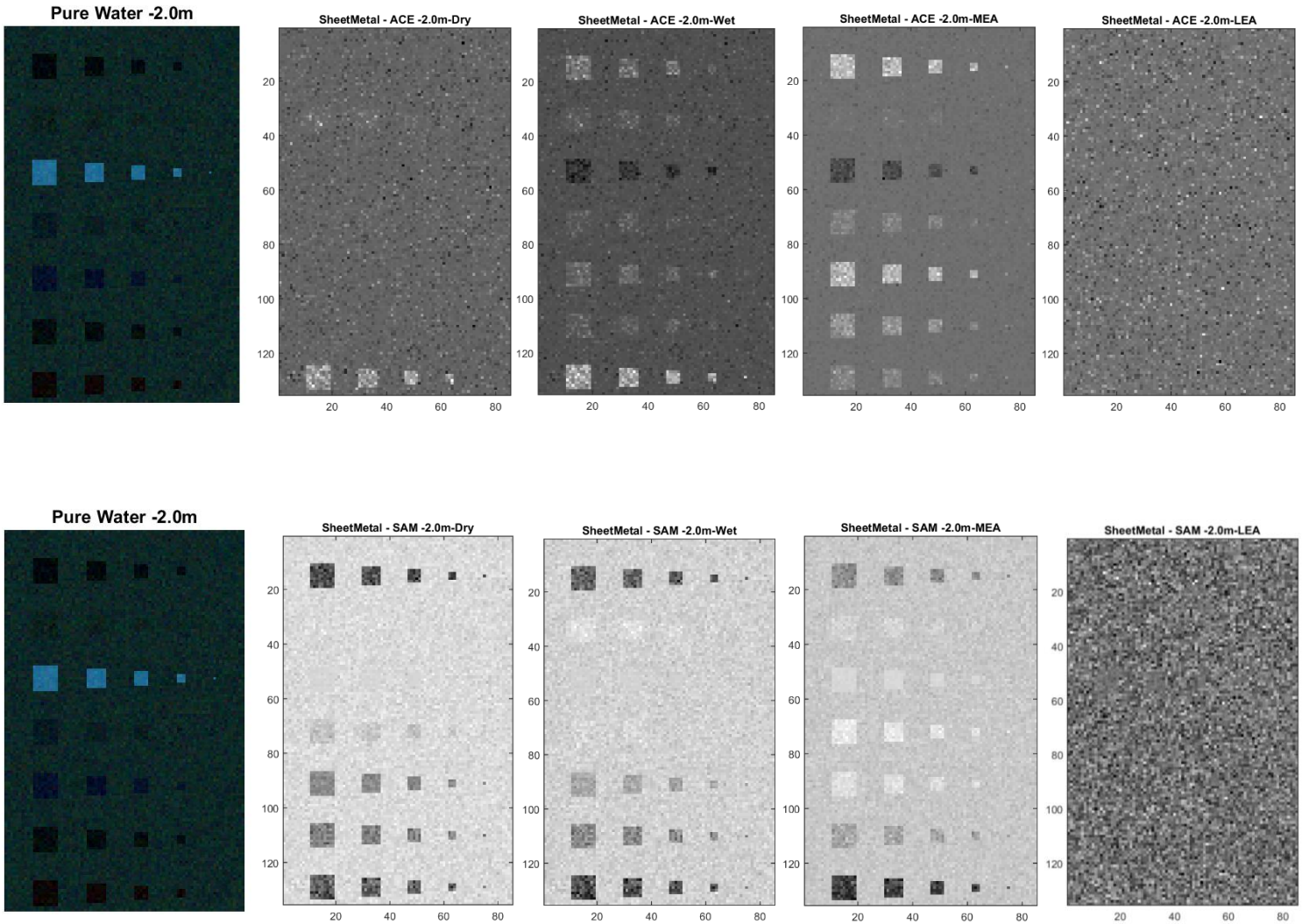

Figure 43: Detection Results of Sheet Metal with Different Target Reflectance (2m depth)

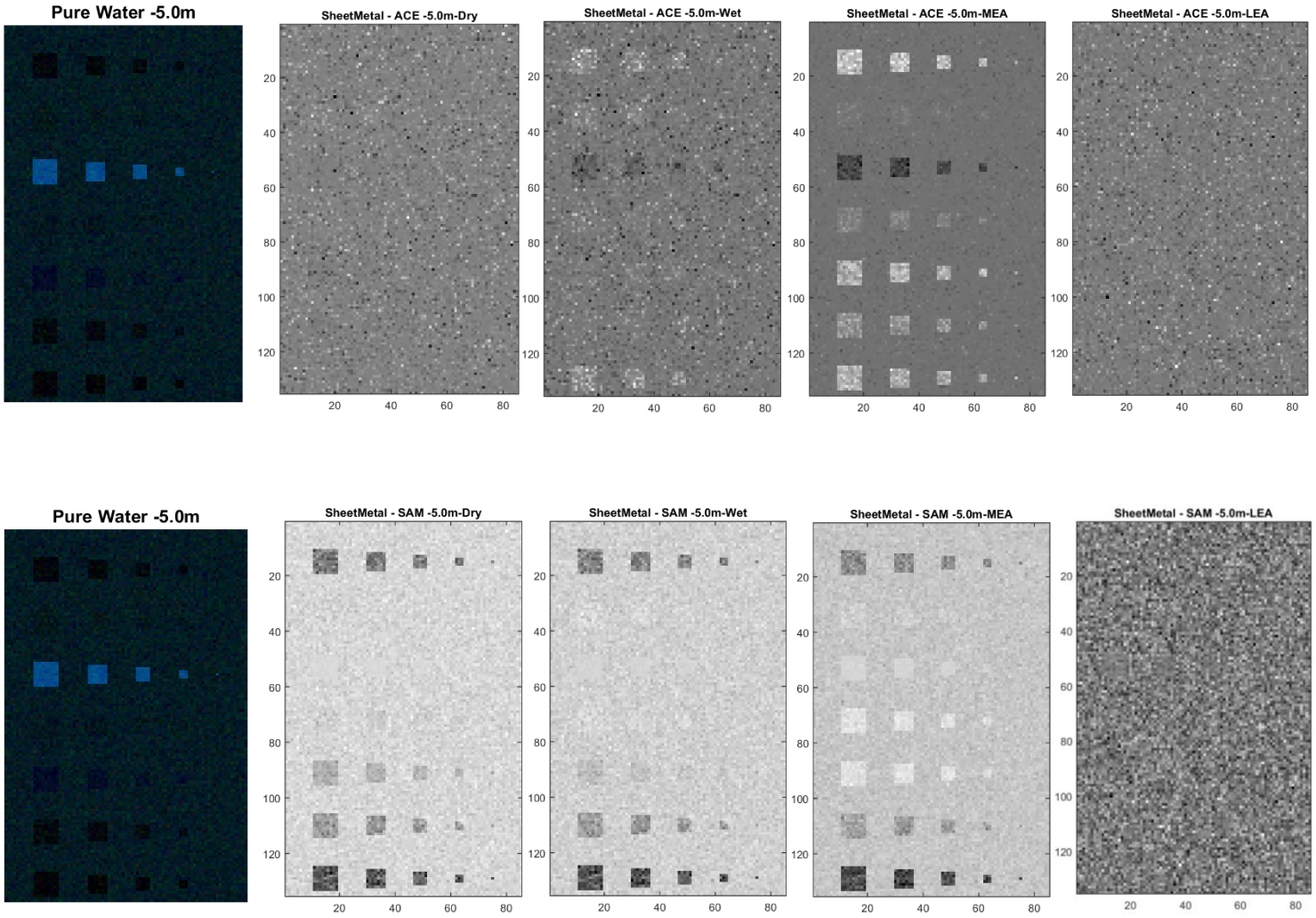

Figure 44: Detection Results of Sheet Metal with Different Target Reflectance (5m depth)

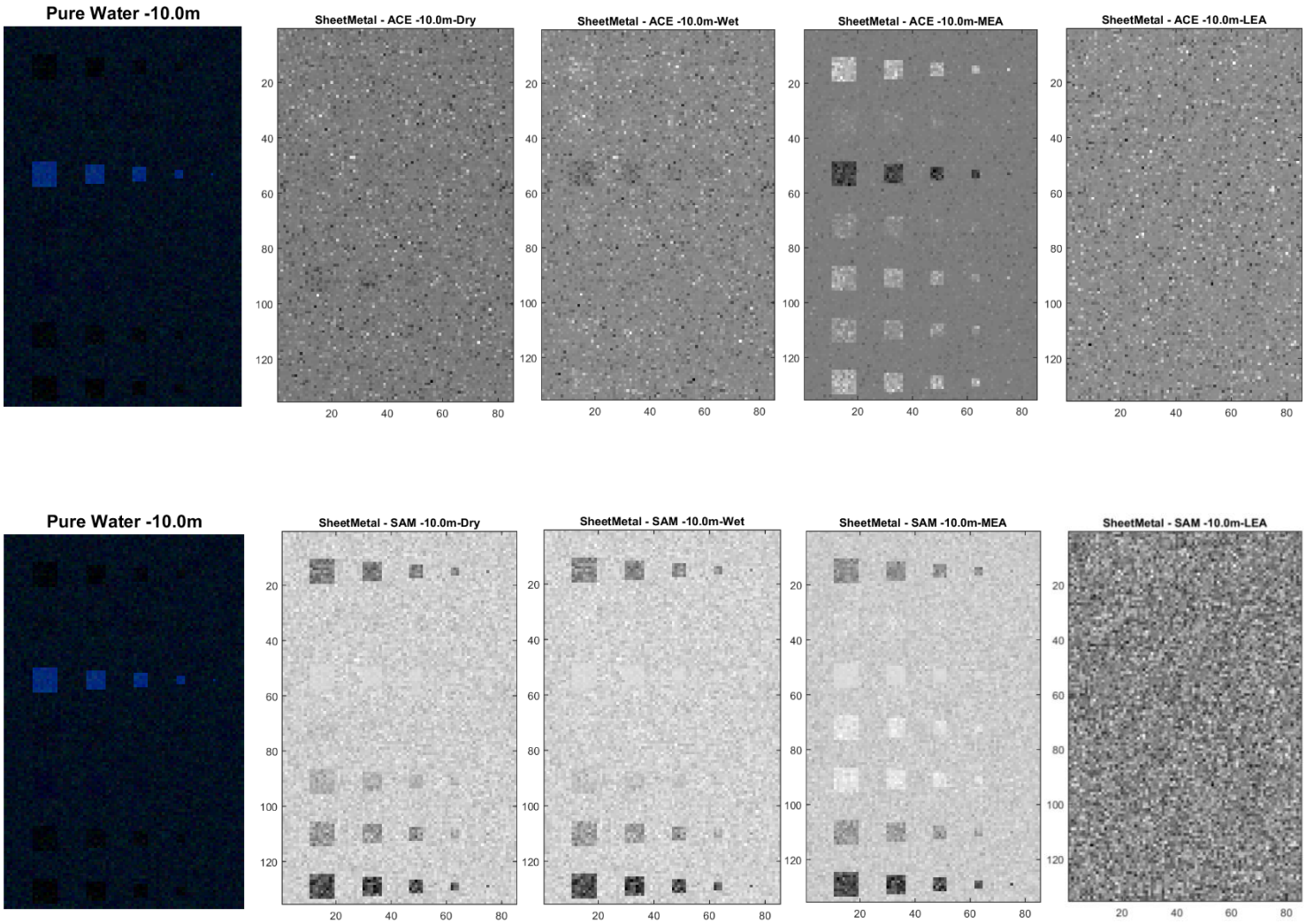

Figure 45: Detection Results of Sheet Metal with Different Target Reflectance (10m depth)

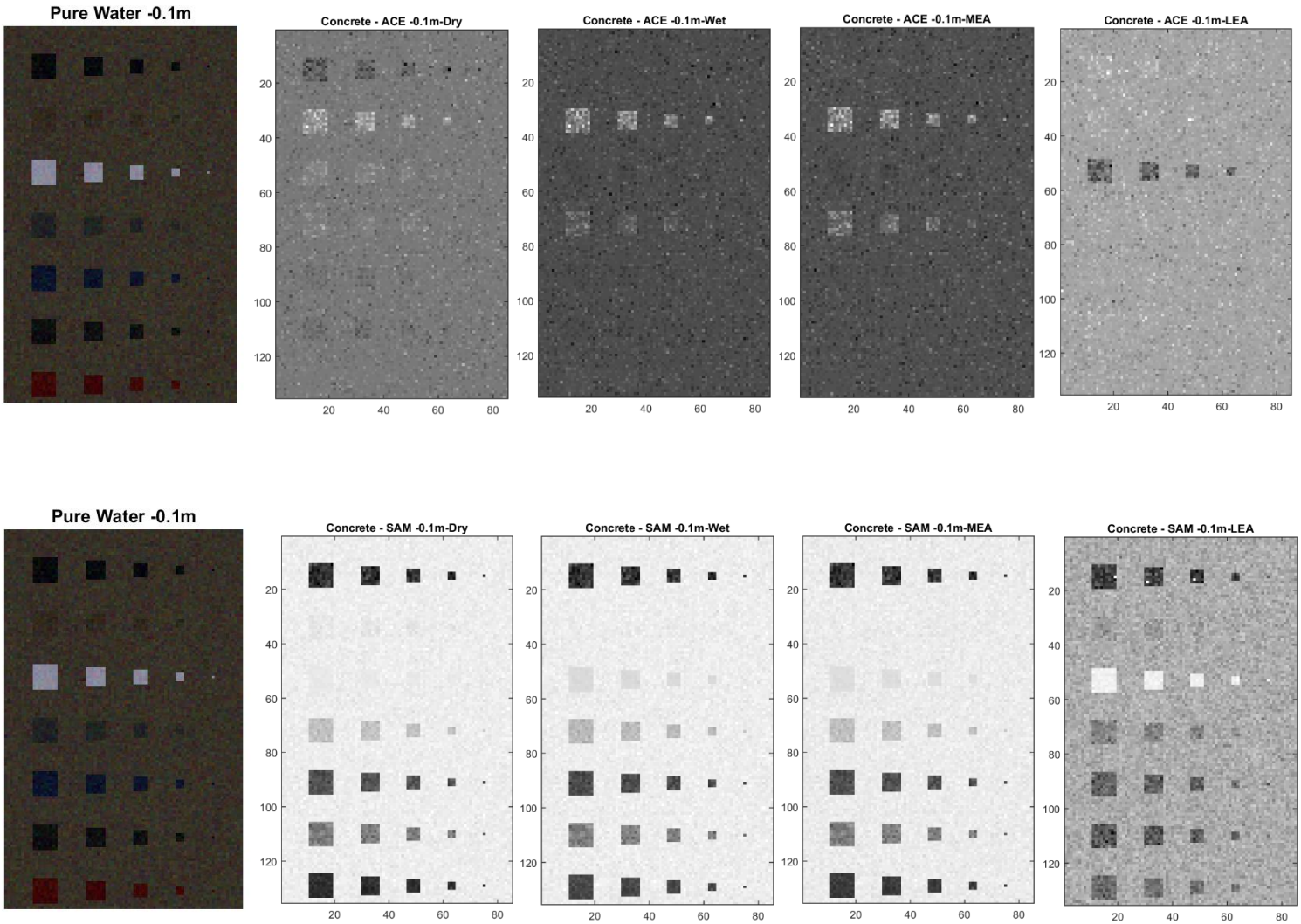

Figure 46: Detection Results of Concrete with Different Target Reflectance (0.1m depth)

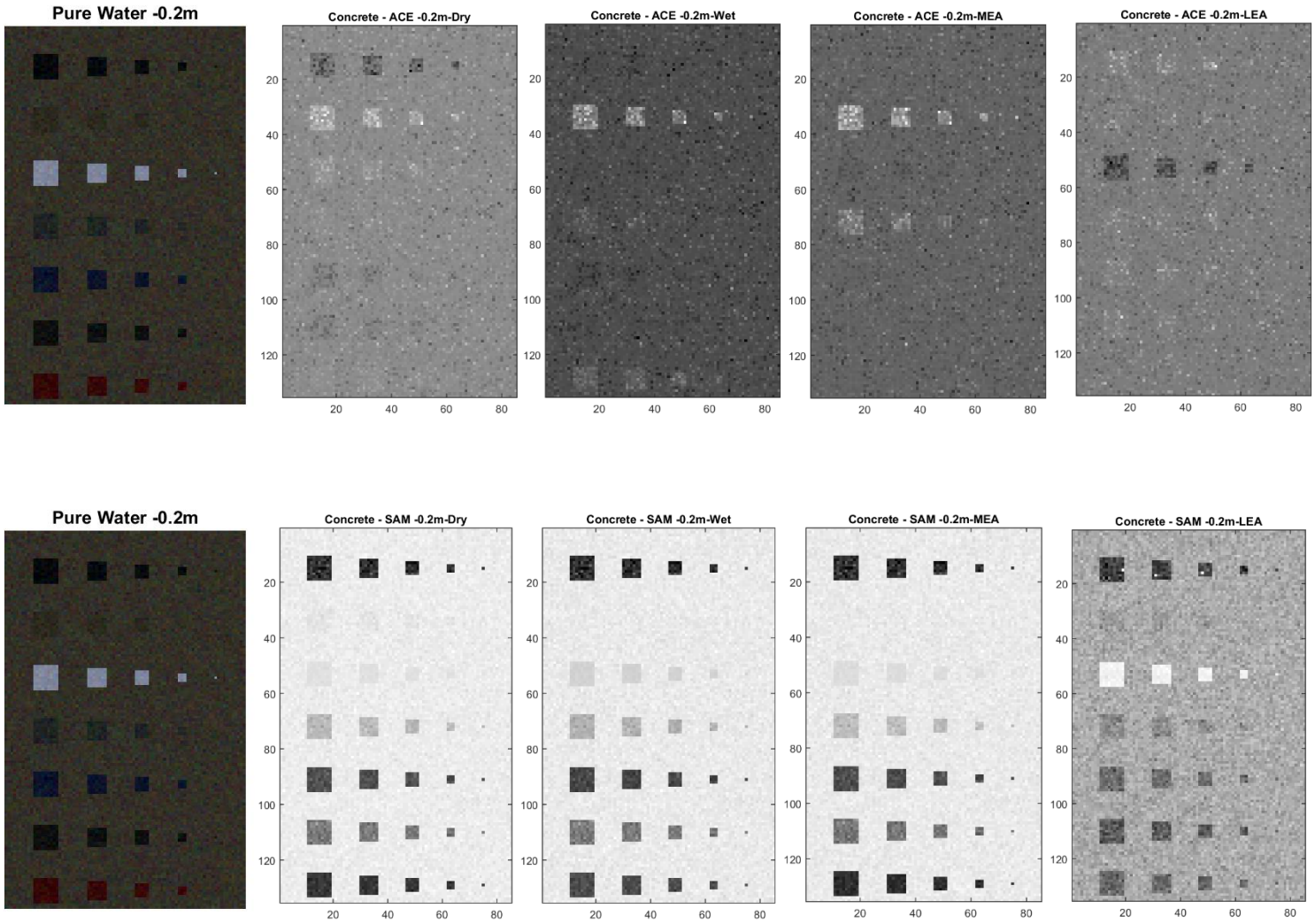

Figure 47: Detection Results of Concrete with Different Target Reflectance (0.2m depth)

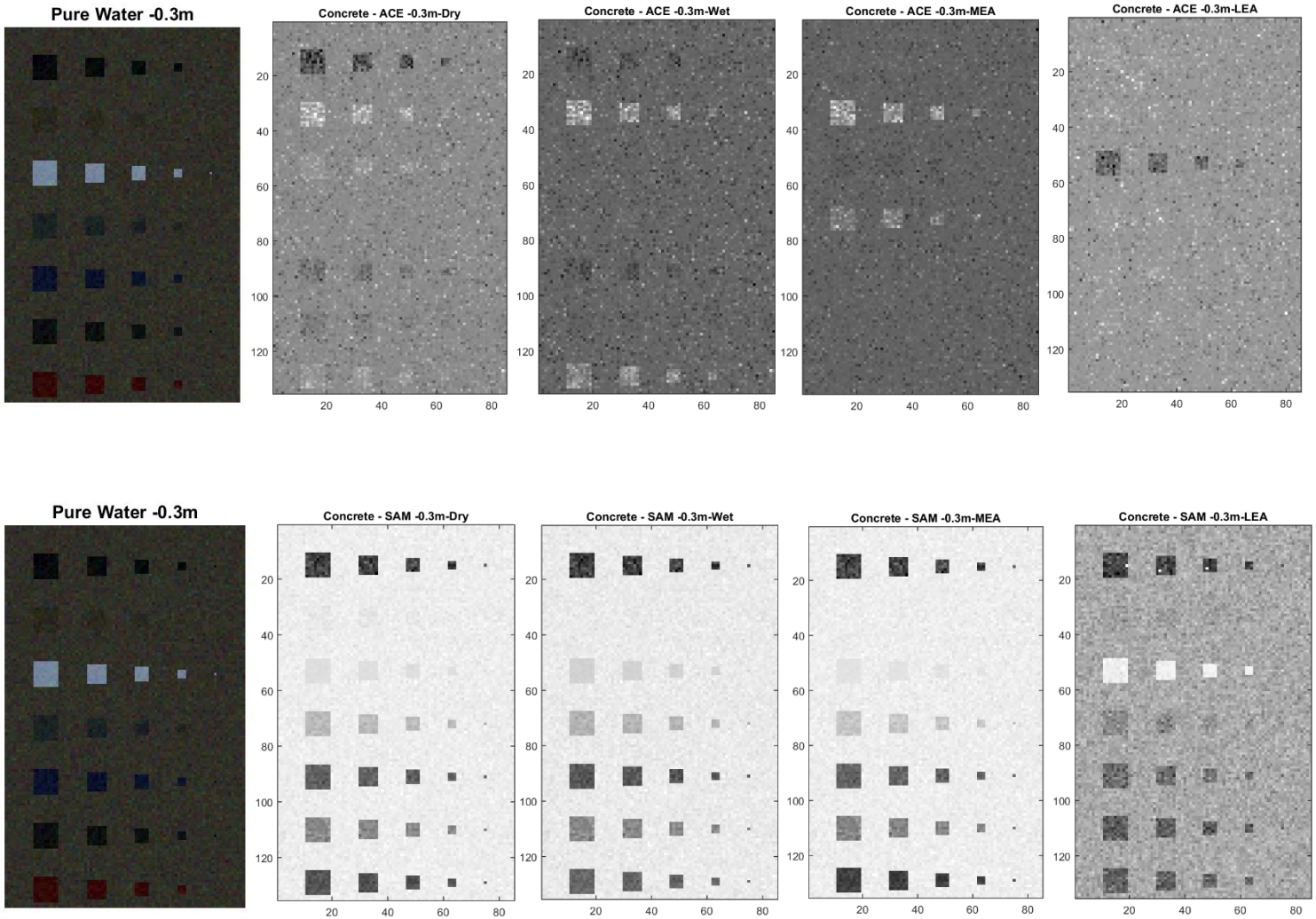

Figure 48: Detection Results of Concrete with Different Target Reflectance (0.3m depth)

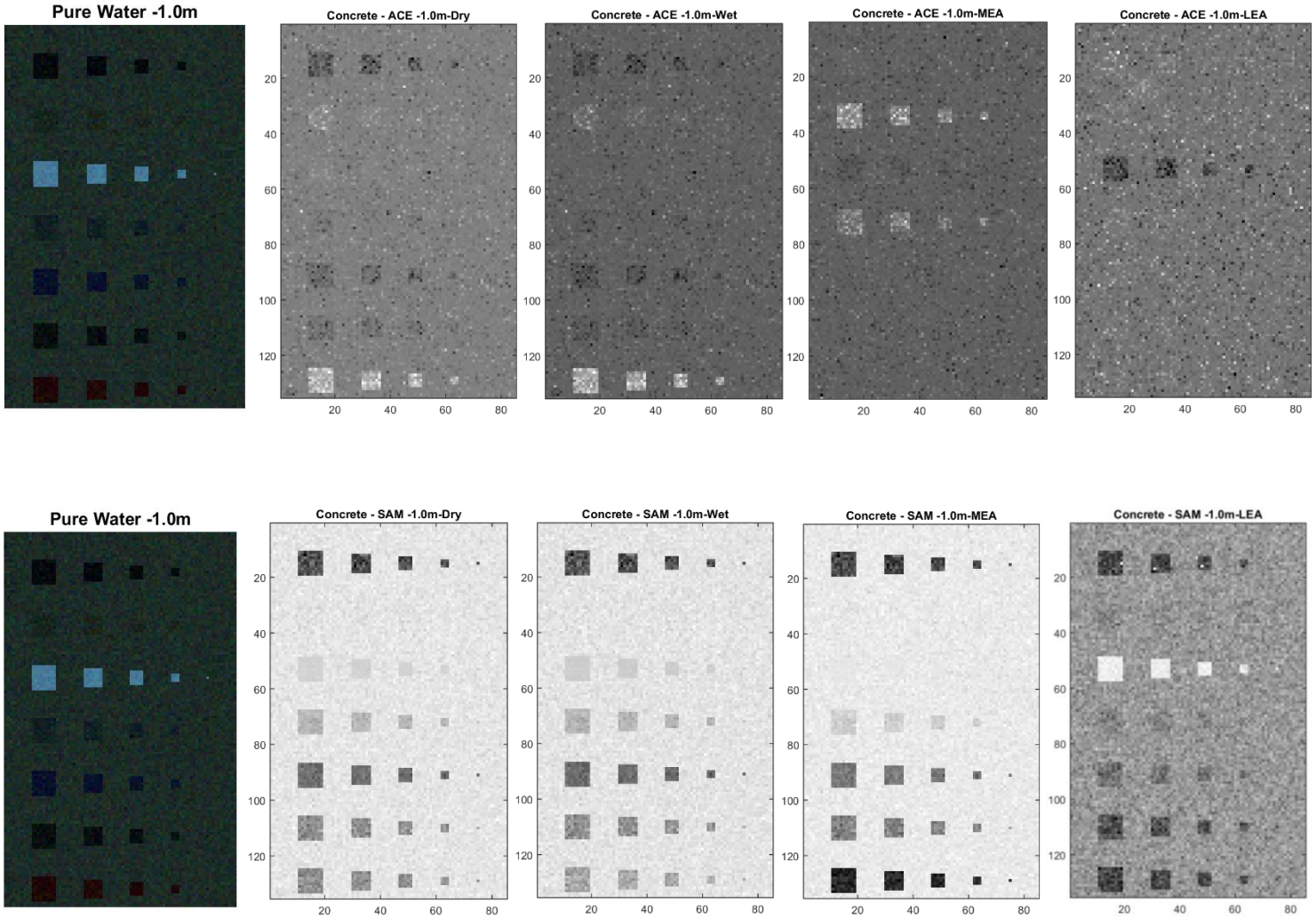

Figure 49: Detection Results of Concrete with Different Target Reflectance (1m depth)

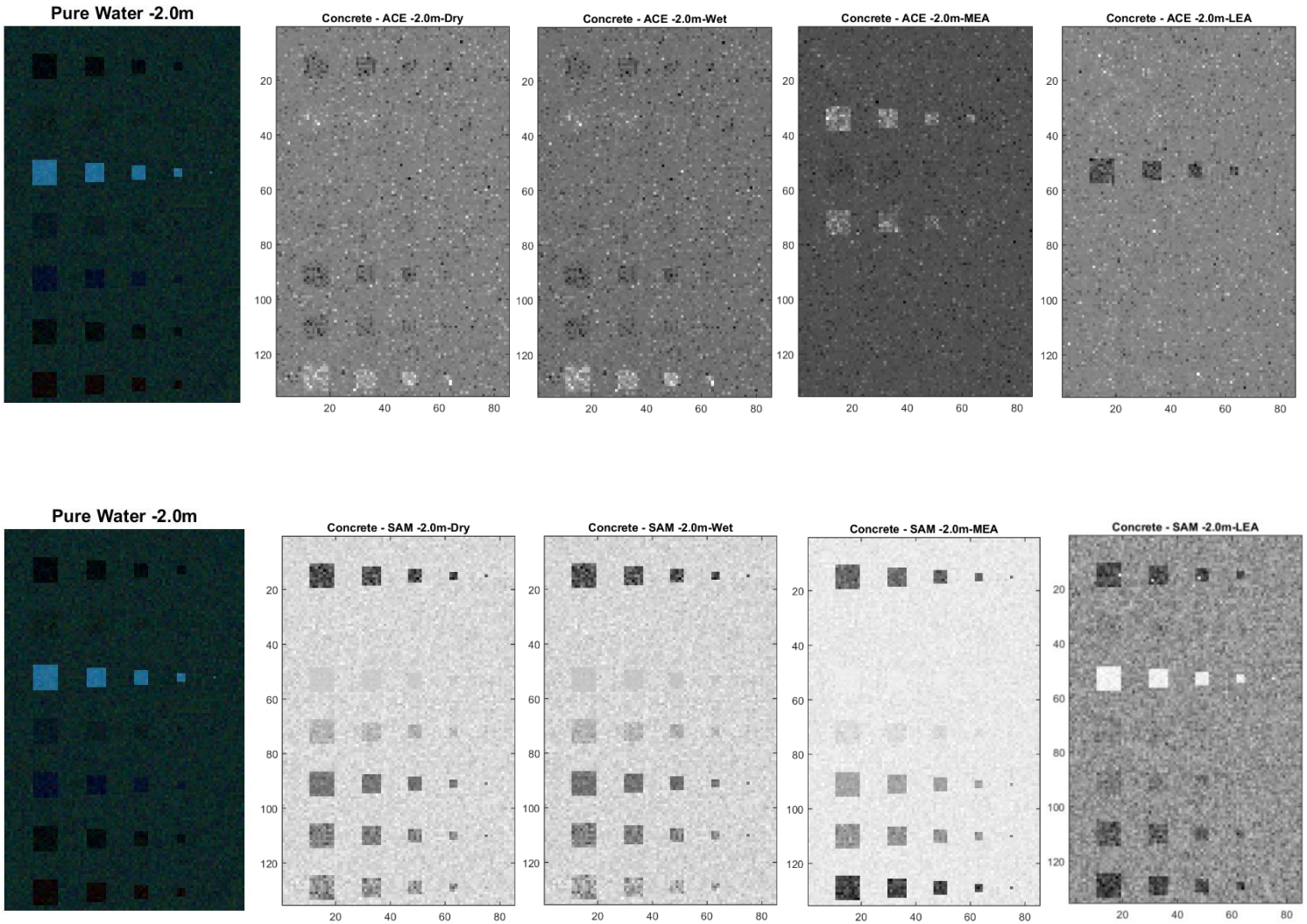

Figure 50: Detection Results of Concrete with Different Target Reflectance (2m depth)

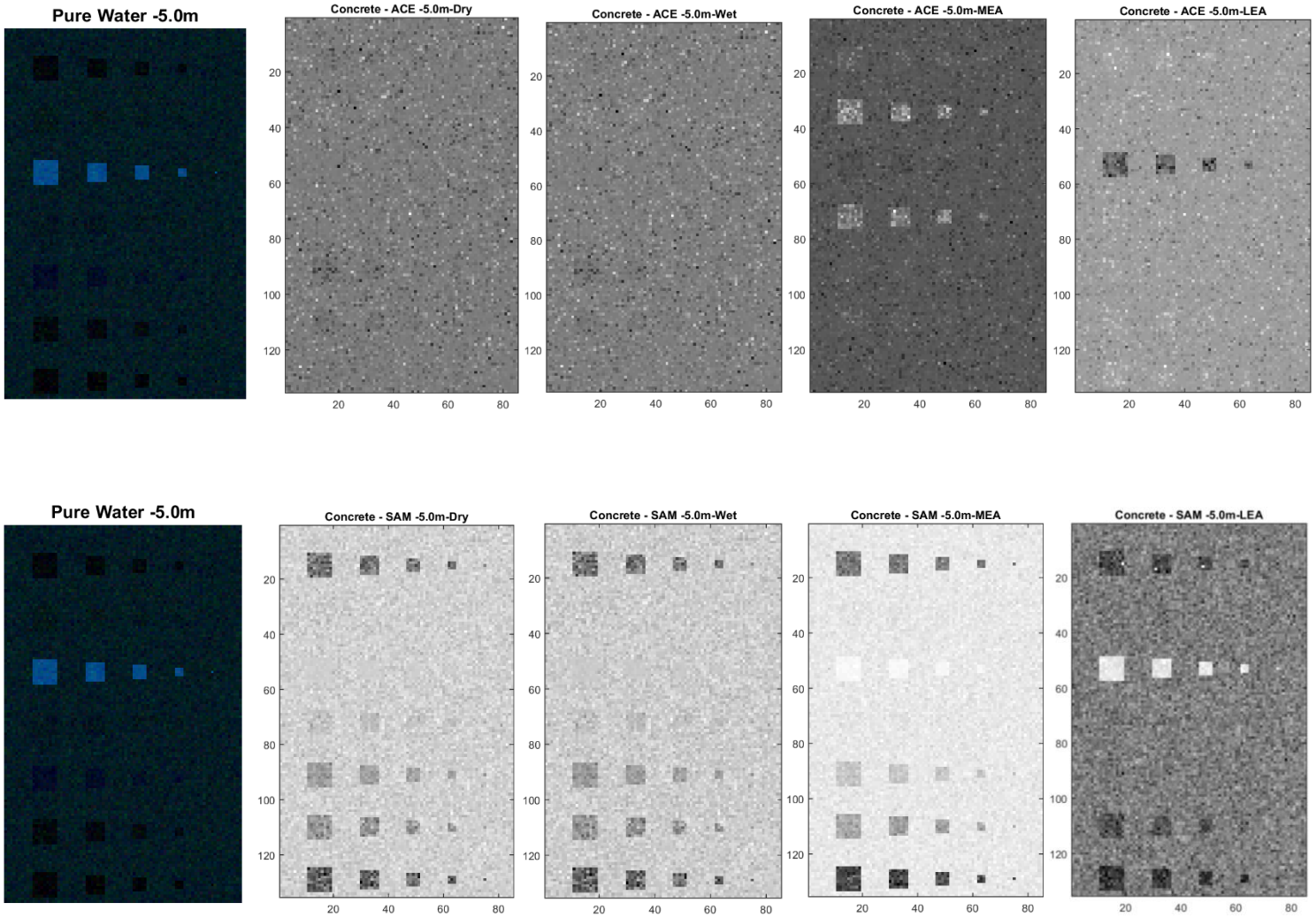

Figure 51: Detection Results of Concrete with Different Target Reflectance (5m depth)

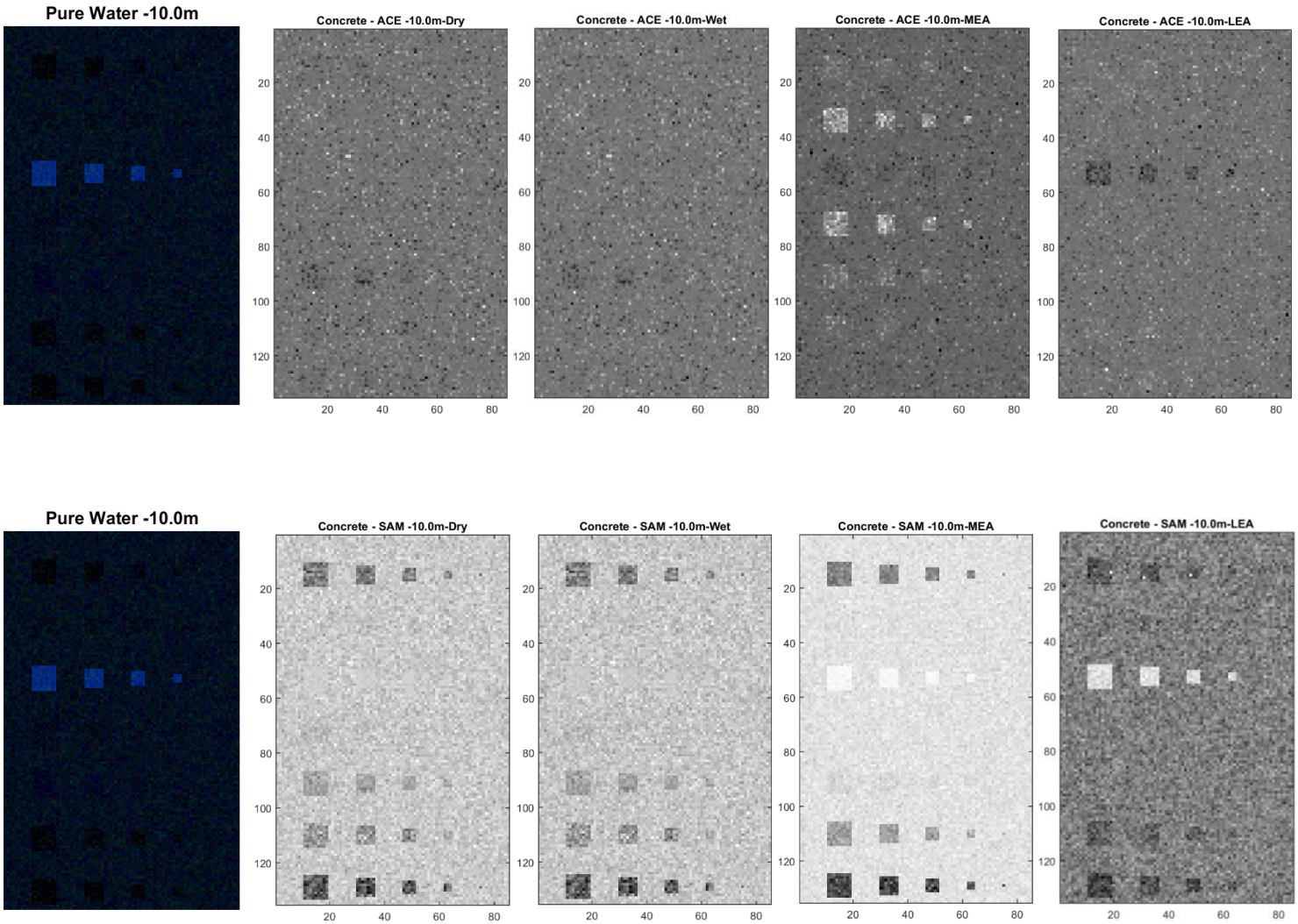

Figure 52: Detection Results of Concrete with Different Target Reflectance (10m depth)

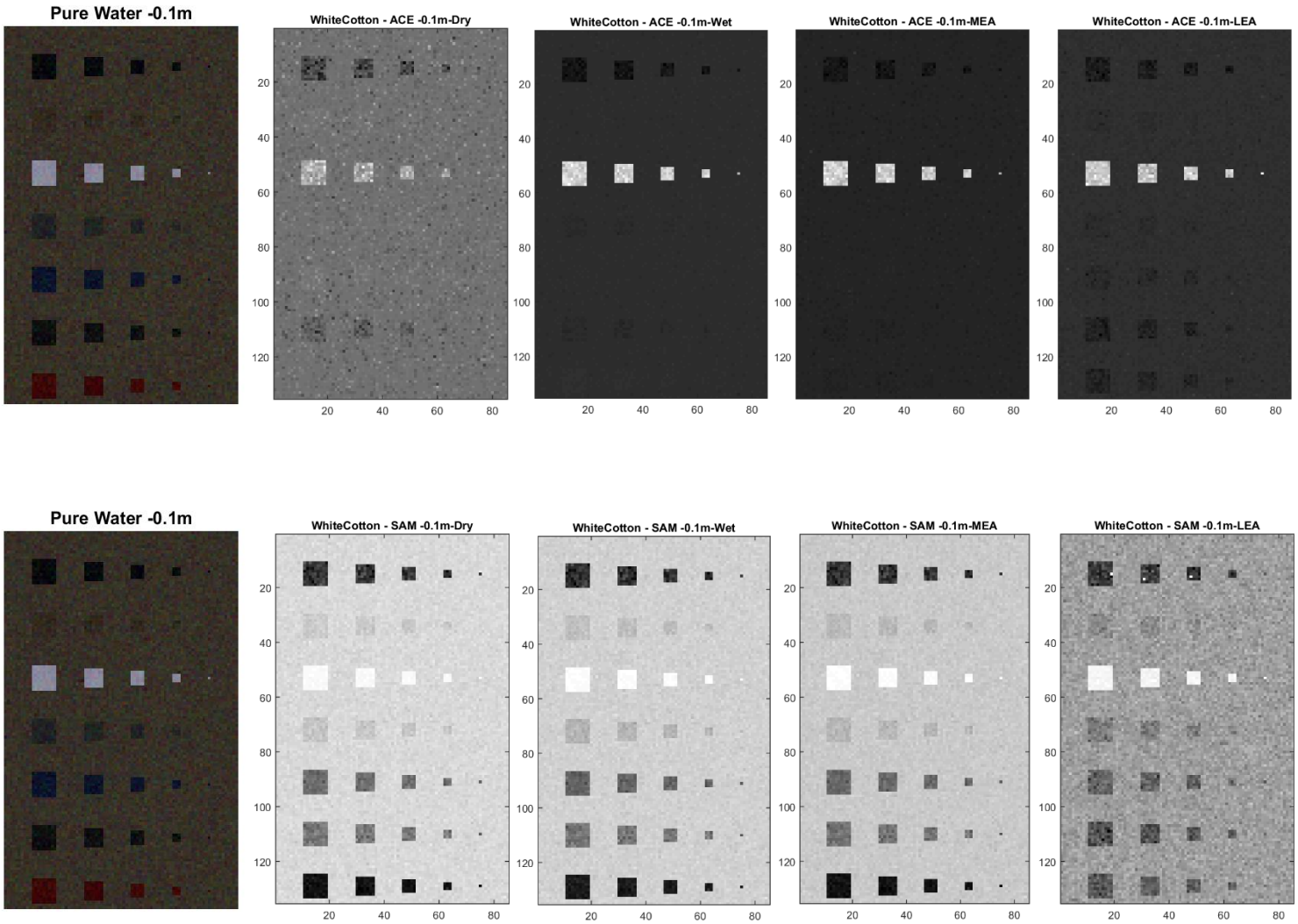

Figure 53: Detection Results of White Cotton Fabric with Different Target Reflectance (0.1m depth)

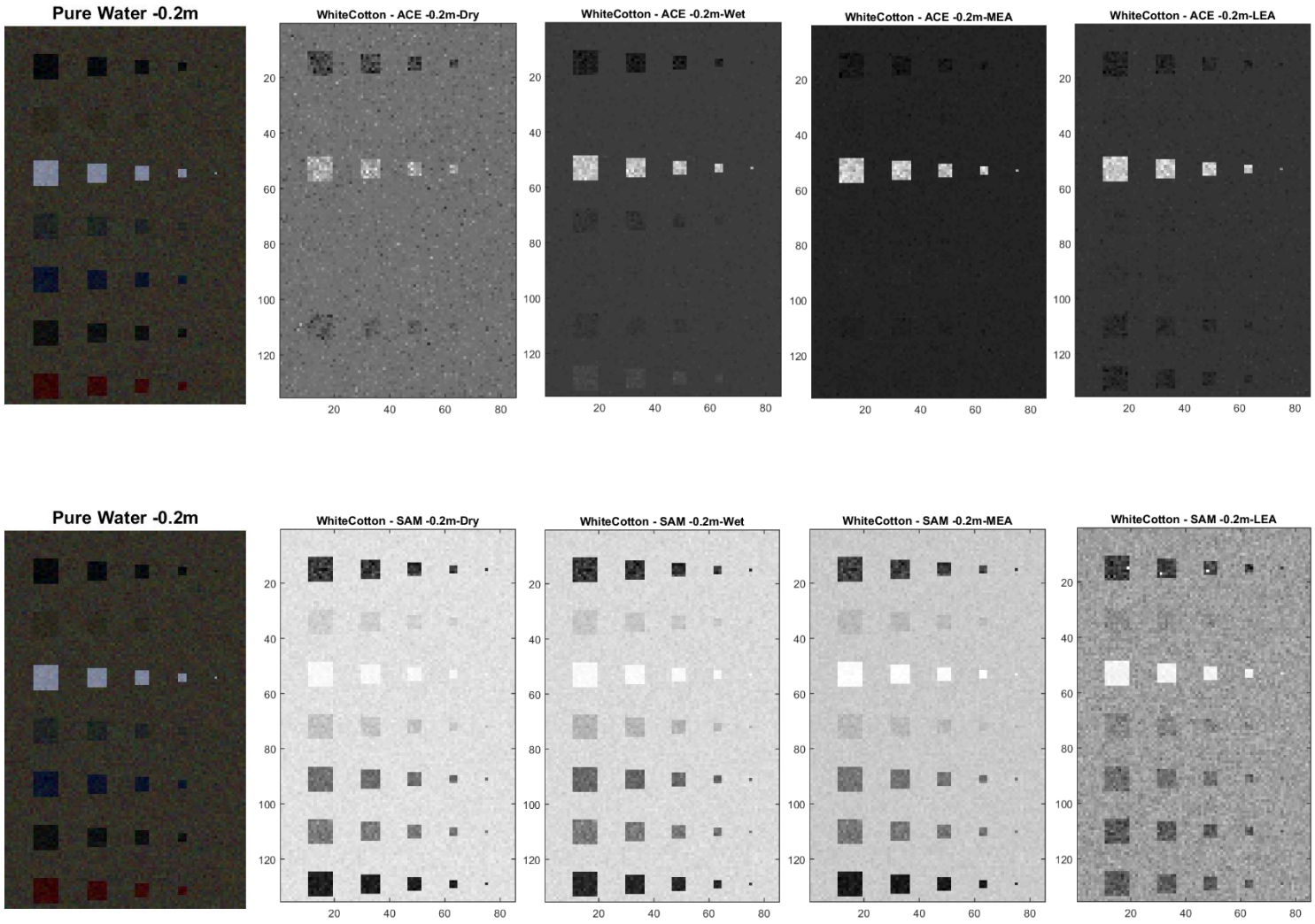

Figure 54: Detection Results of White Cotton Fabric with Different Target Reflectance (0.2m depth)

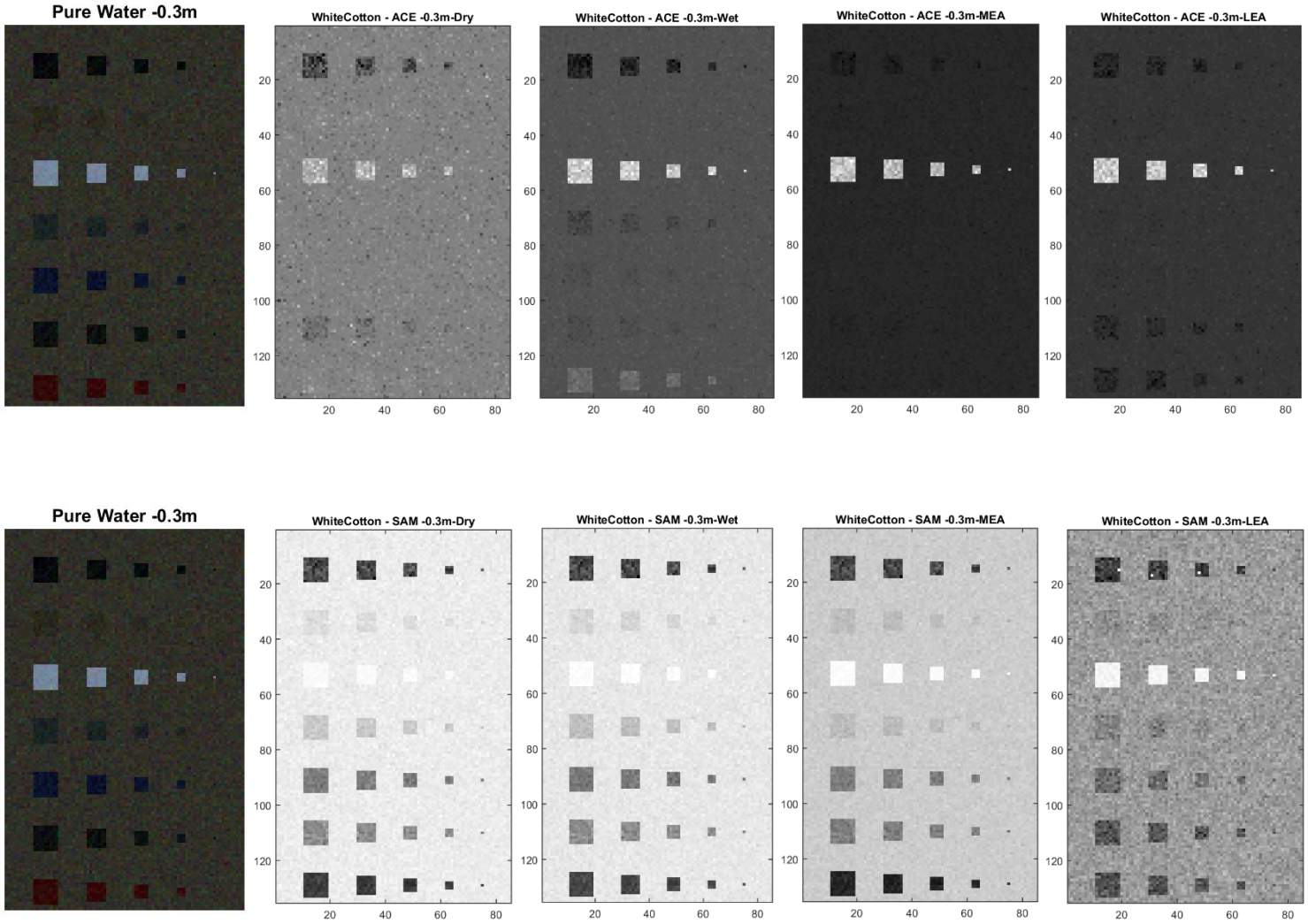

Figure 55: Detection Results of White Cotton Fabric with Different Target Reflectance (0.3m depth)

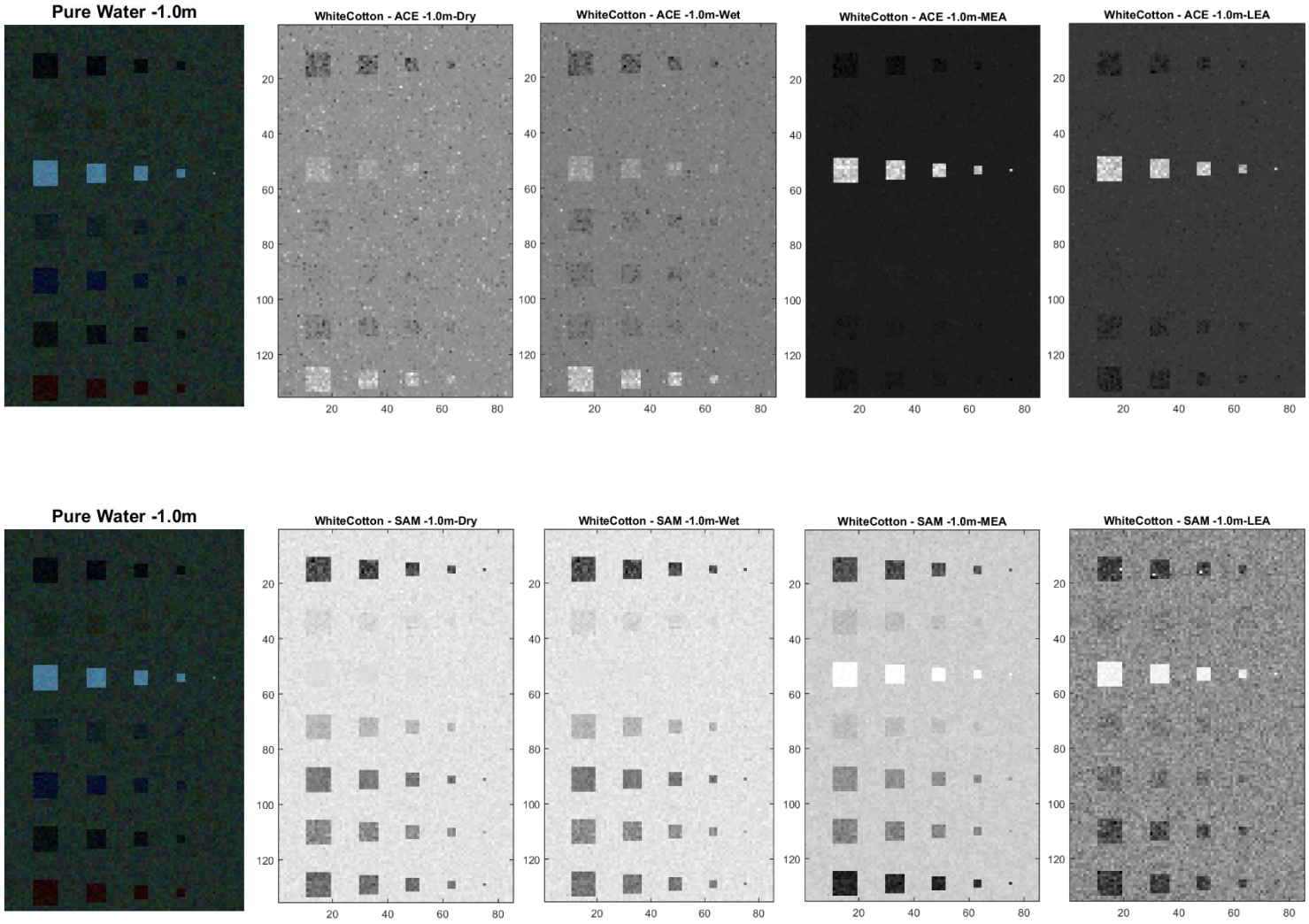

Figure 56: Detection Results of White Cotton Fabric with Different Target Reflectance (1m depth)

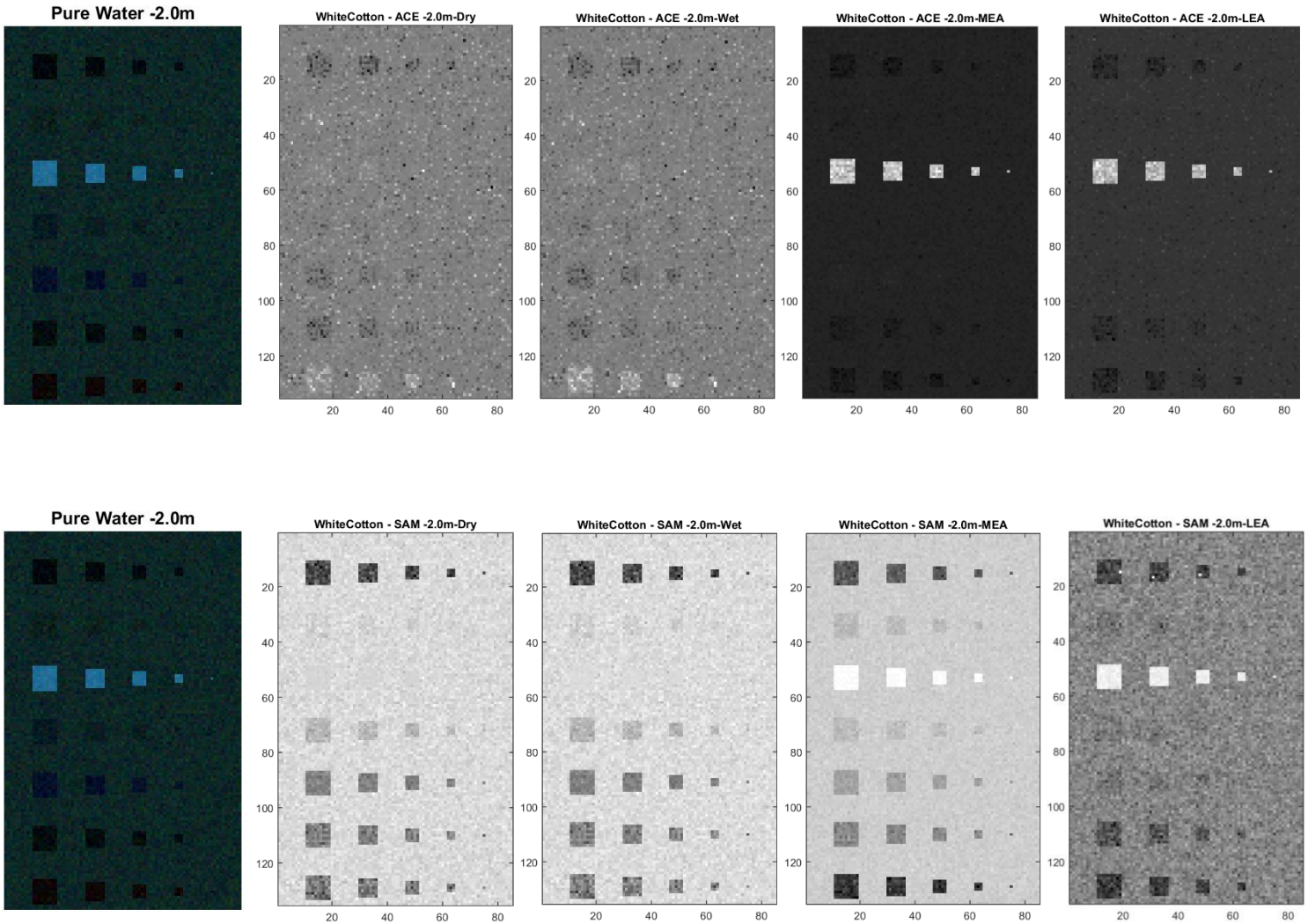

Figure 57: Detection Results of White Cotton Fabric with Different Target Reflectance (2m depth)

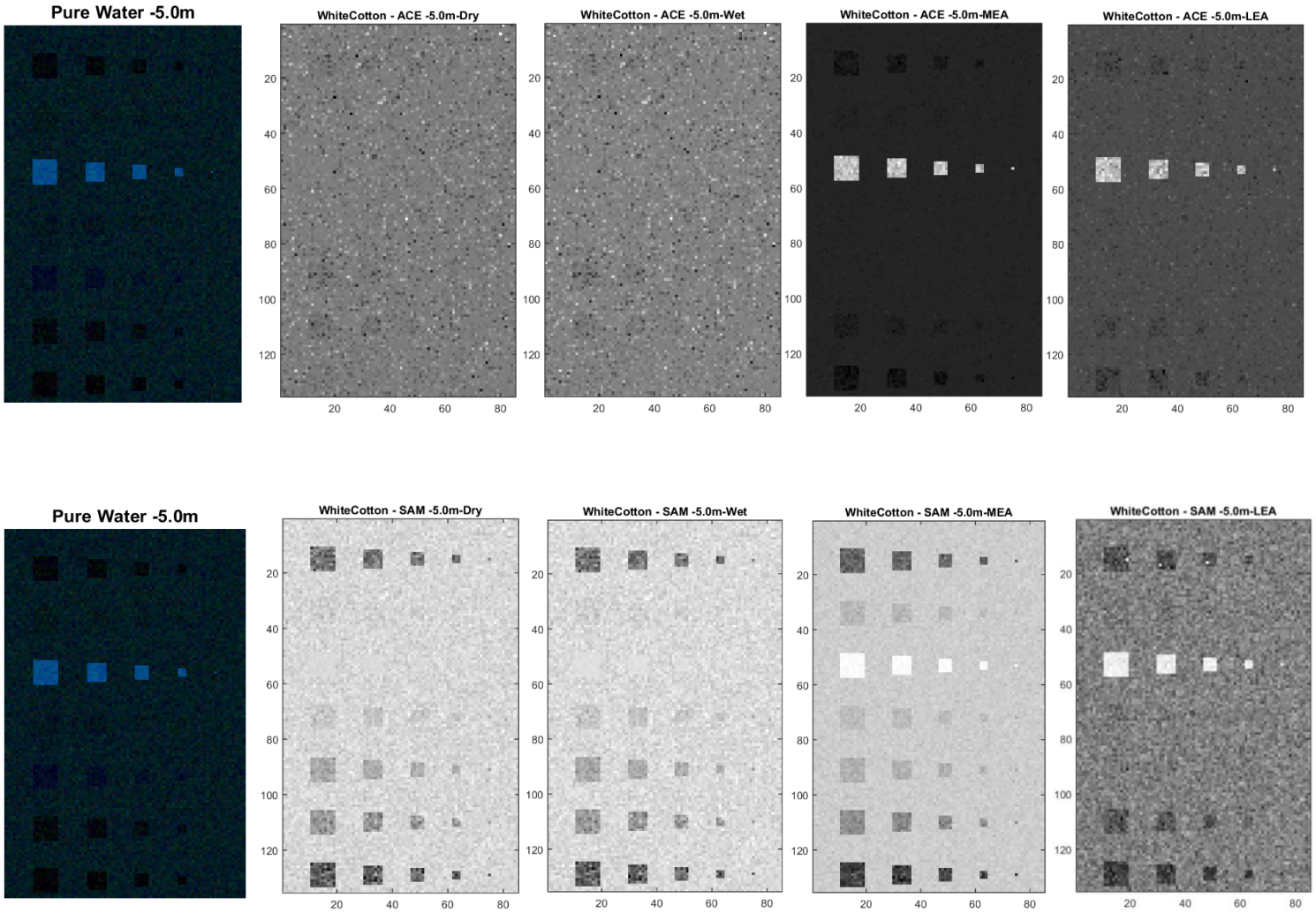

Figure 58: Detection Results of White Cotton Fabric with Different Target Reflectance (5m depth)

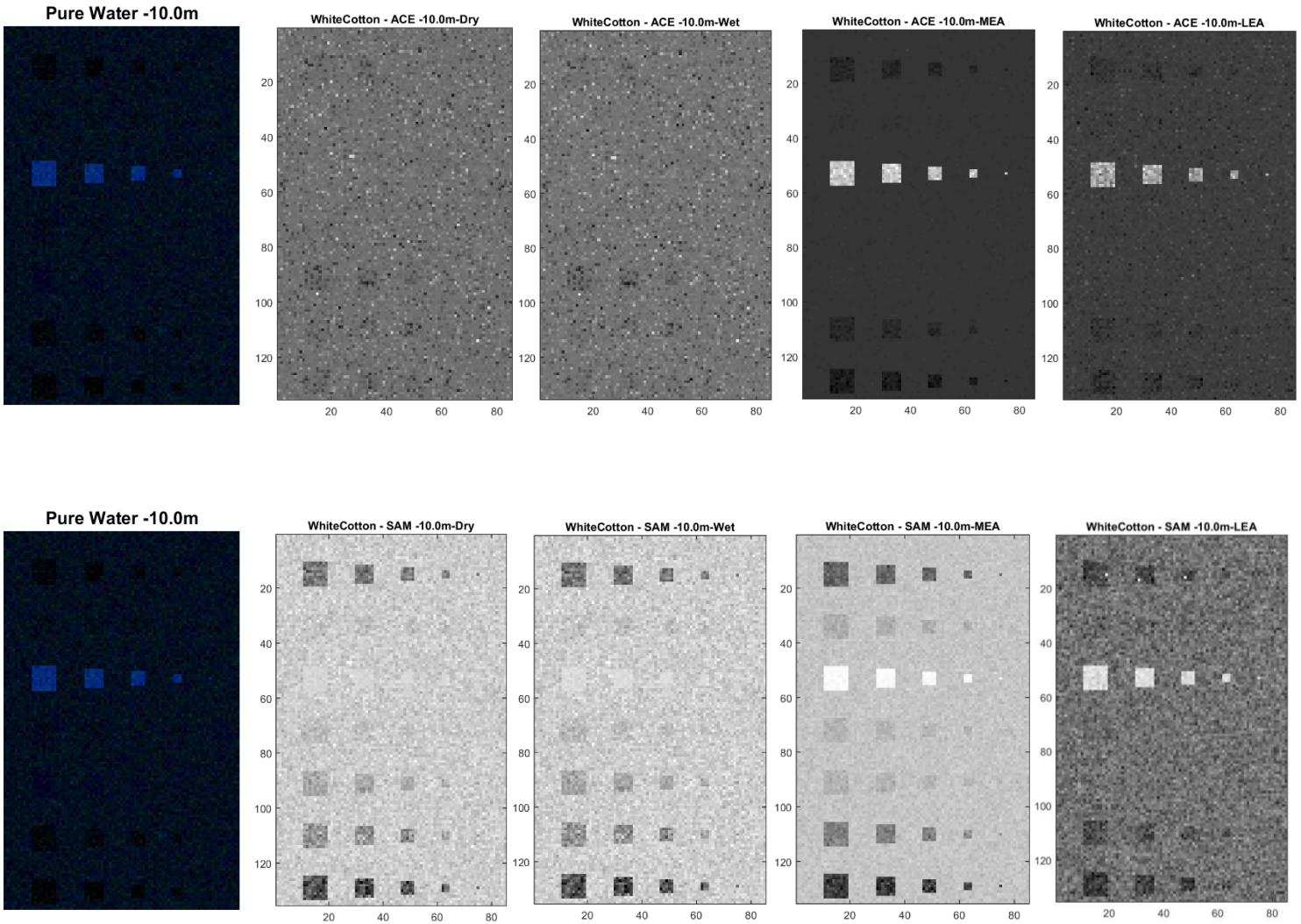

Figure 59: Detection Results of White Cotton Fabric with Different Target Reflectance (10m depth)

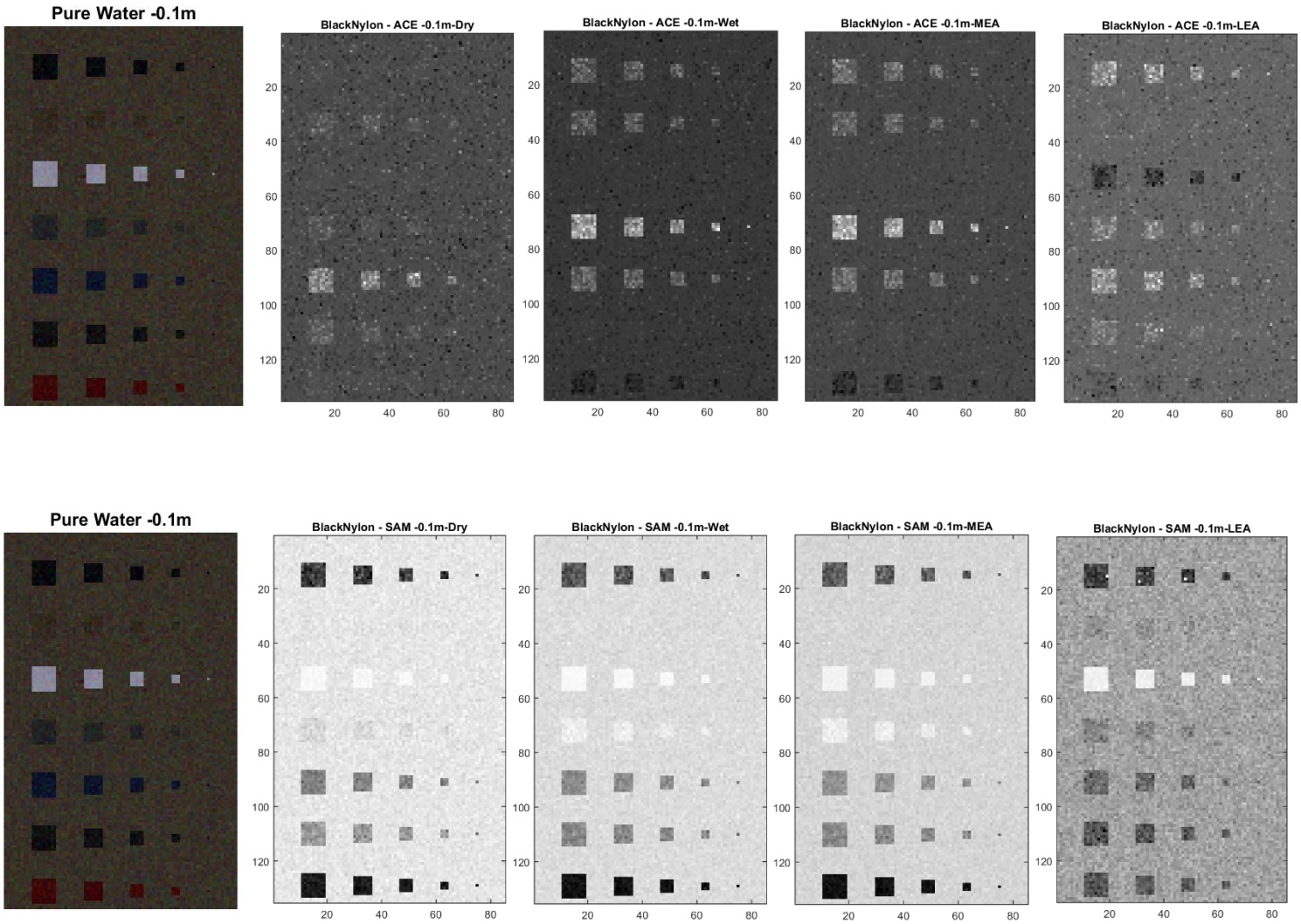

Figure 60: Detection Results of Black Nylon Fabric with Different Target Reflectance (0.1m depth)

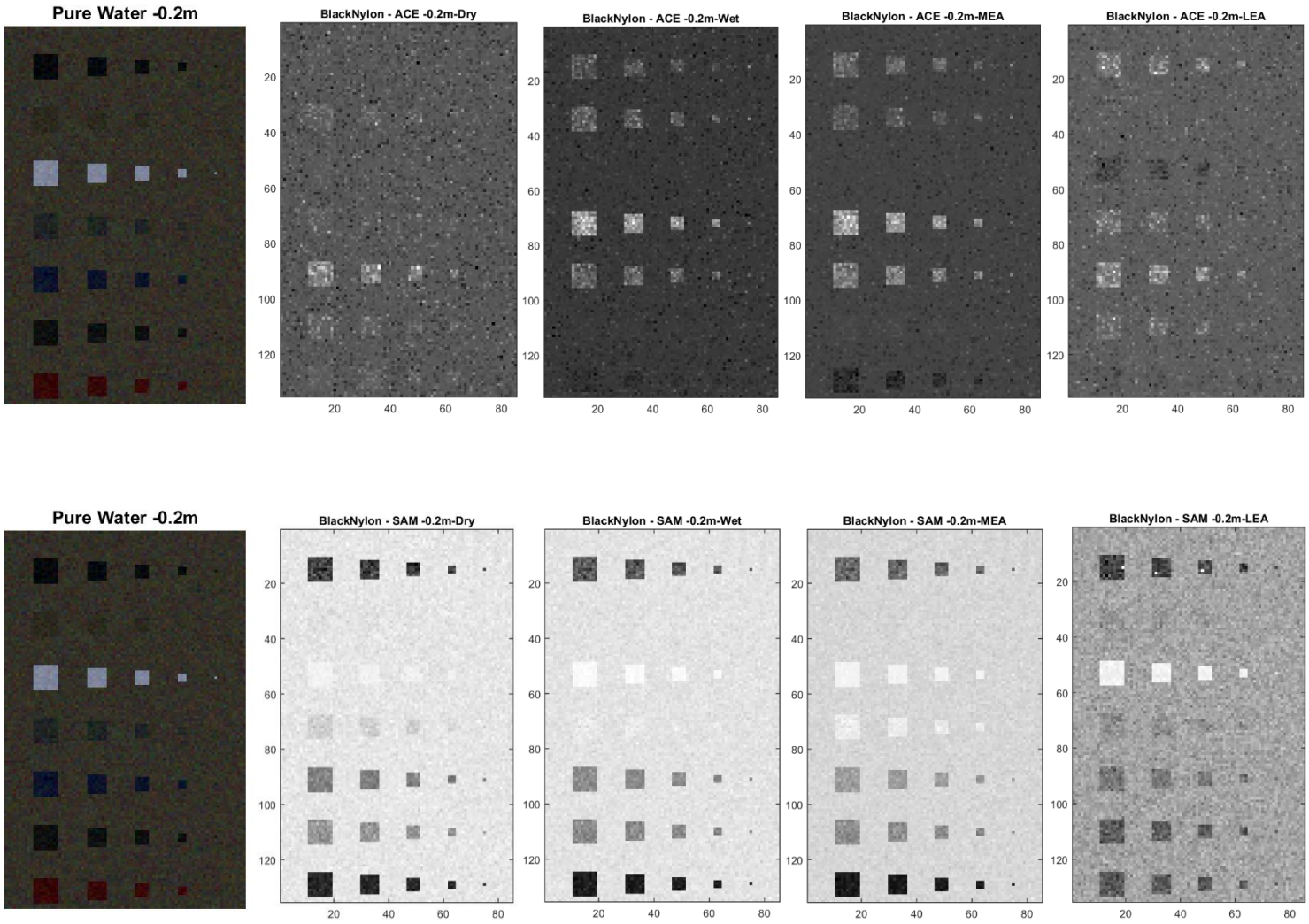

Figure 61: Detection Results of Black Nylon Fabric with Different Target Reflectance (0.2m depth)

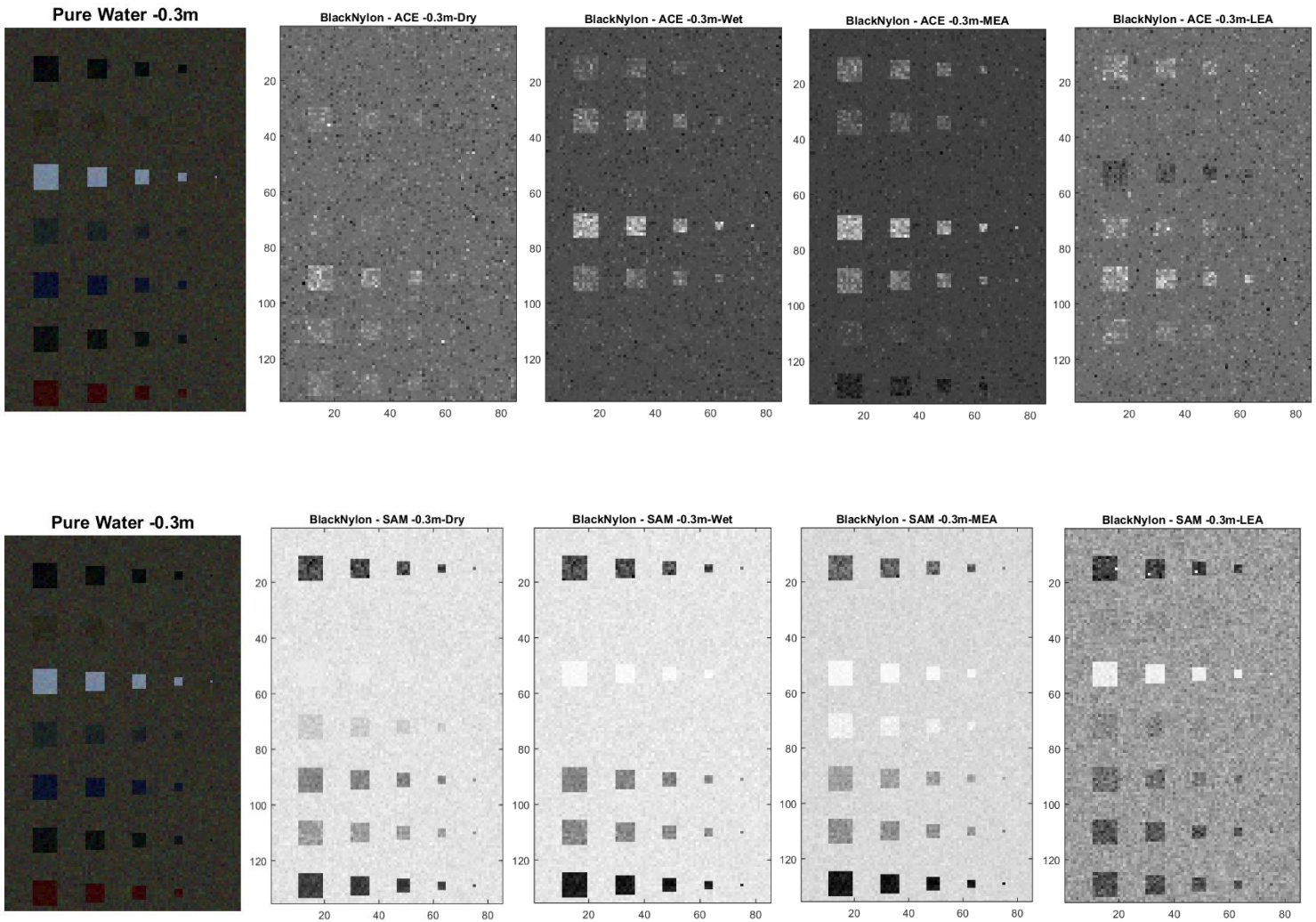

Figure 62: Detection Results of Black Nylon Fabric with Different Target Reflectance (0.3m depth)

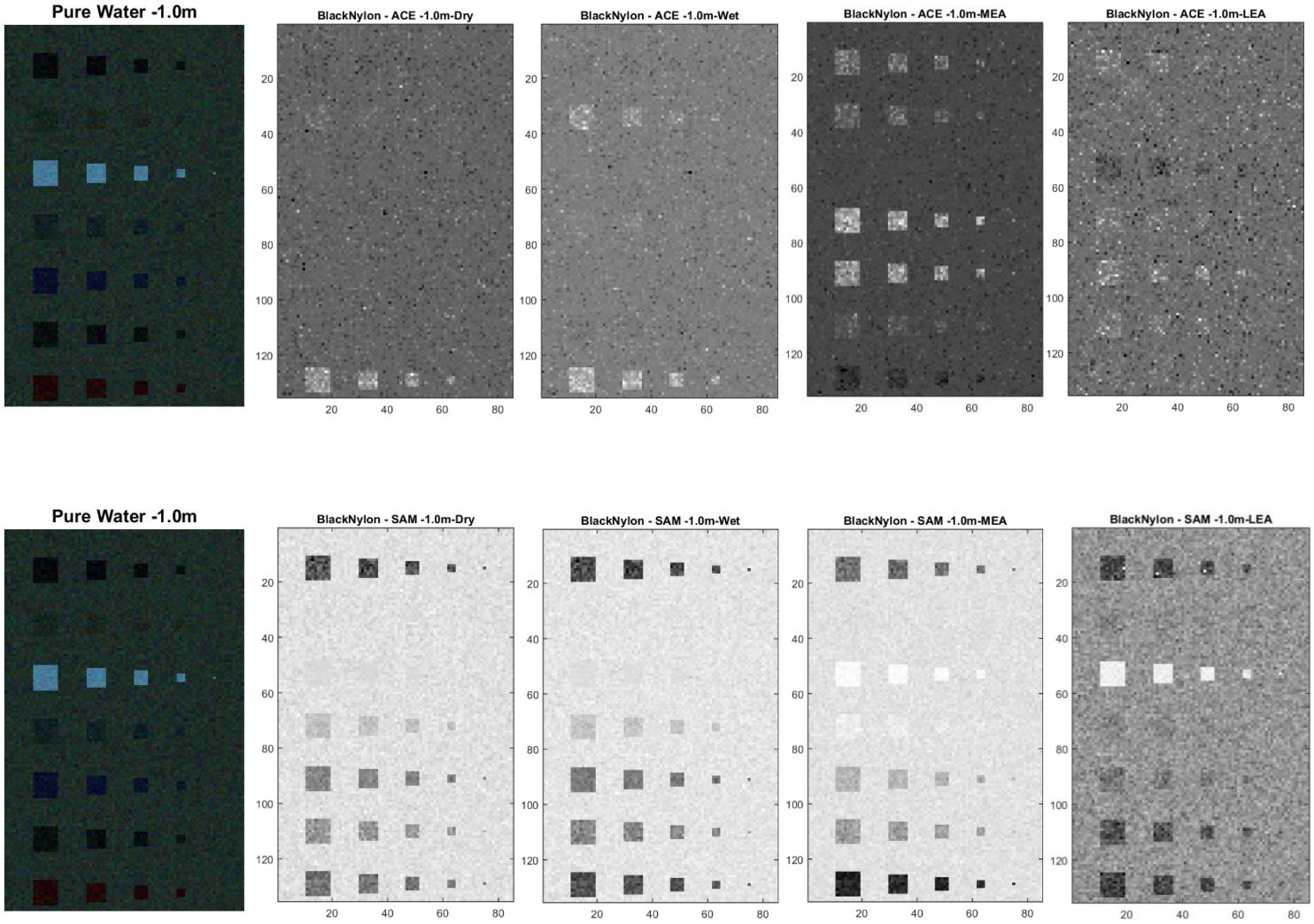

Figure 63: Detection Results of Black Nylon Fabric with Different Target Reflectance (1m depth)

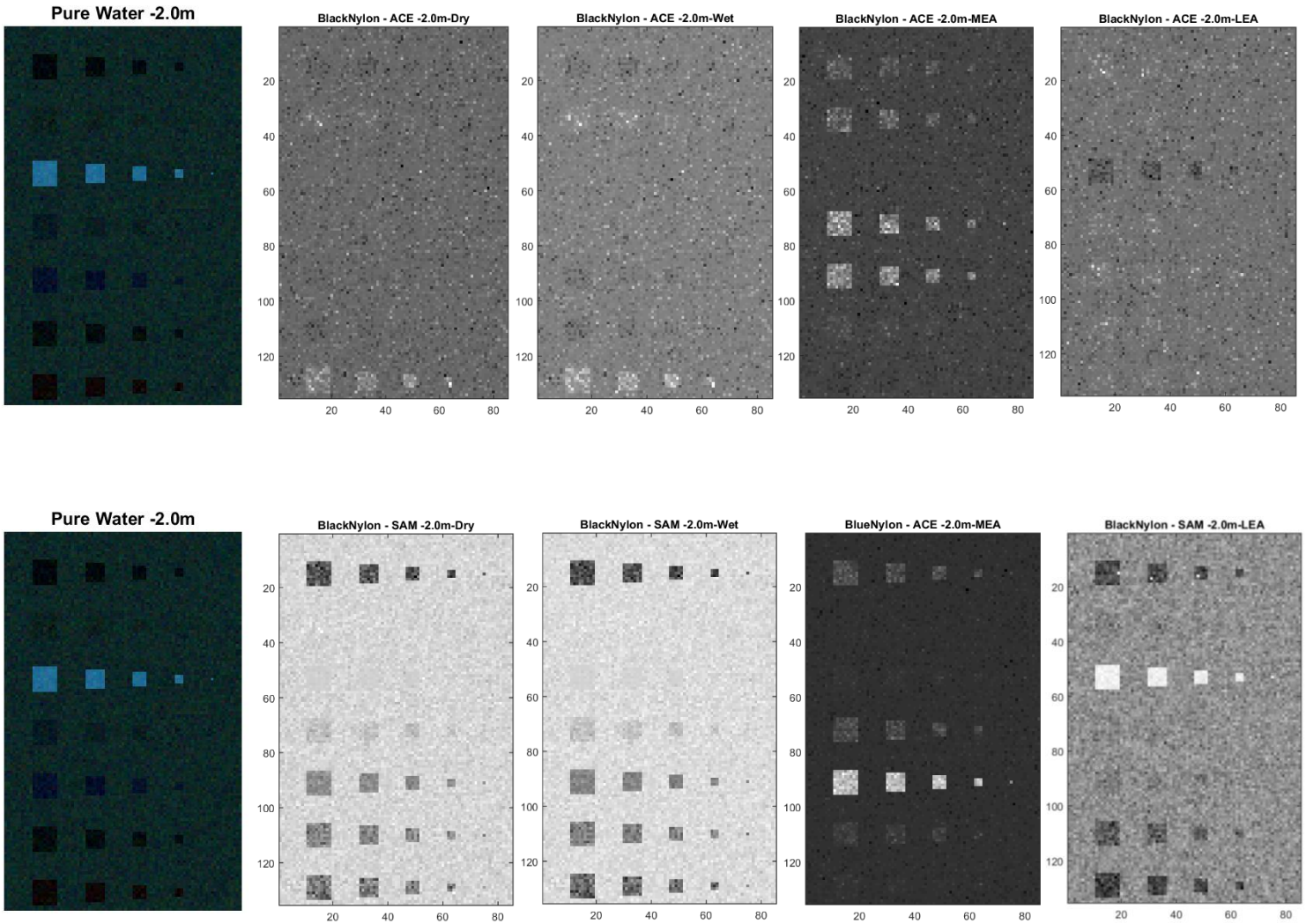

Figure 64: Detection Results of Black Nylon Fabric with Different Target Reflectance (2m depth)

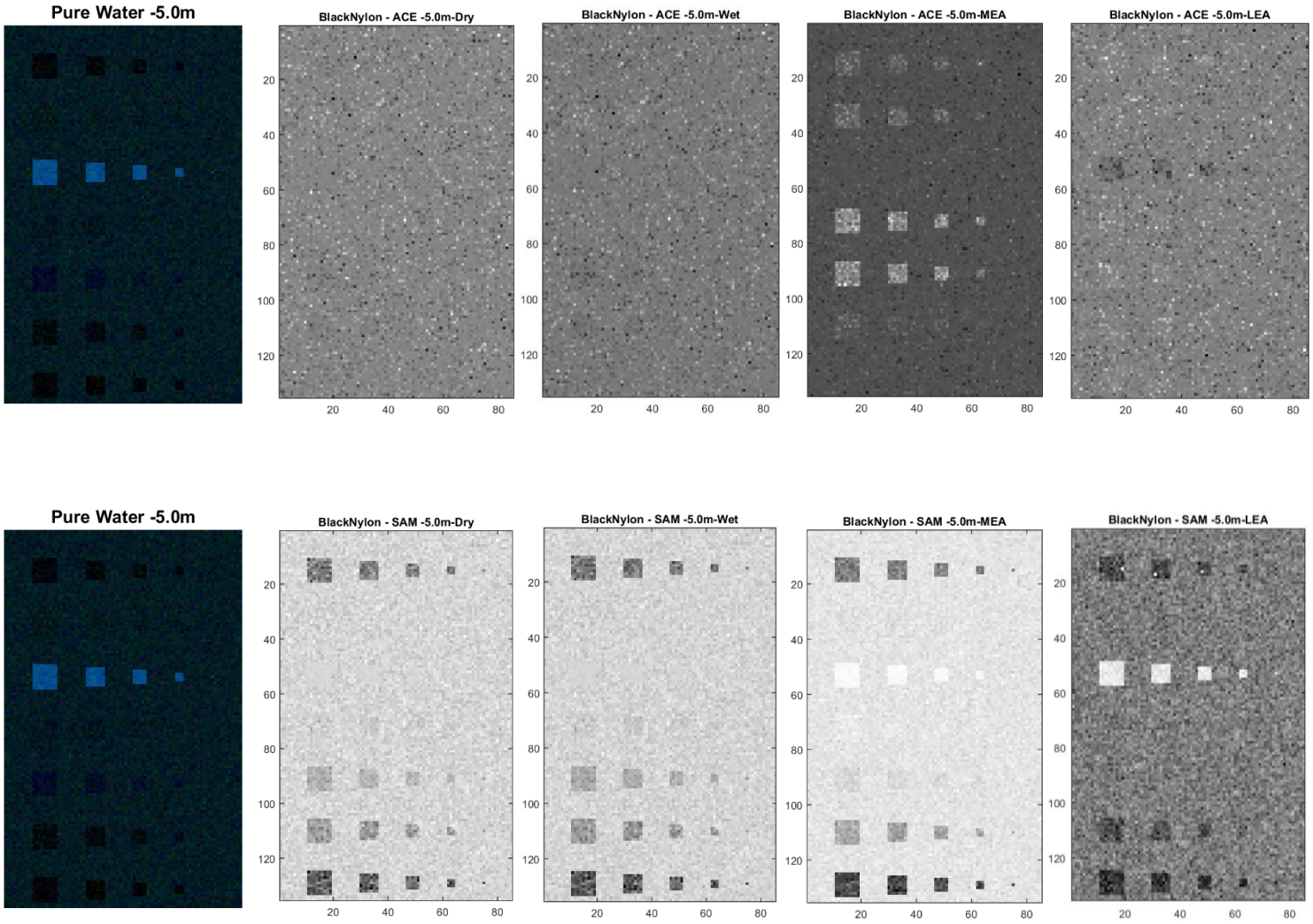

Figure 65: Detection Results of Black Nylon Fabric with Different Target Reflectance (5m depth)

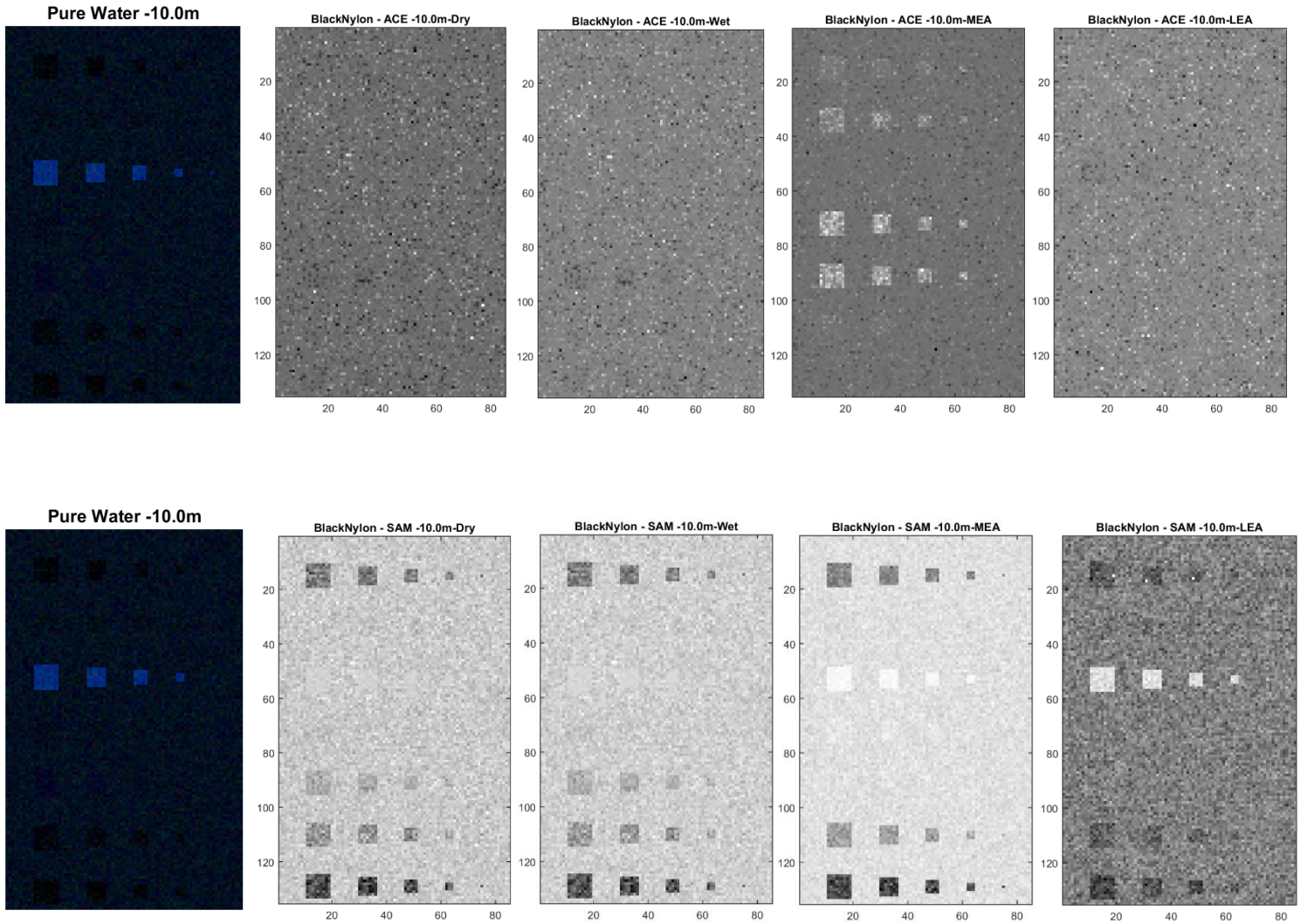

Figure 66: Detection Results of Black Nylon Fabric with Different Target Reflectance (10m depth)

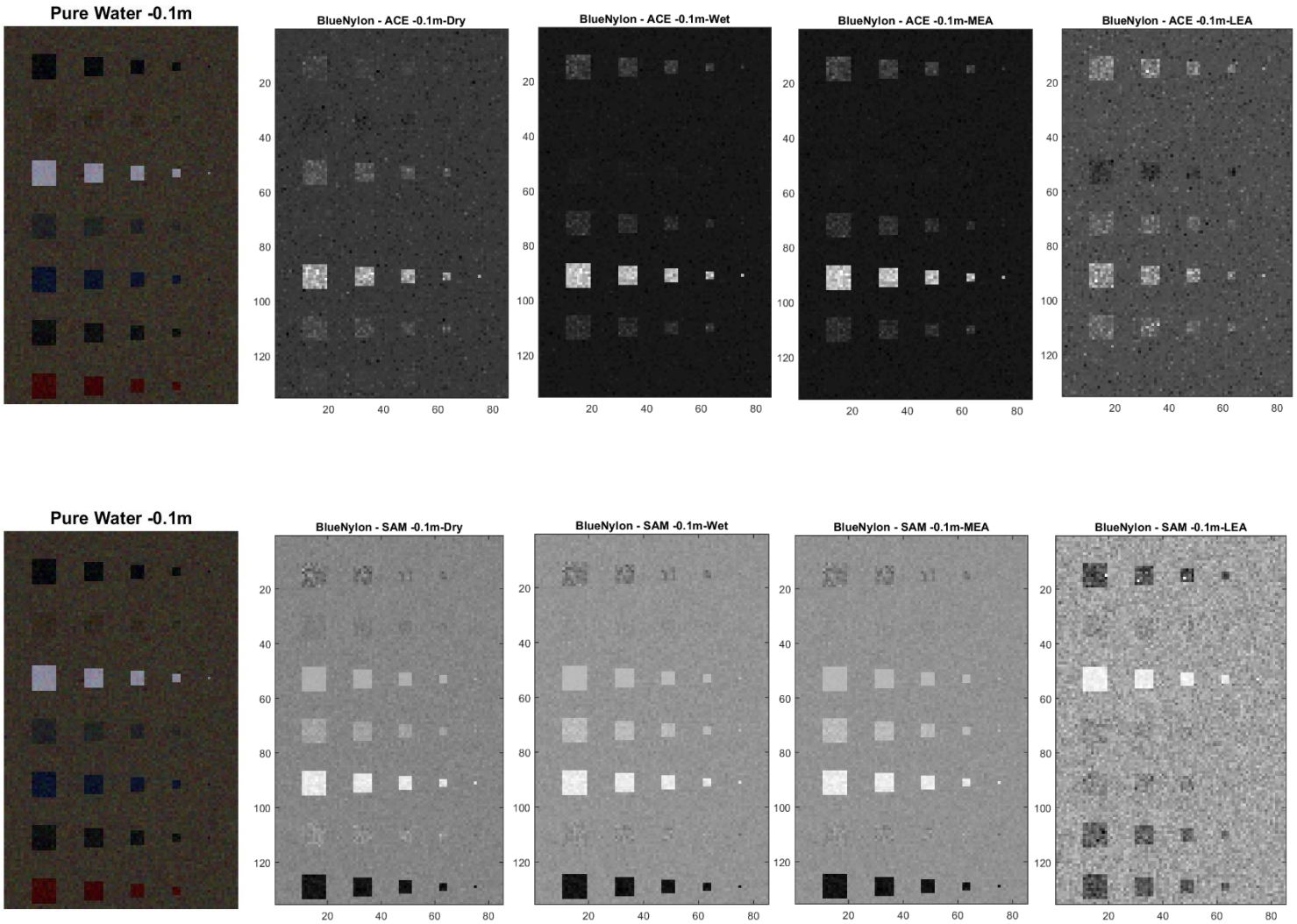

Figure 67: Detection Results of Blue Nylon Fabric with Different Target Reflectance (0.1m depth)

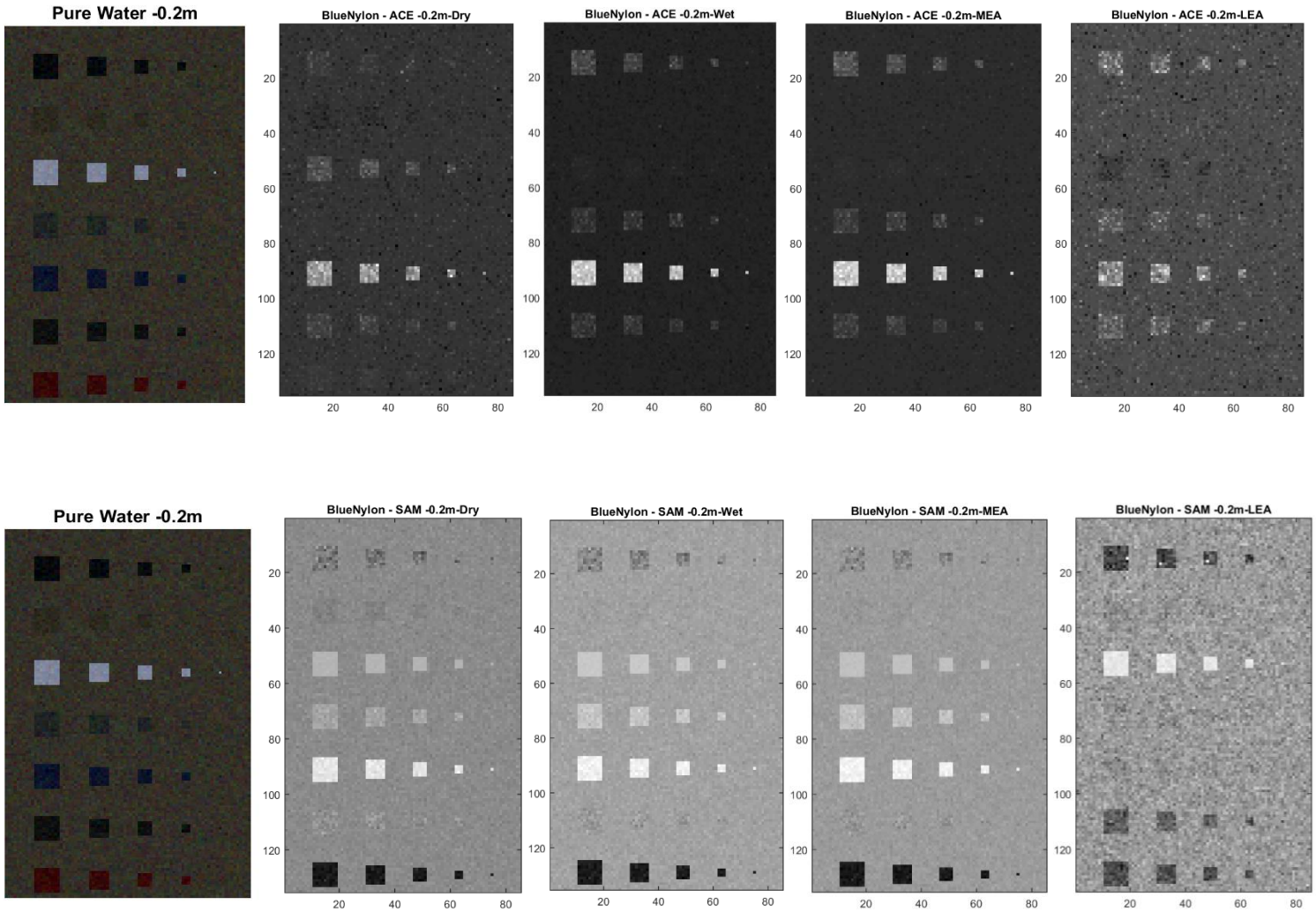

Figure 68: Detection Results of Blue Nylon Fabric with Different Target Reflectance (0.2m depth)

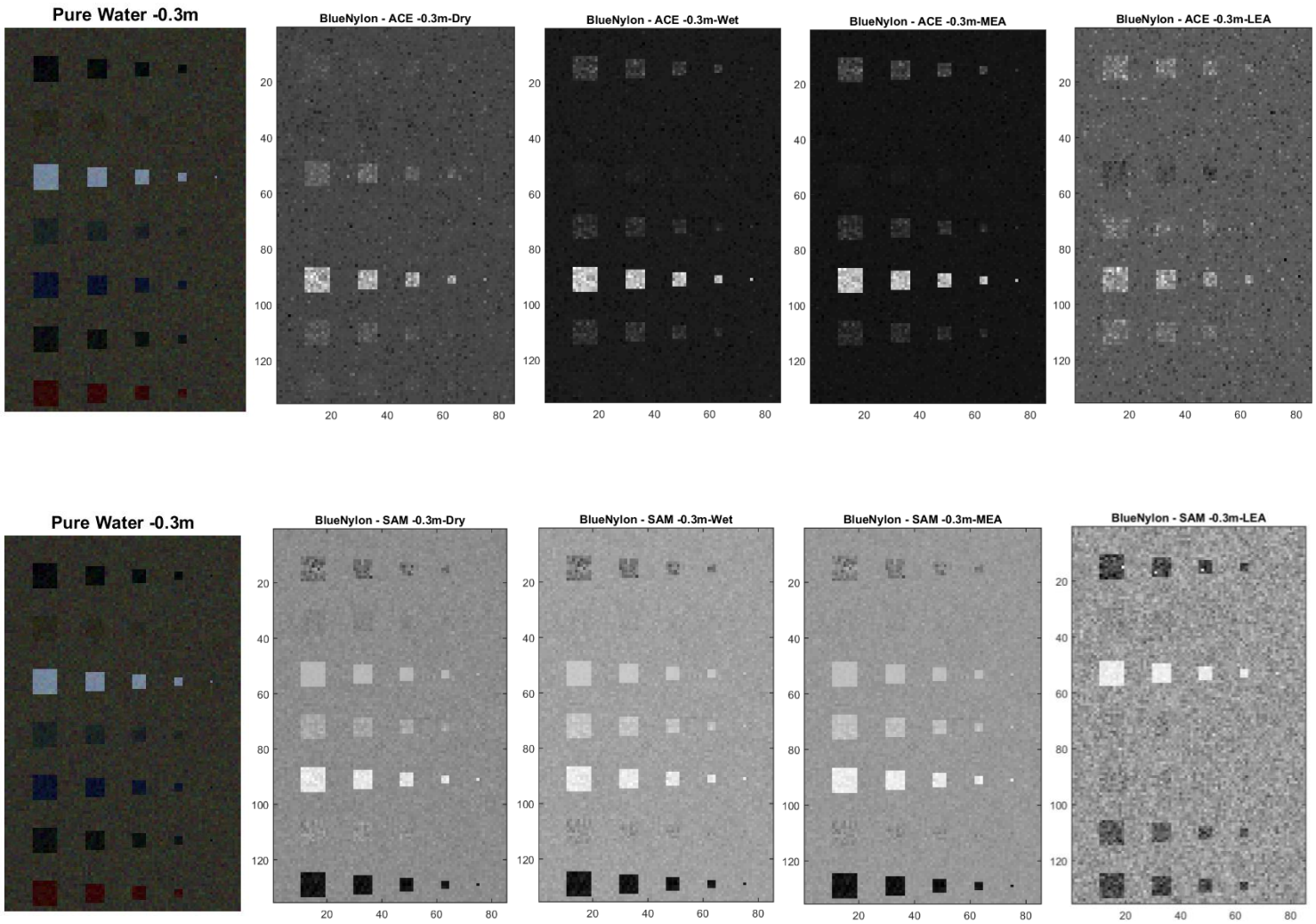

Figure 69: Detection Results of Blue Nylon Fabric with Different Target Reflectance (0.3m depth)

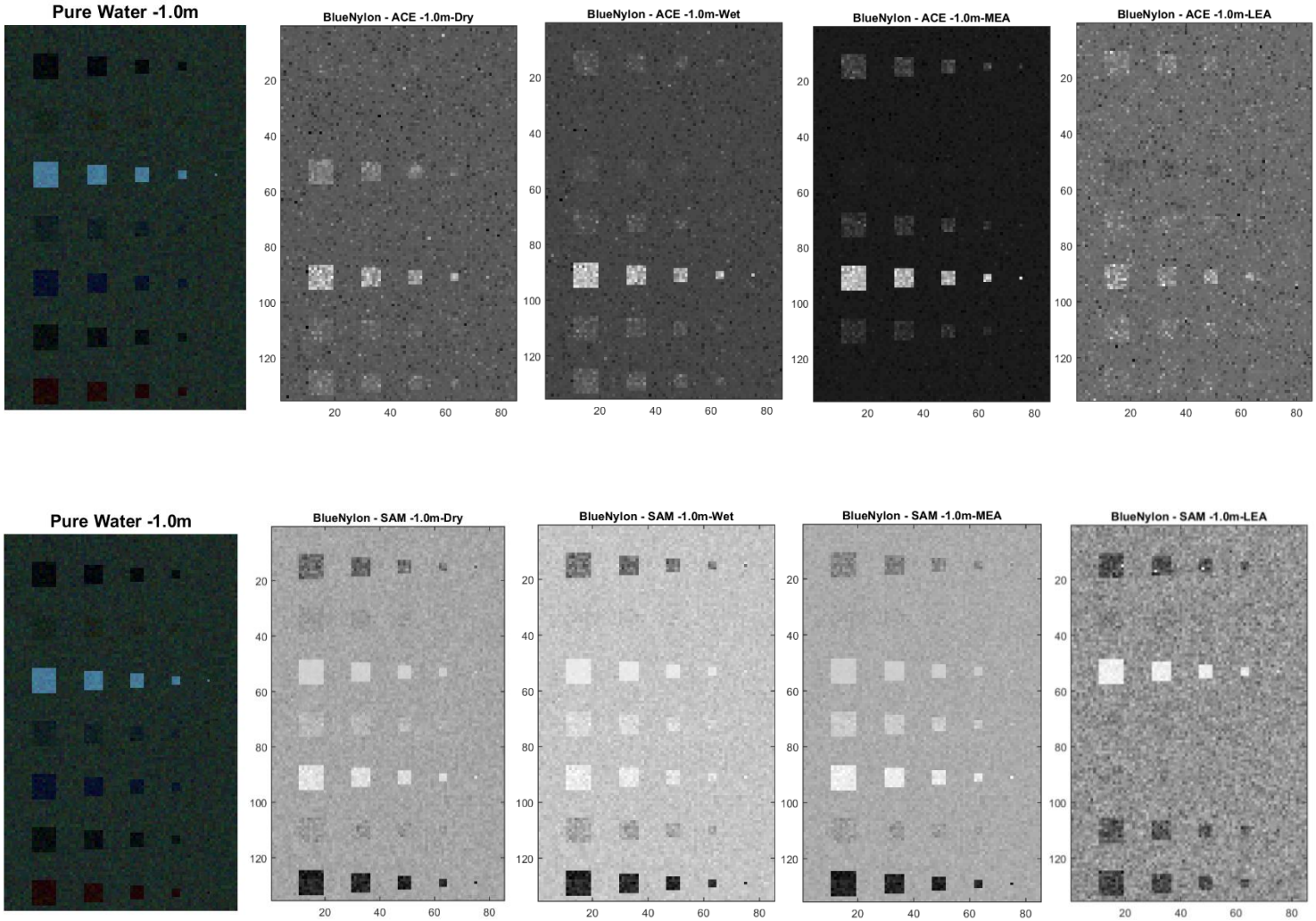

Figure 70: Detection Results of Blue Nylon Fabric with Different Target Reflectance (1m depth)

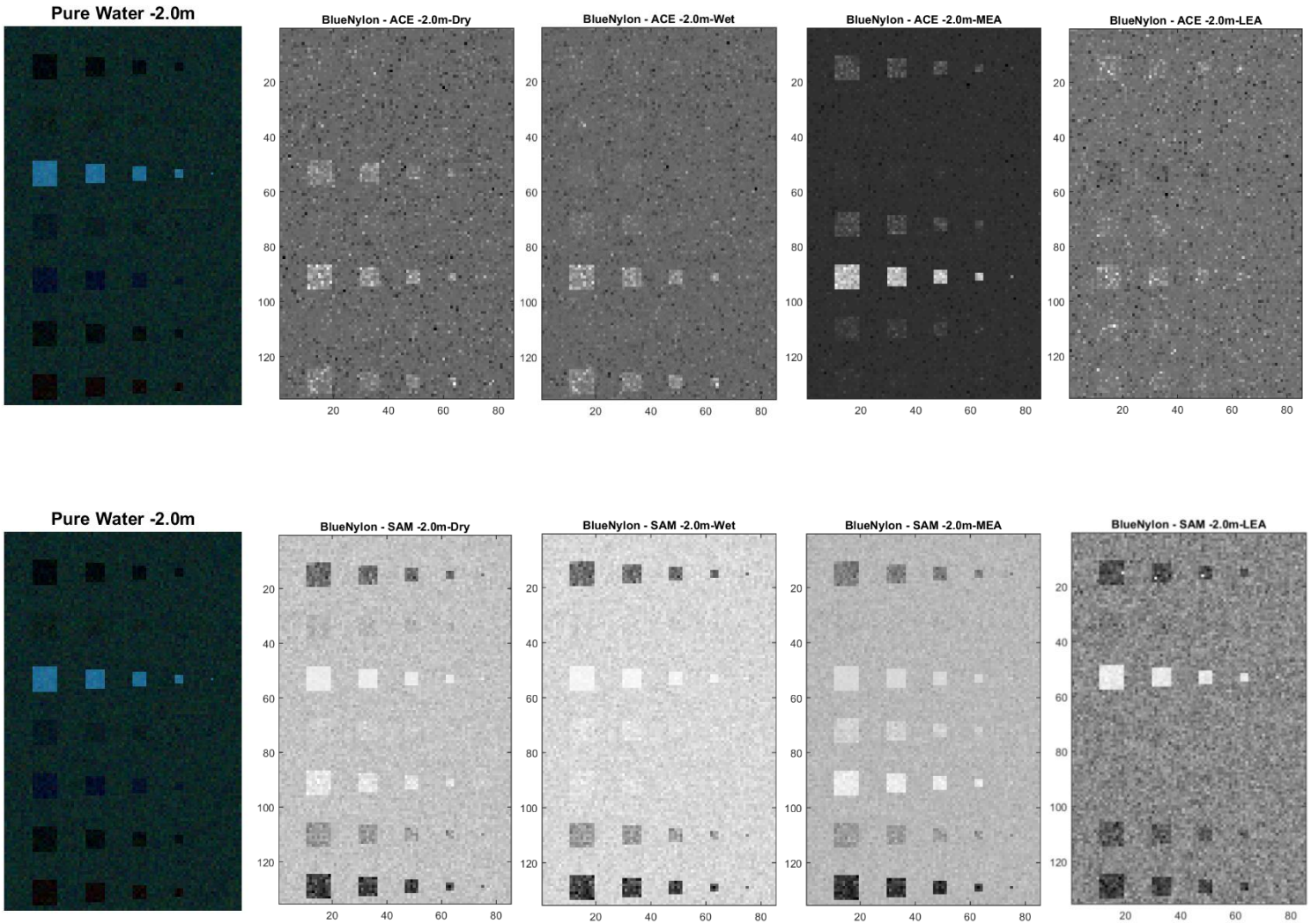

Figure 71: Detection Results of Blue Nylon Fabric with Different Target Reflectance (2m depth)

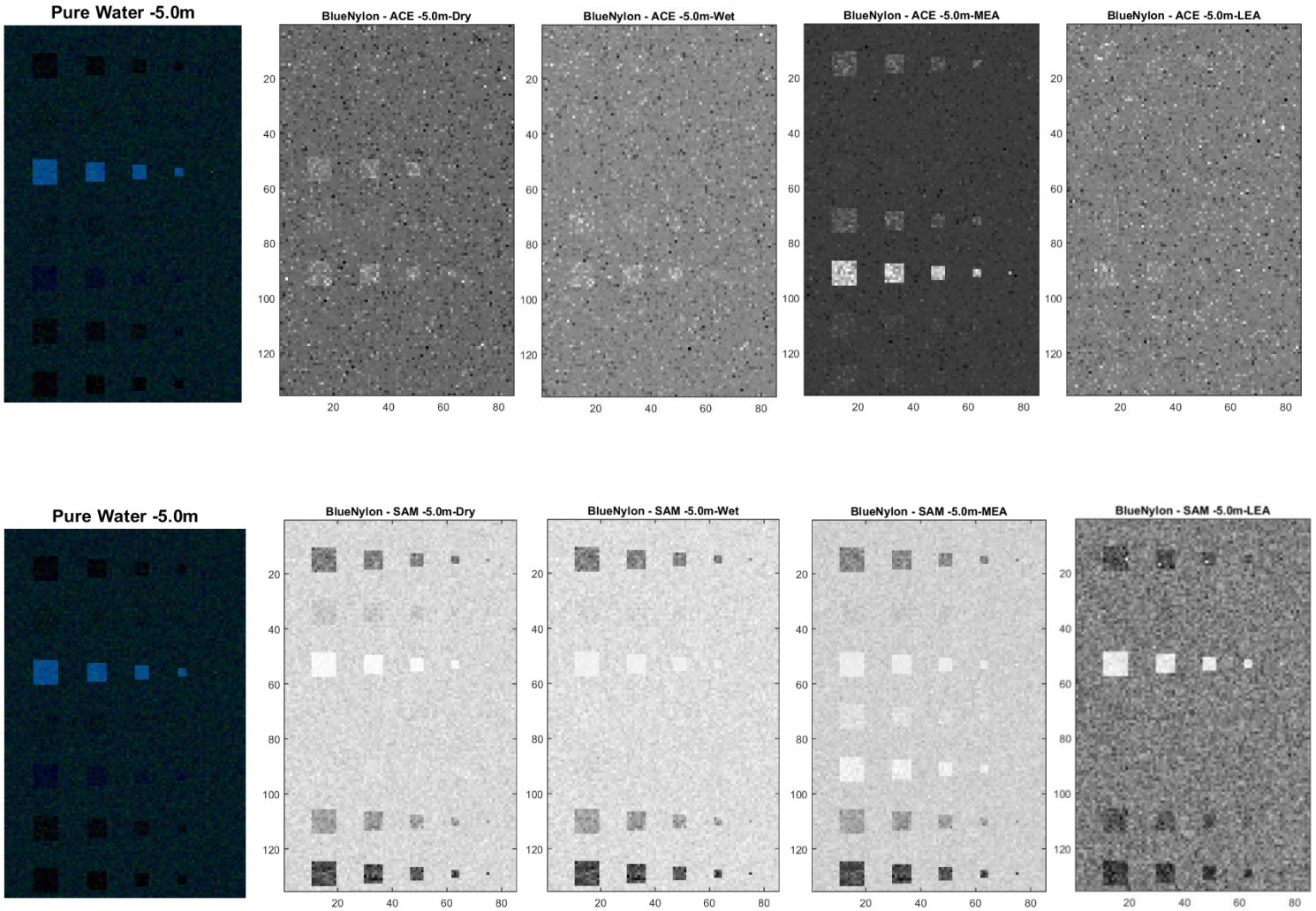

Figure 72: Detection Results of Blue Nylon Fabric with Different Target Reflectance (5m depth)

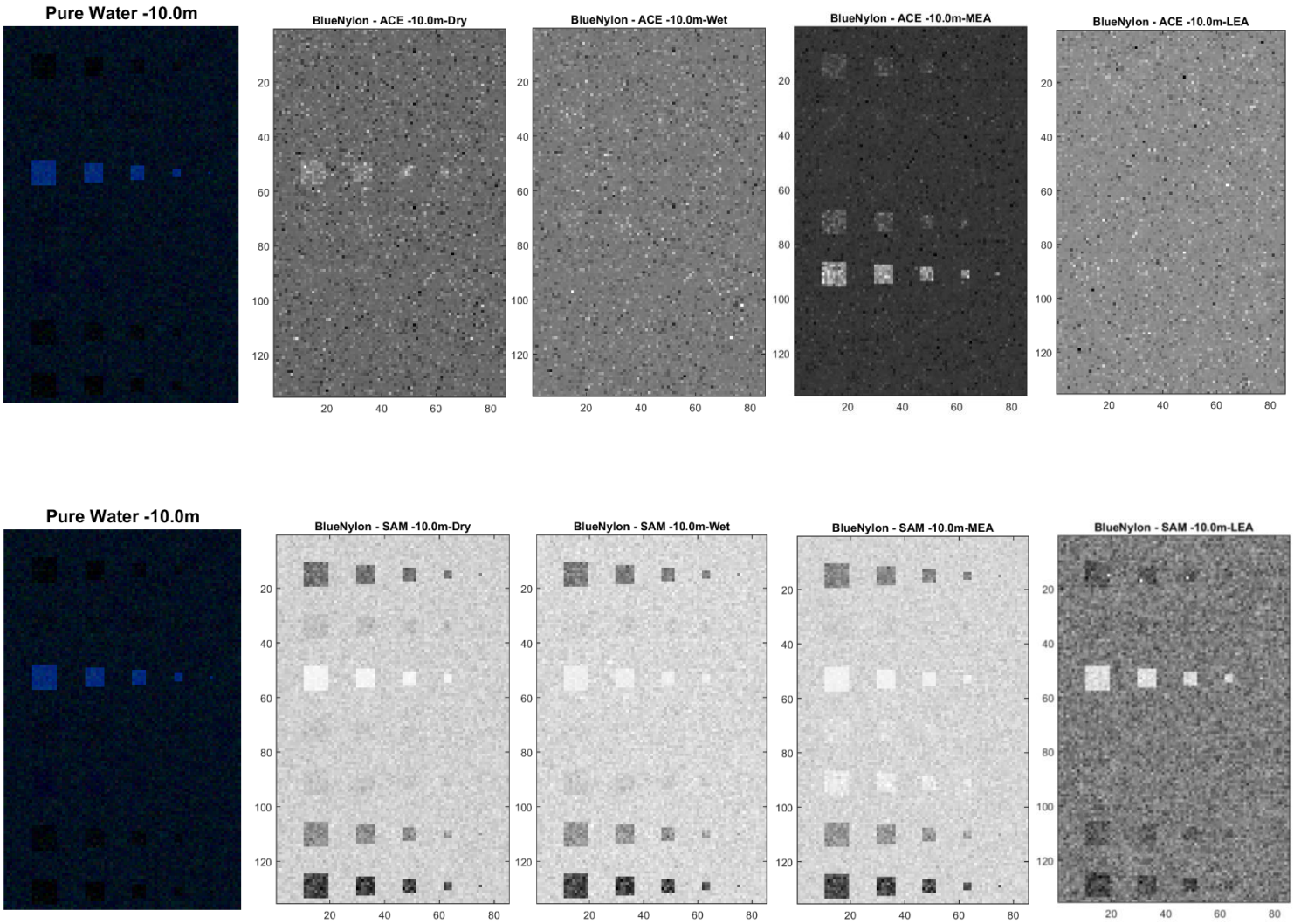

Figure 73: Detection Results of Blue Nylon Fabric with Different Target Reflectance (10m depth)

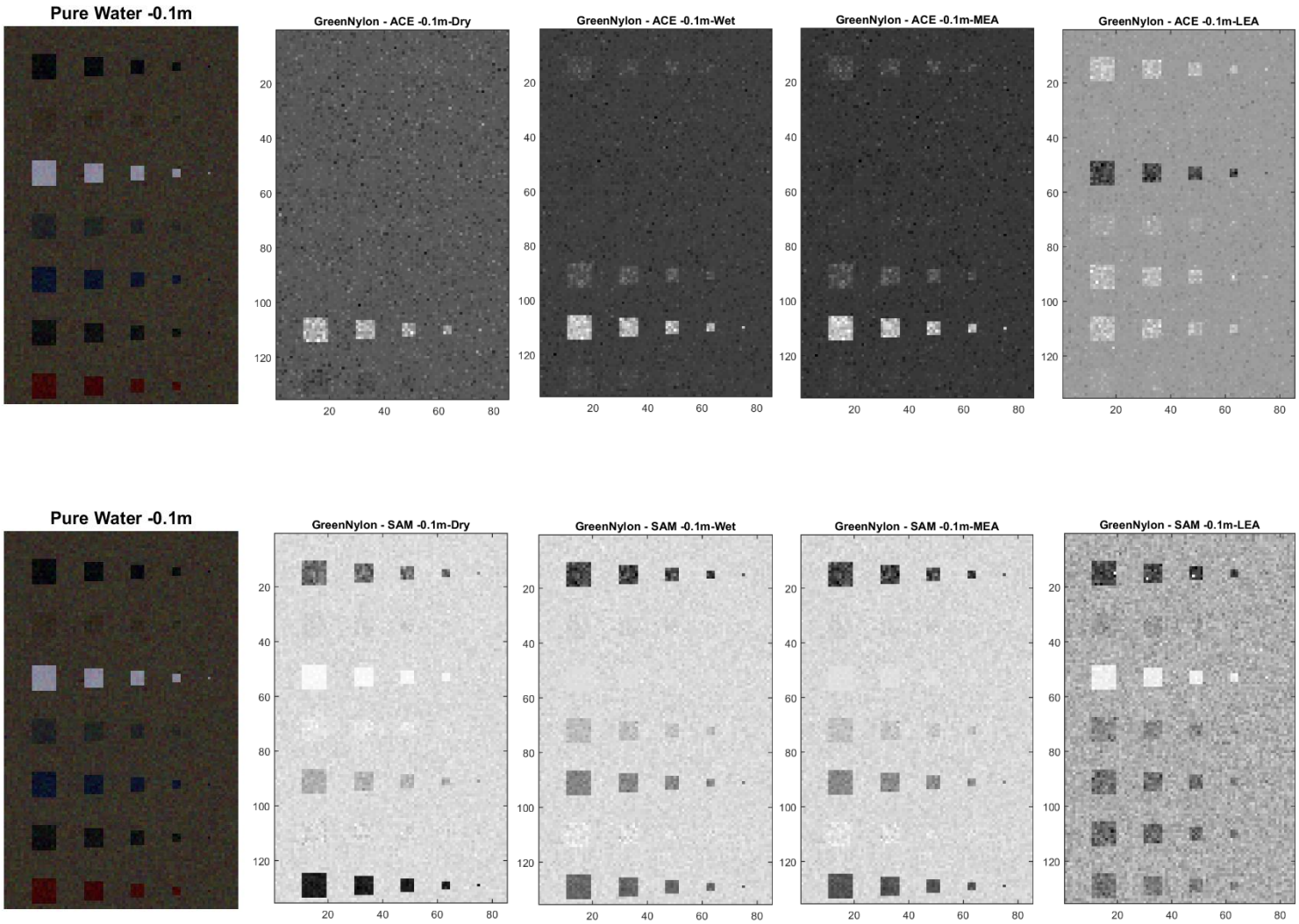

Figure 74: Detection Results of Green Nylon Fabric with Different Target Reflectance (0.1m depth)

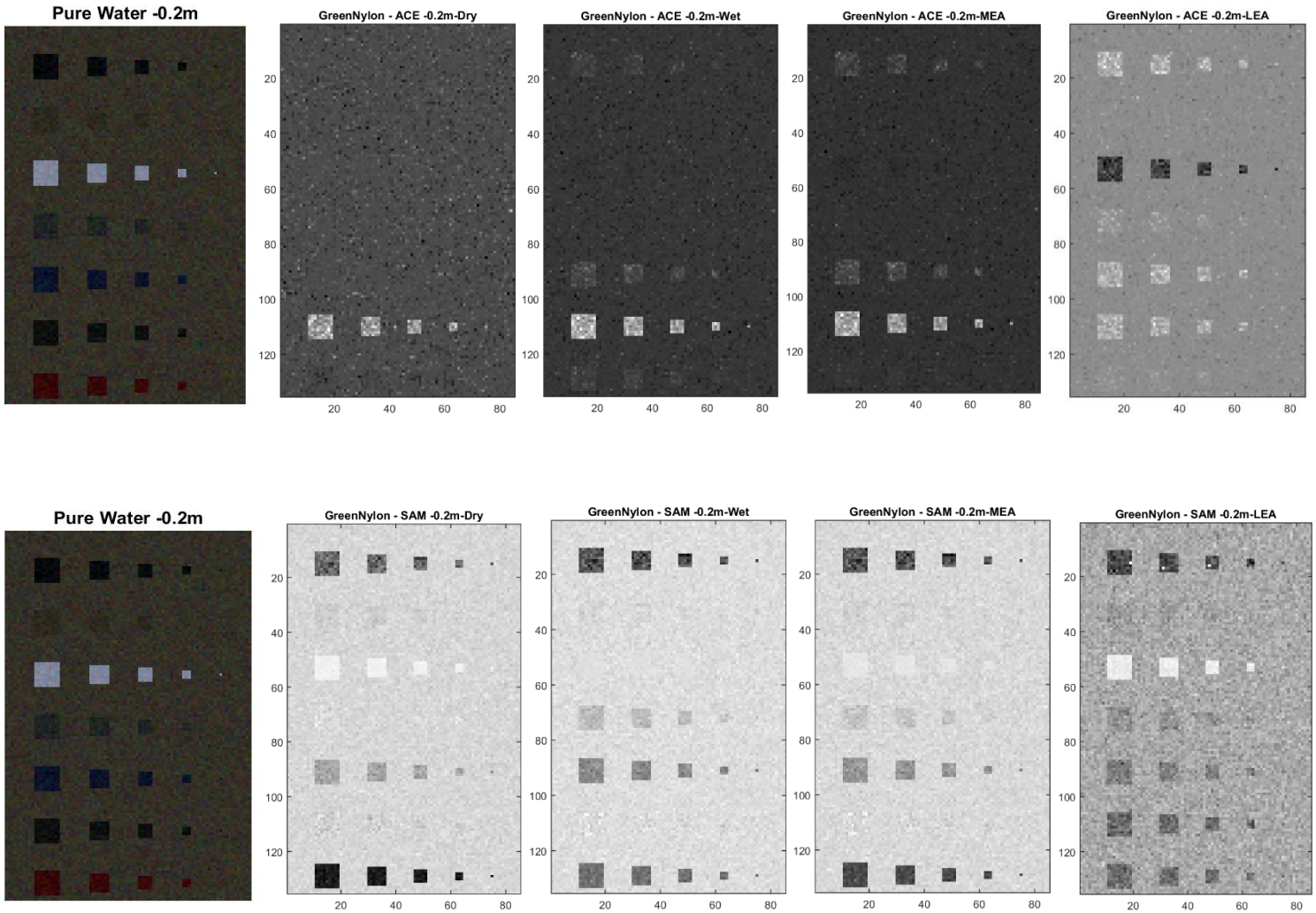

Figure 75: Detection Results of Green Nylon Fabric with Different Target Reflectance (0.2m depth)

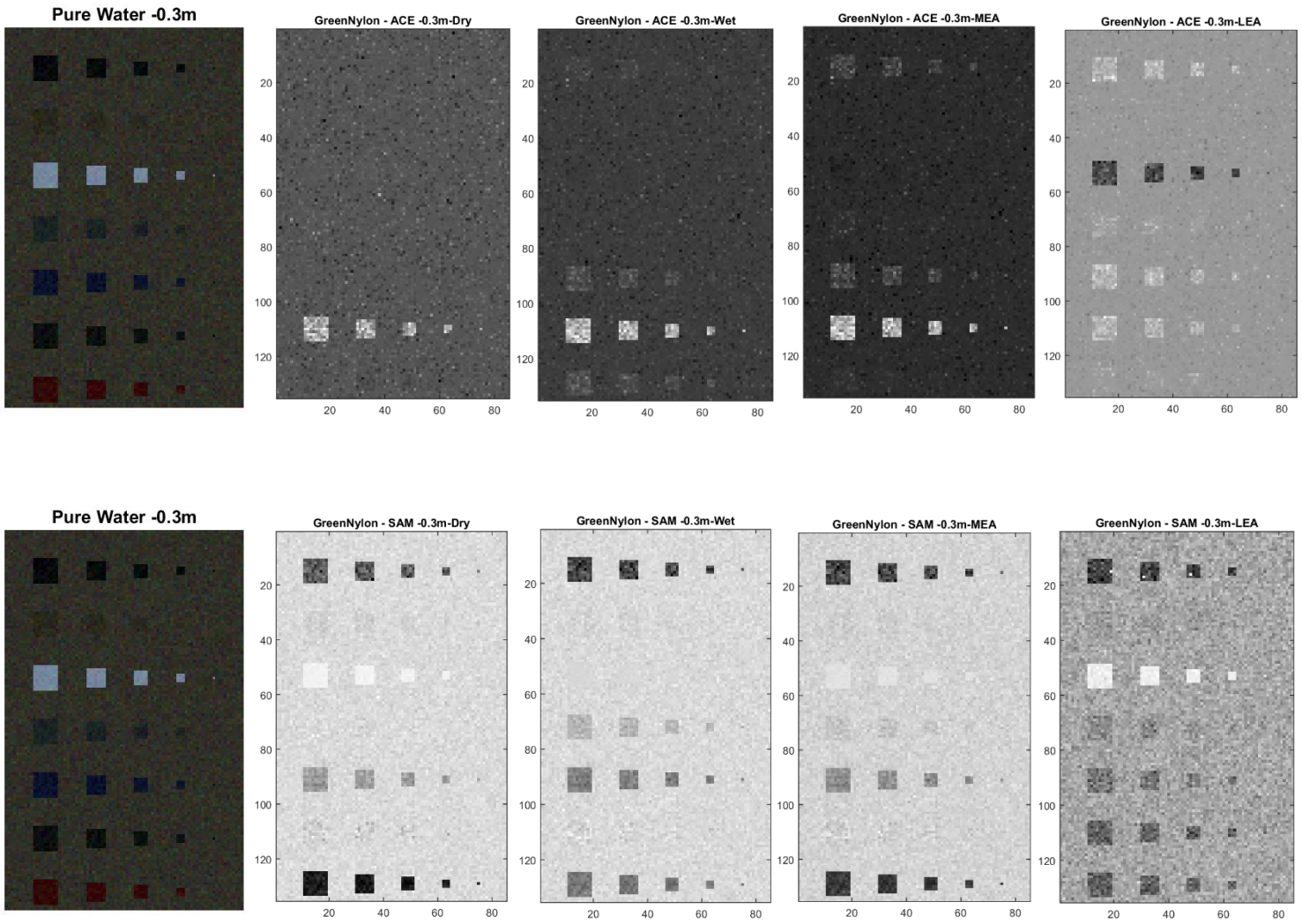

Figure 76: Detection Results of Green Nylon Fabric with Different Target Reflectance (0.3m depth)

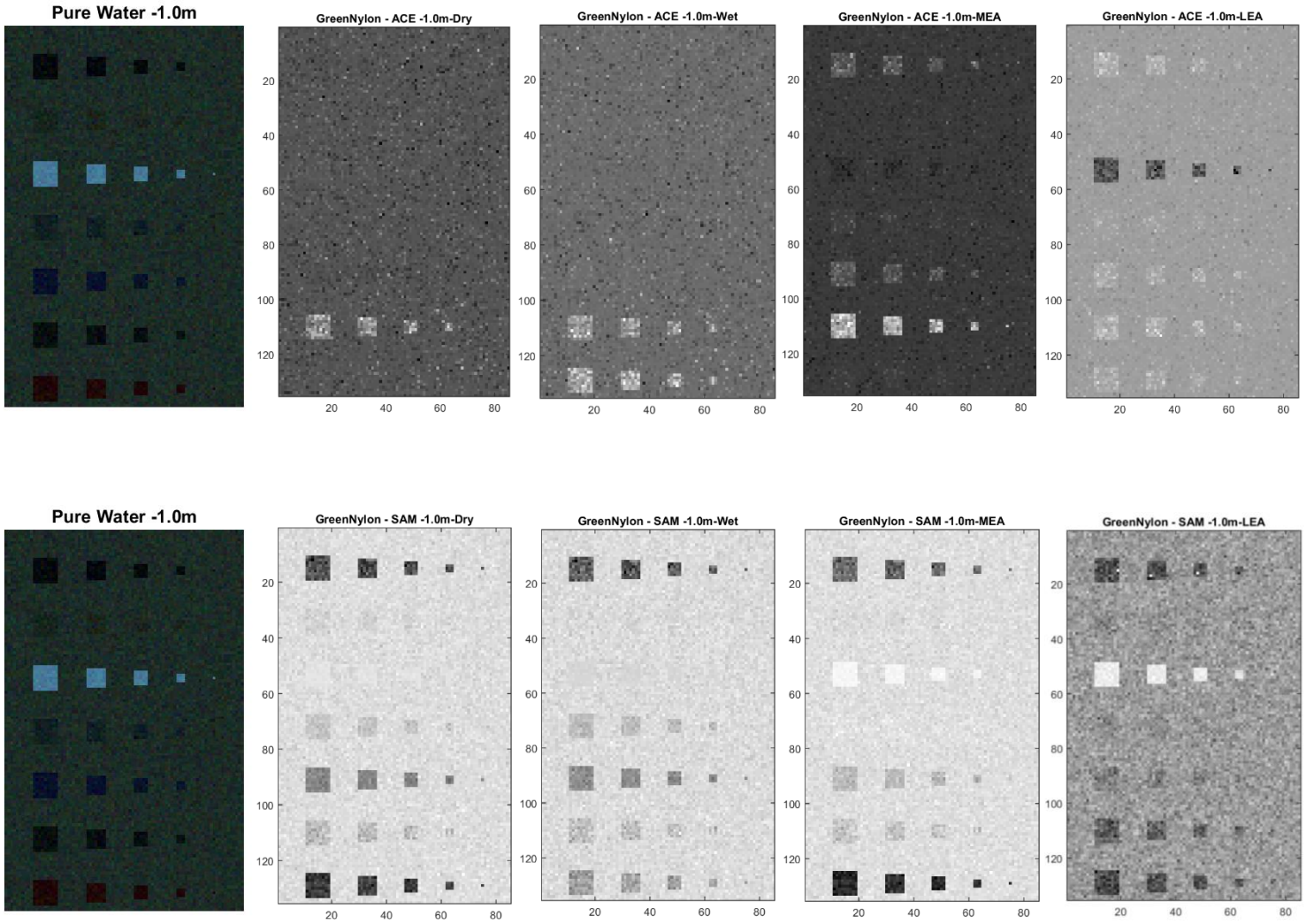

Figure 77: Detection Results of Green Nylon Fabric with Different Target Reflectance (1m depth)

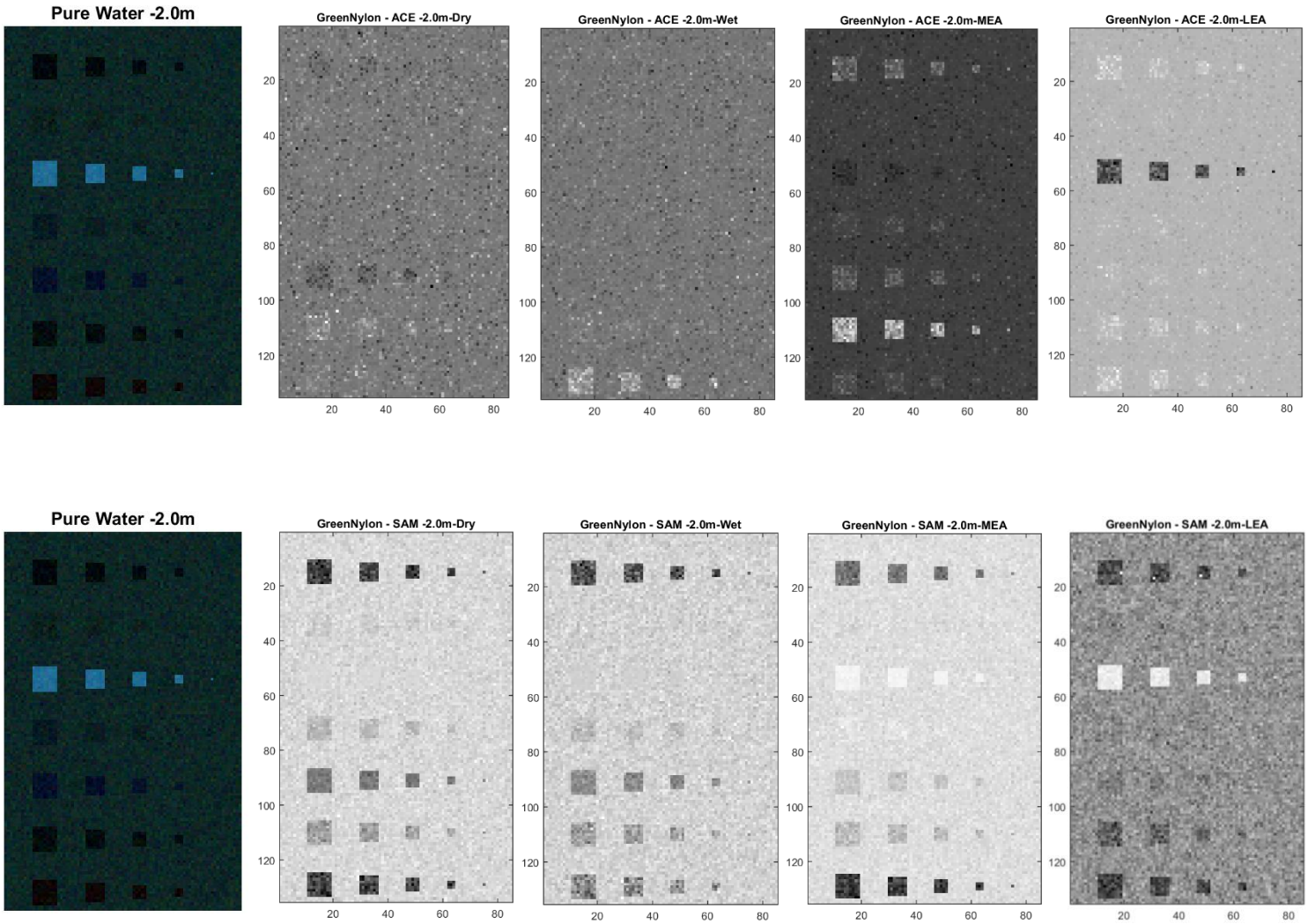

Figure 78: Detection Results of Green Nylon Fabric with Different Target Reflectance (2m depth)

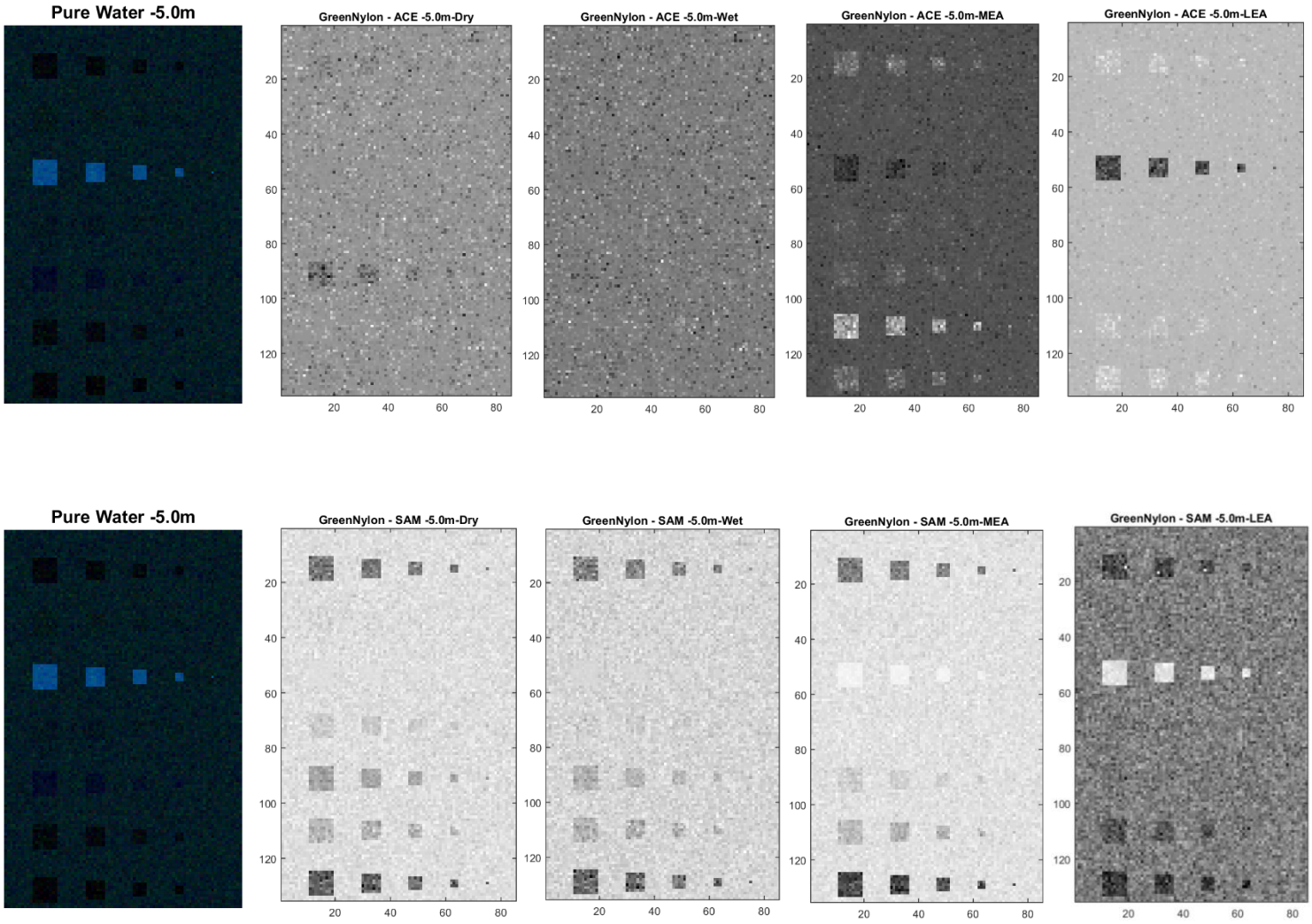

Figure 79: Detection Results of Green Nylon Fabric with Different Target Reflectance (5m depth)

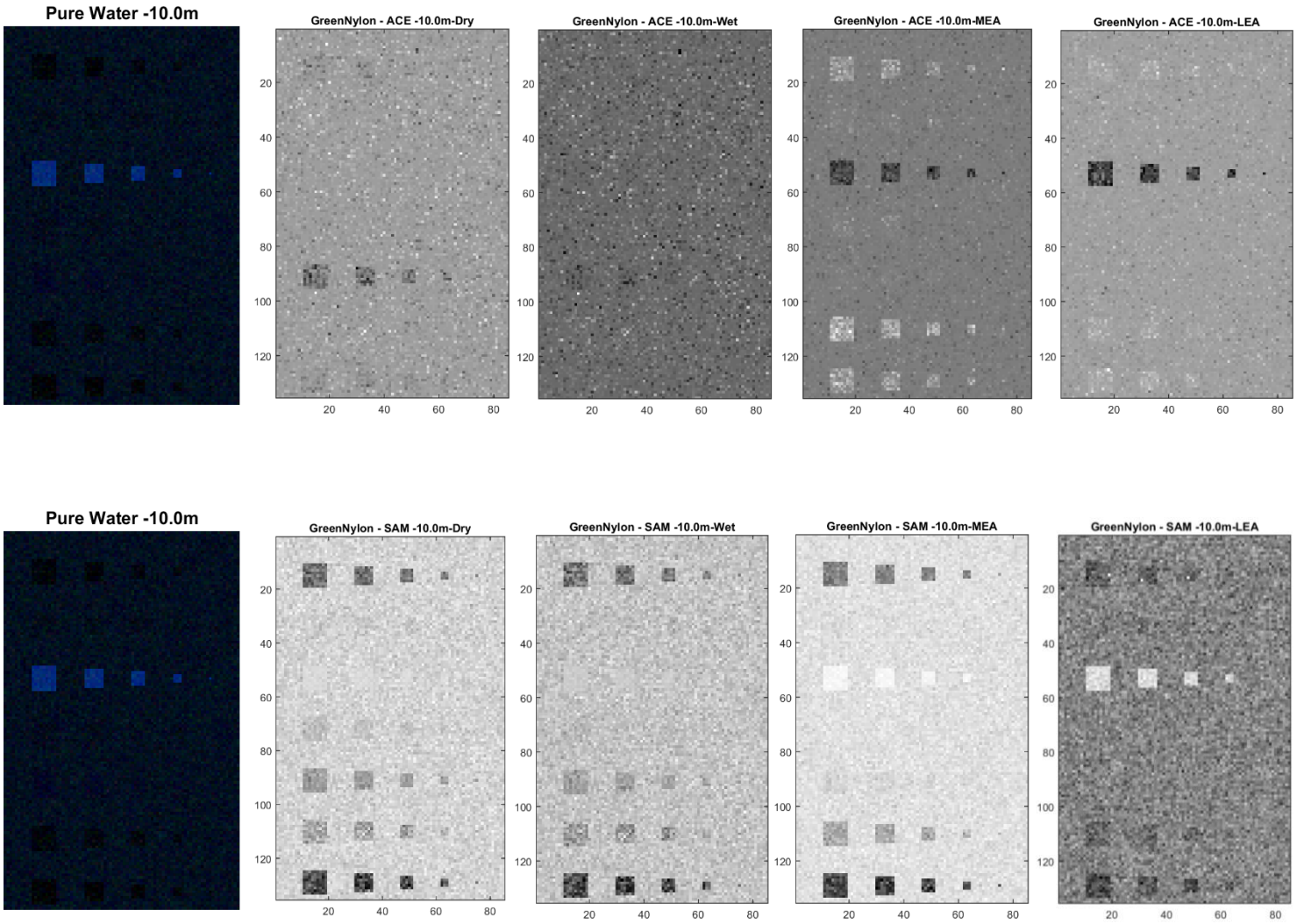

Figure 80: Detection Results of Green Nylon Fabric with Different Target Reflectance (10m depth)

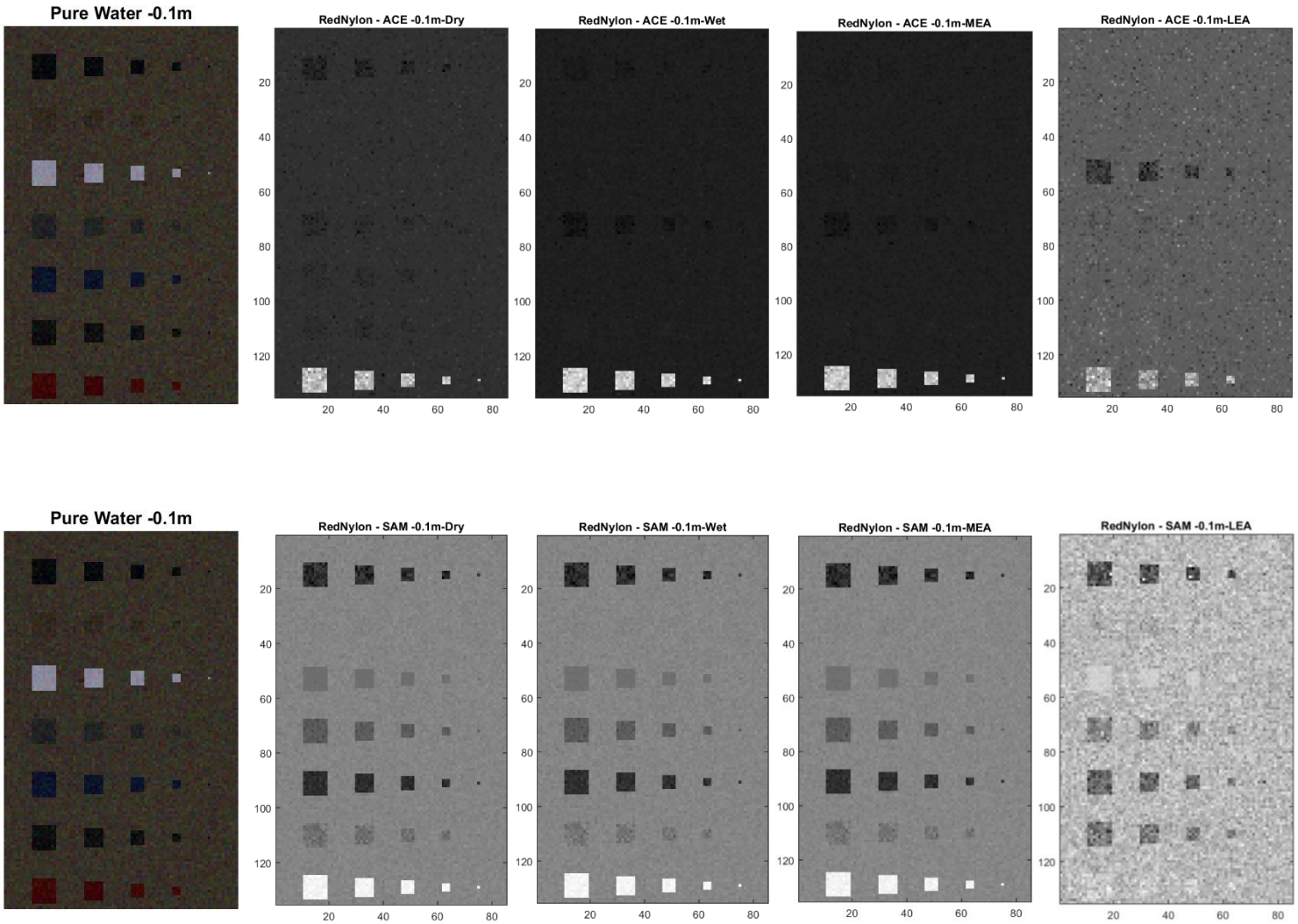

Figure 81: Detection Results of Red Nylon Fabric with Different Target Reflectance (0.1m depth)

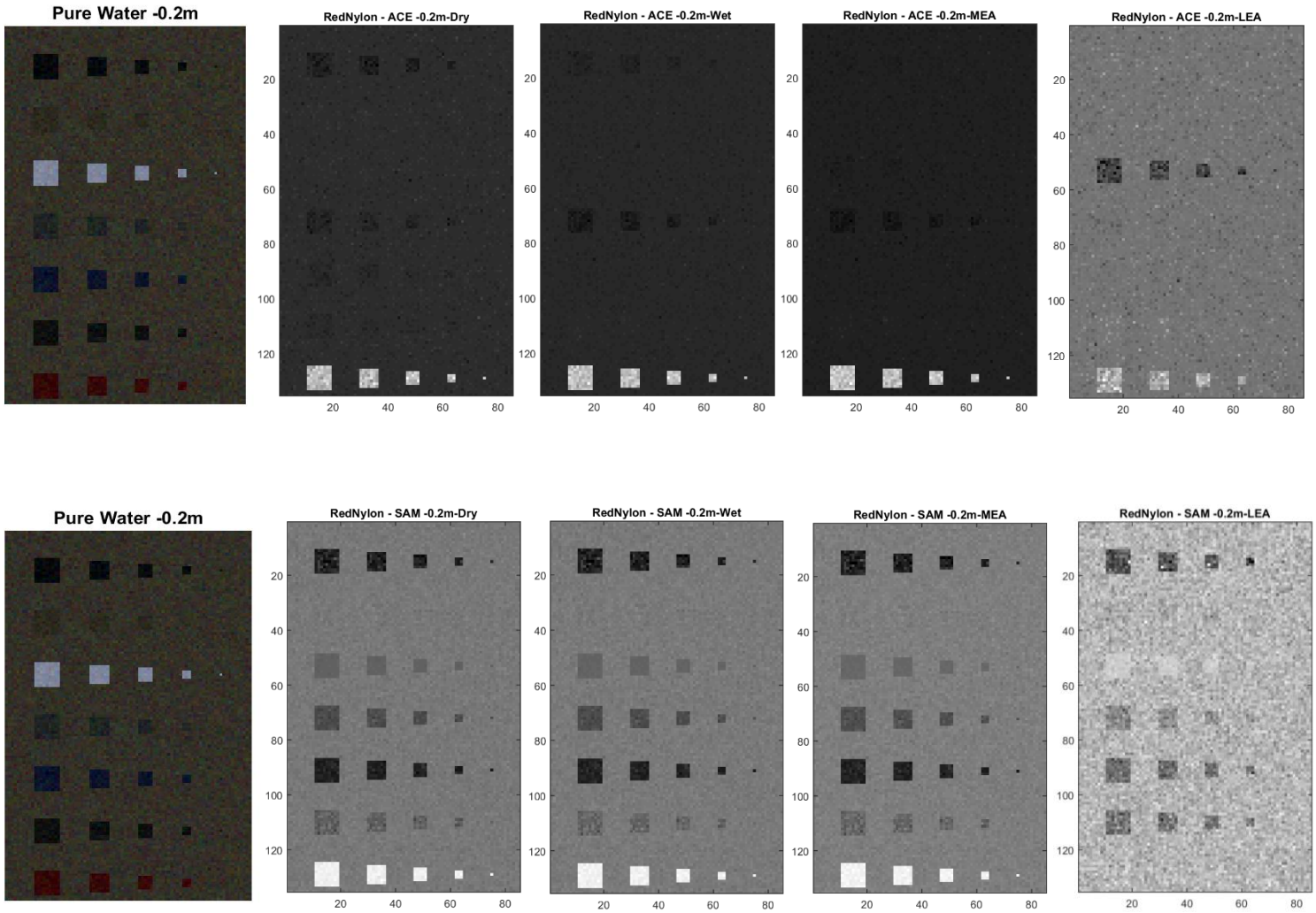

Figure 82: Detection Results of Red Nylon Fabric with Different Target Reflectance (0.2m depth)

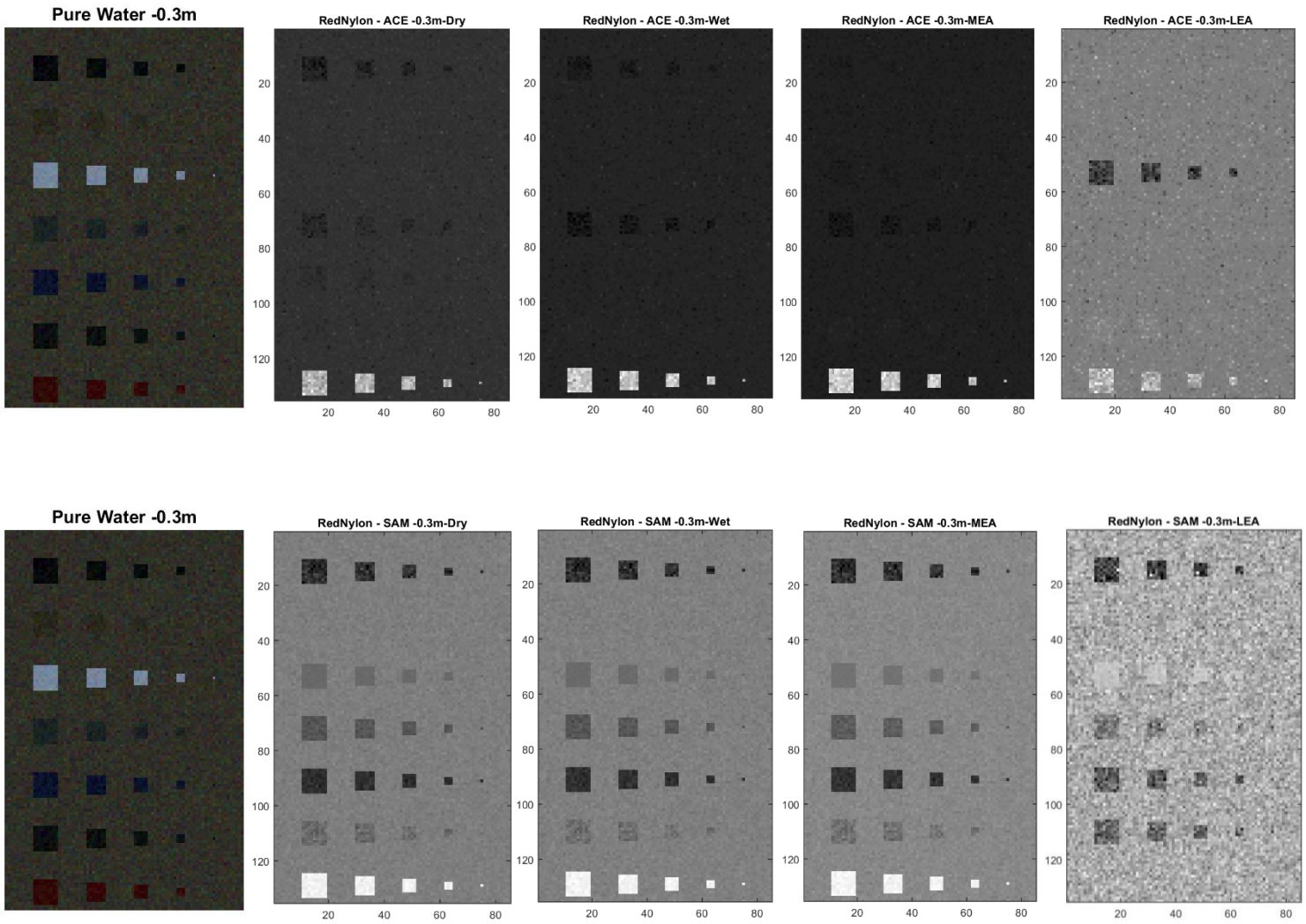

Figure 83: Detection Results of Red Nylon Fabric with Different Target Reflectance (0.3m depth)

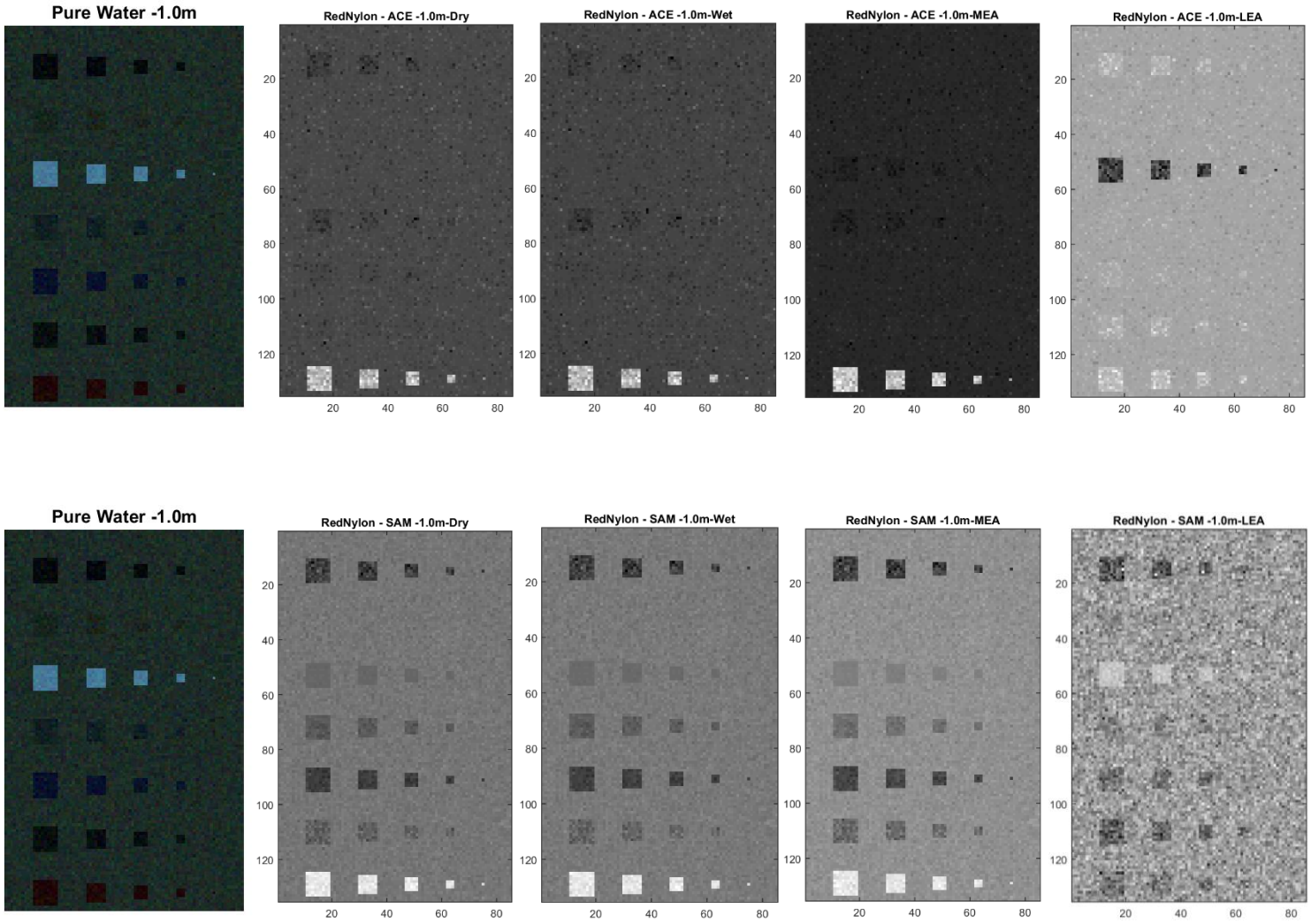

Figure 84: Detection Results of Red Nylon Fabric with Different Target Reflectance (1m depth)

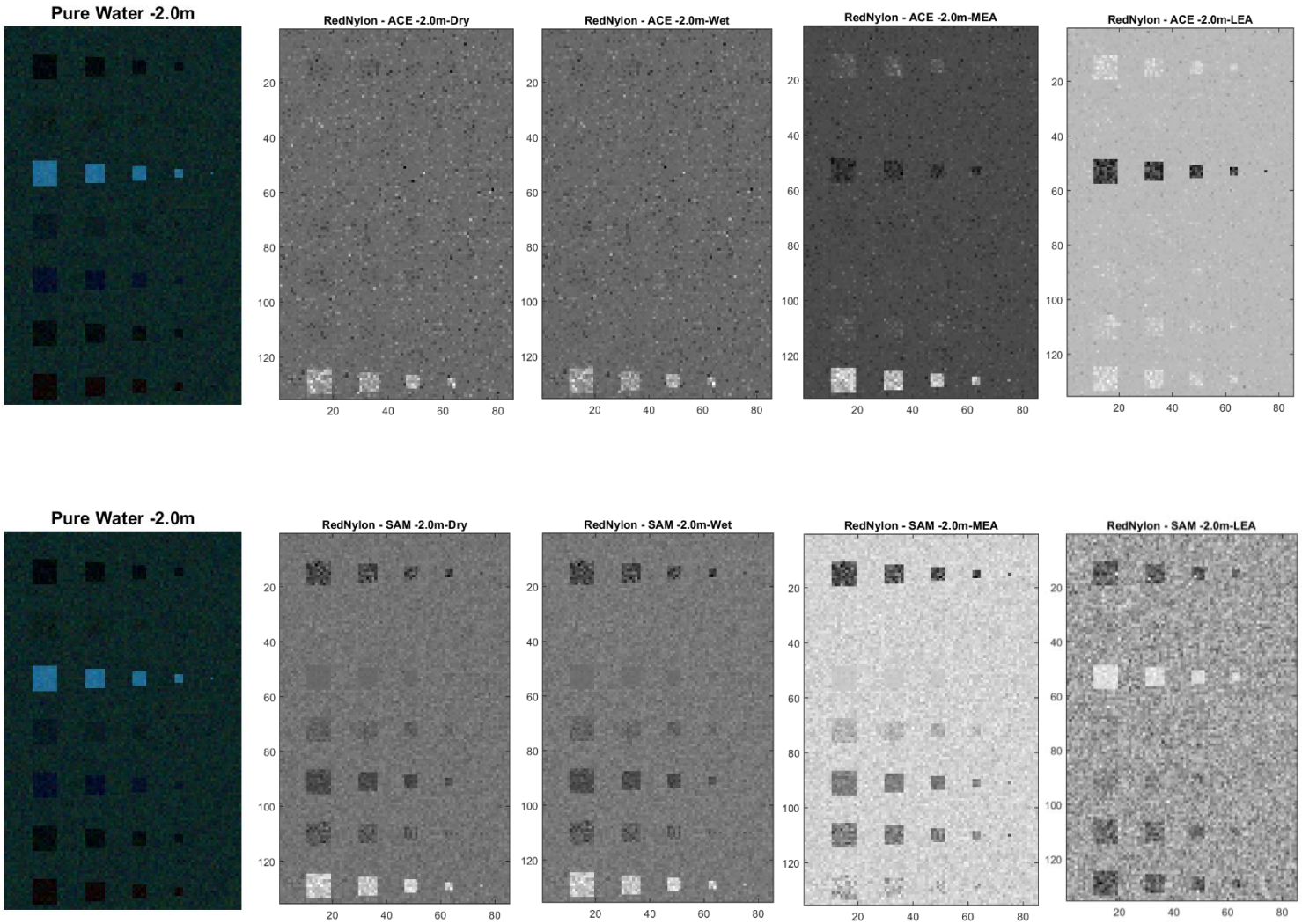

Figure 85: Detection Results of Red Nylon Fabric with Different Target Reflectance (2m depth)

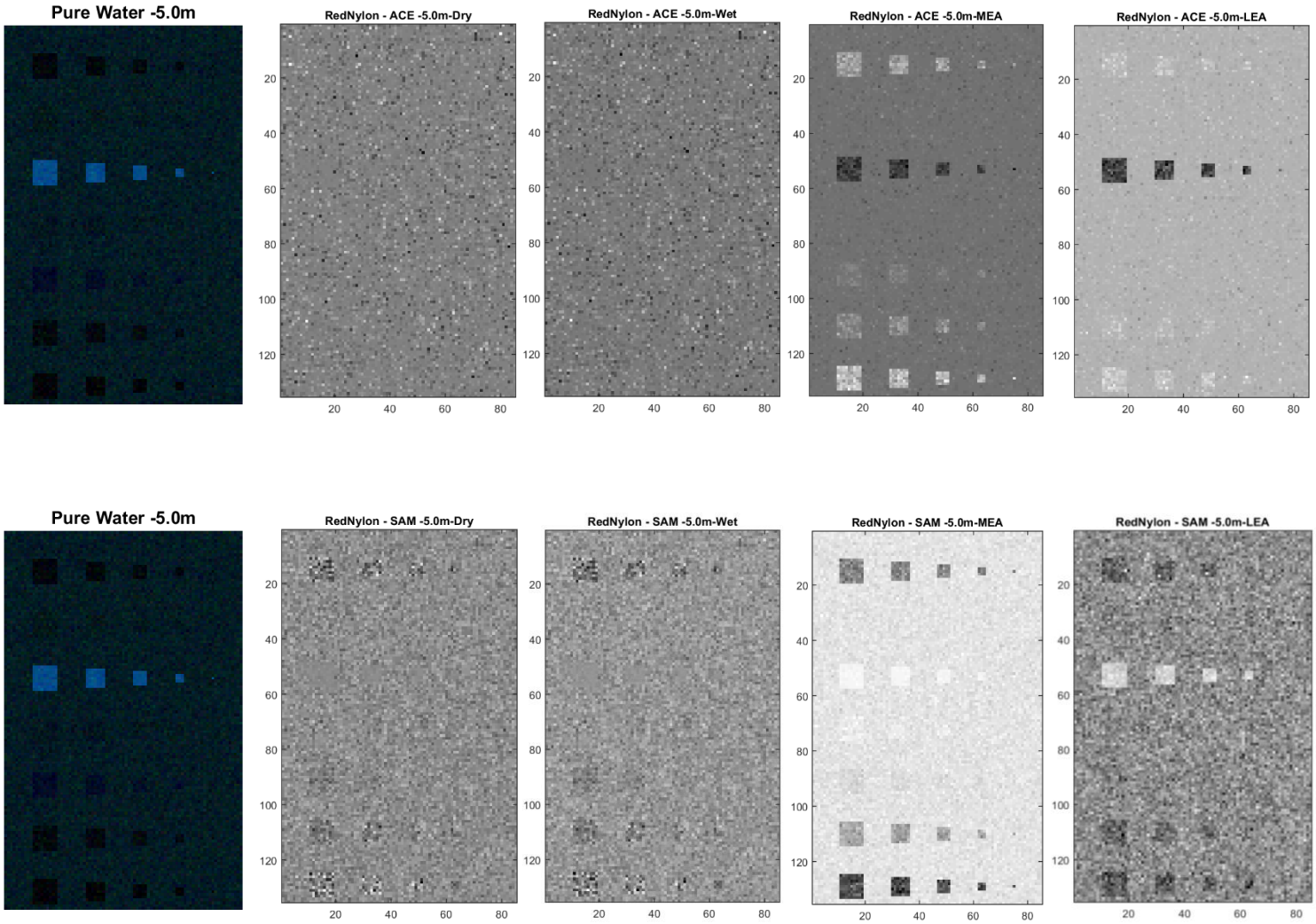

Figure 86: Detection Results of Red Nylon Fabric with Different Target Reflectance (5m depth)

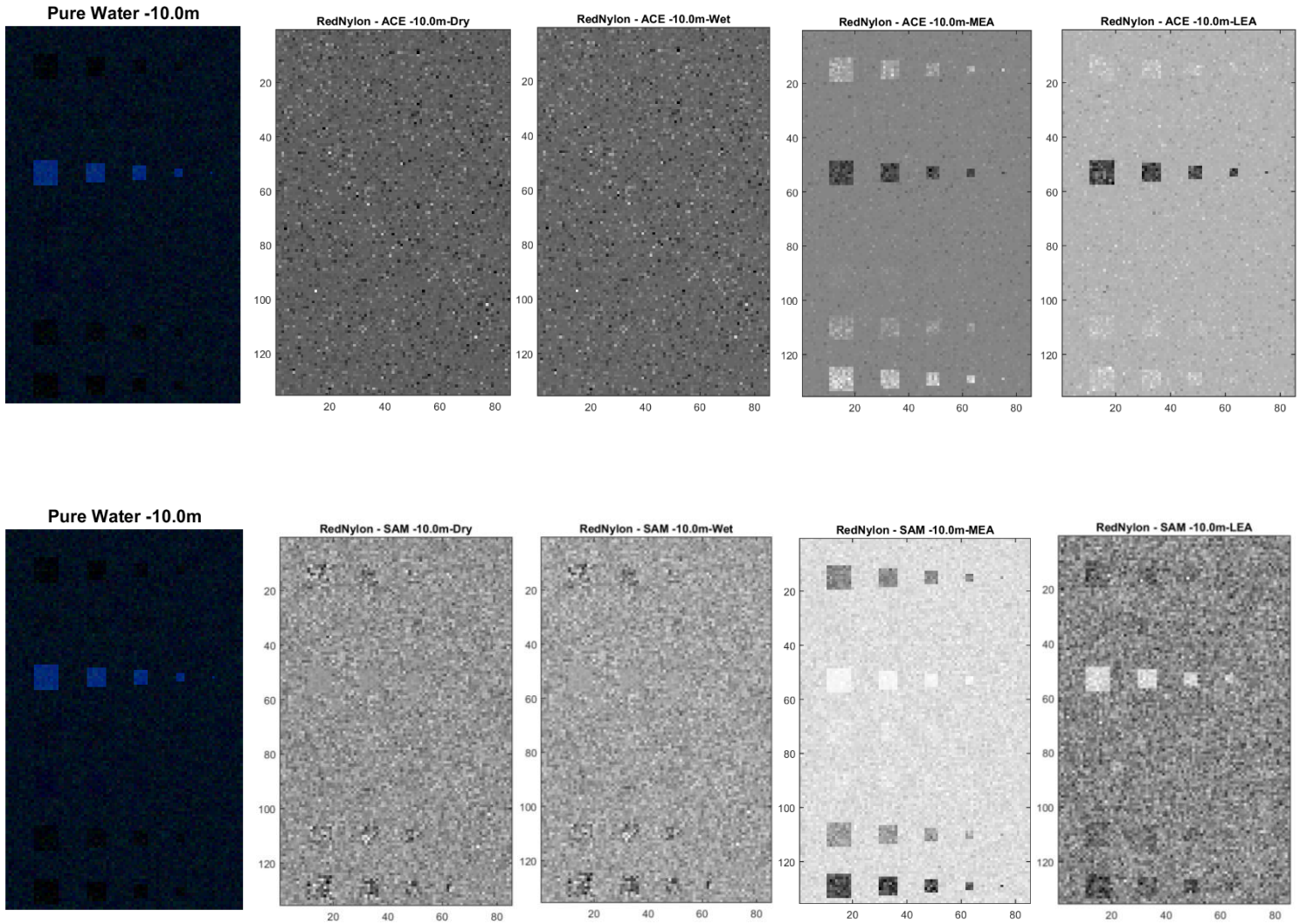

Figure 87: Detection Results of Red Nylon Fabric with Different Target Reflectance (10m depth)

APPENDIX F

DETECTION RESULTS OF MATERIALS

(REAL DATA)

The following figures show the comparison of detection results of all materials with different target signatures in 0.3 meter depth. For both algorithms (ACE, SAM), the colors ranging from black to white indicate the similarity of the materials to target reflectance from least similarity (zero, black) to most similarity (one, white) respectively.

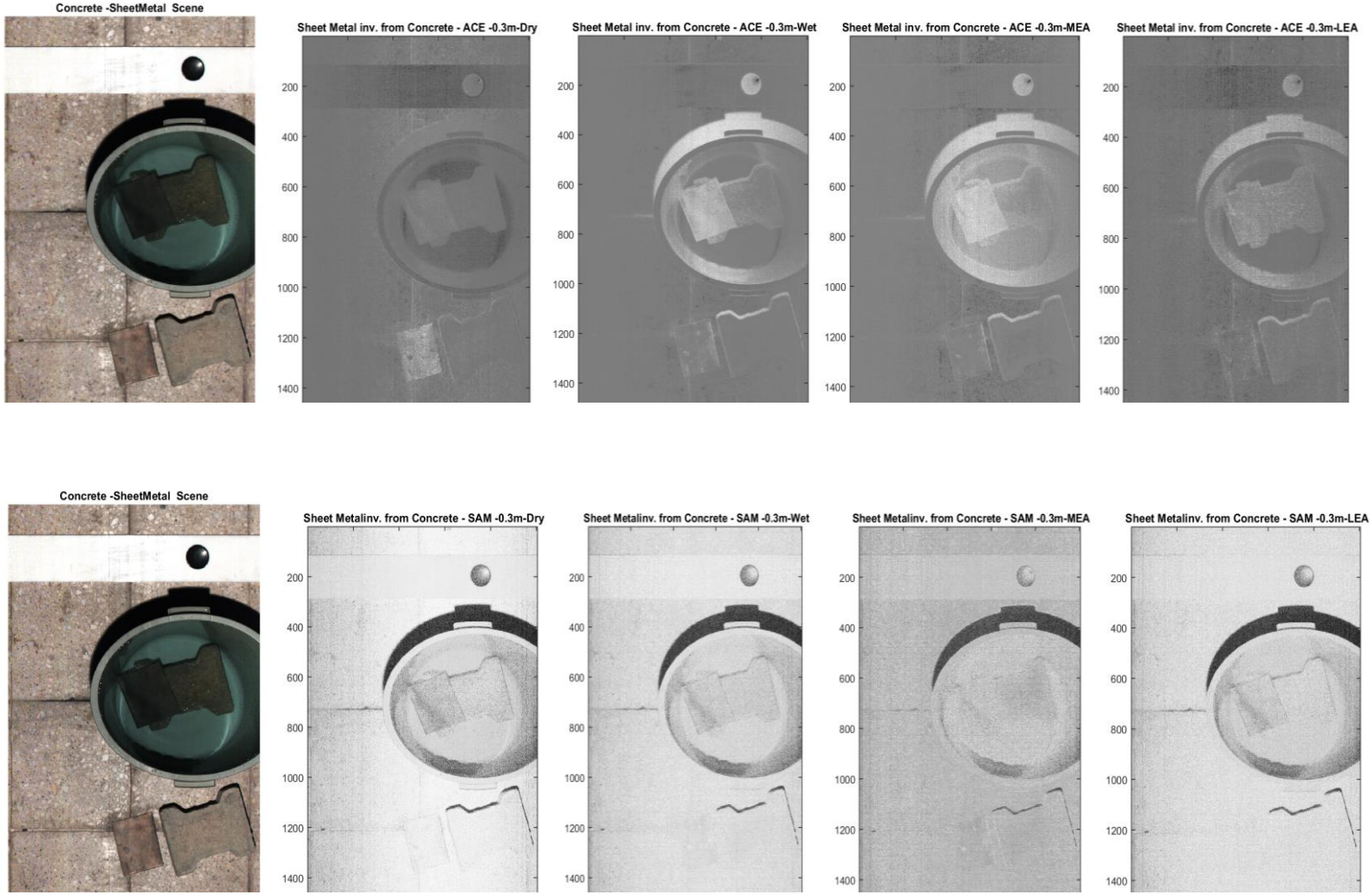

Figure 88: Detection Results of Sheet Metal with Different Target Reflectance

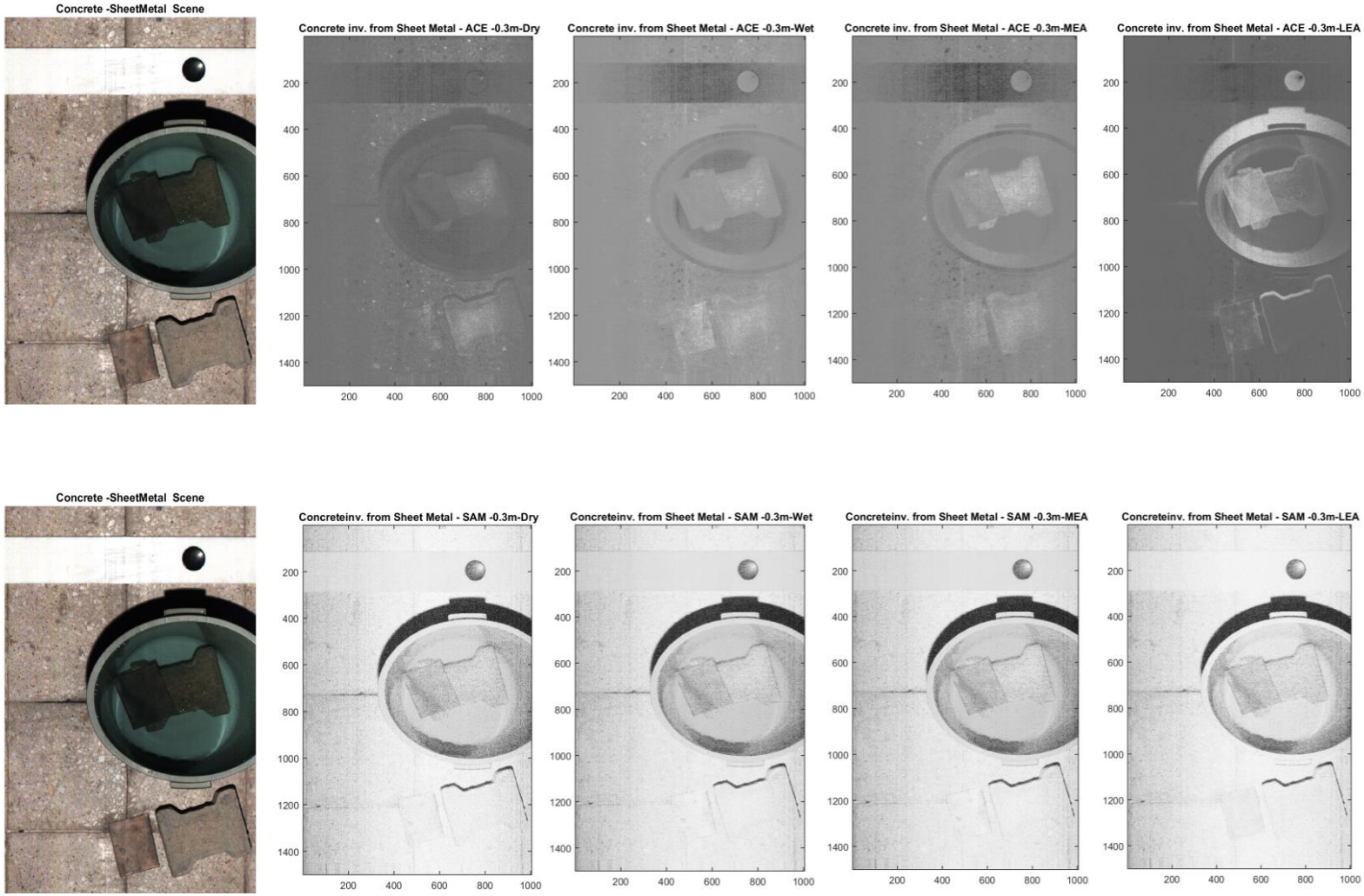

Figure 89: Detection Results of Concrete with Different Target Reflectance

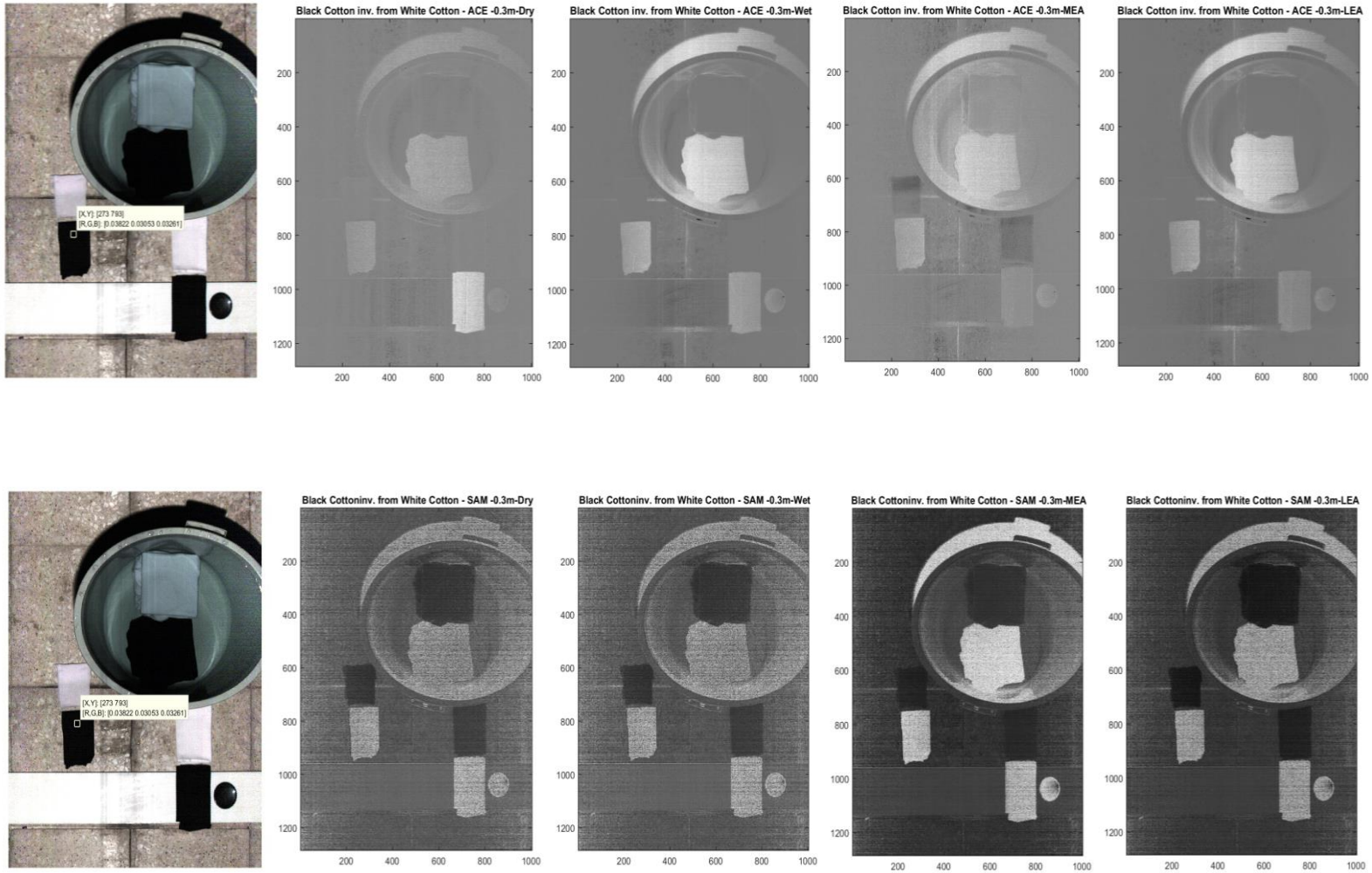

Figure 90: Detection Results of Black Cotton with Different Target Reflectance

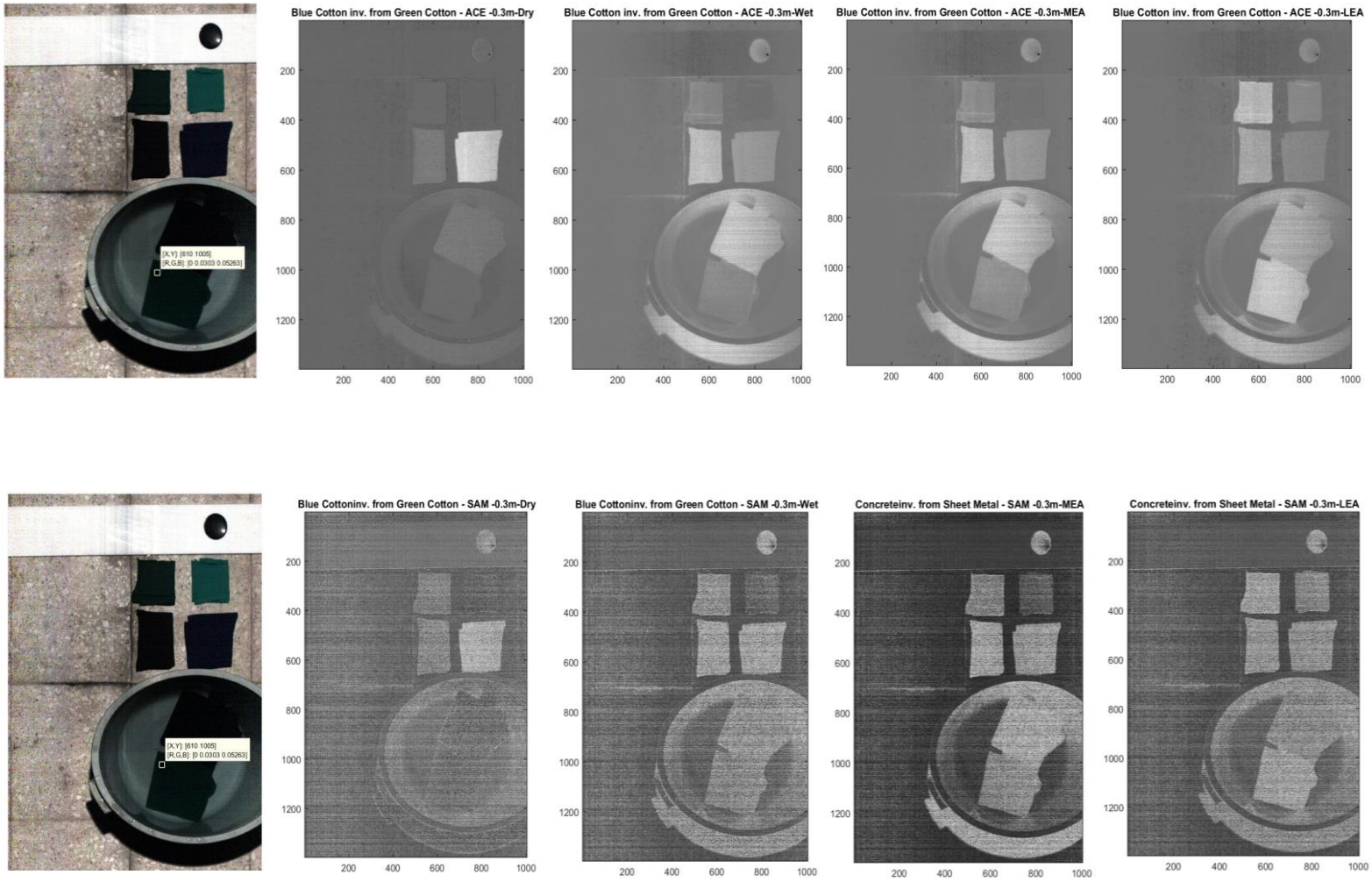

Figure 91: Detection Results of Blue Cotton Inverted from Green Cotton with Different Target Reflectance

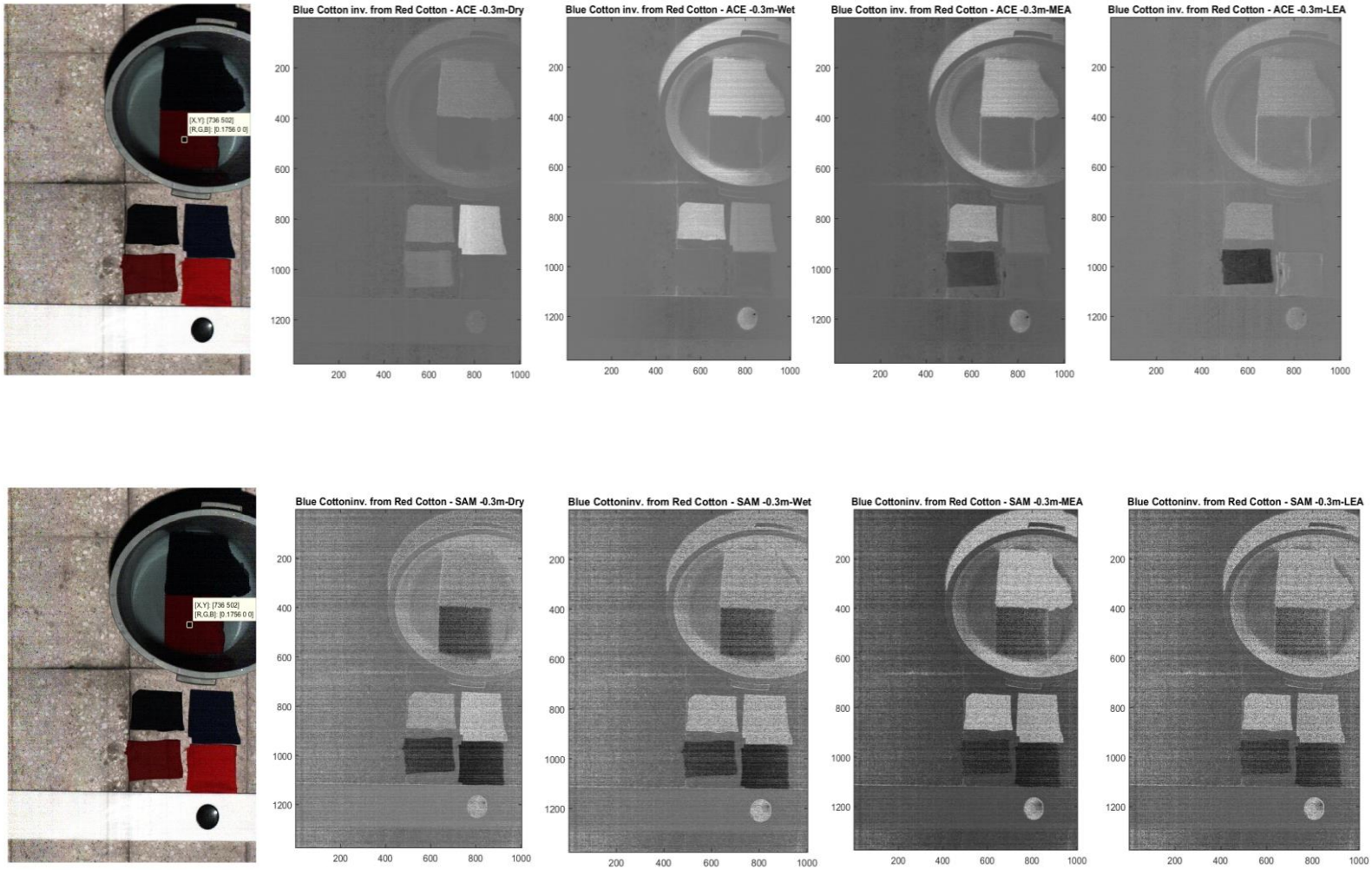

Figure 92: Detection Results of Blue Cotton Inverted from Red Cotton with Different Target Reflectance

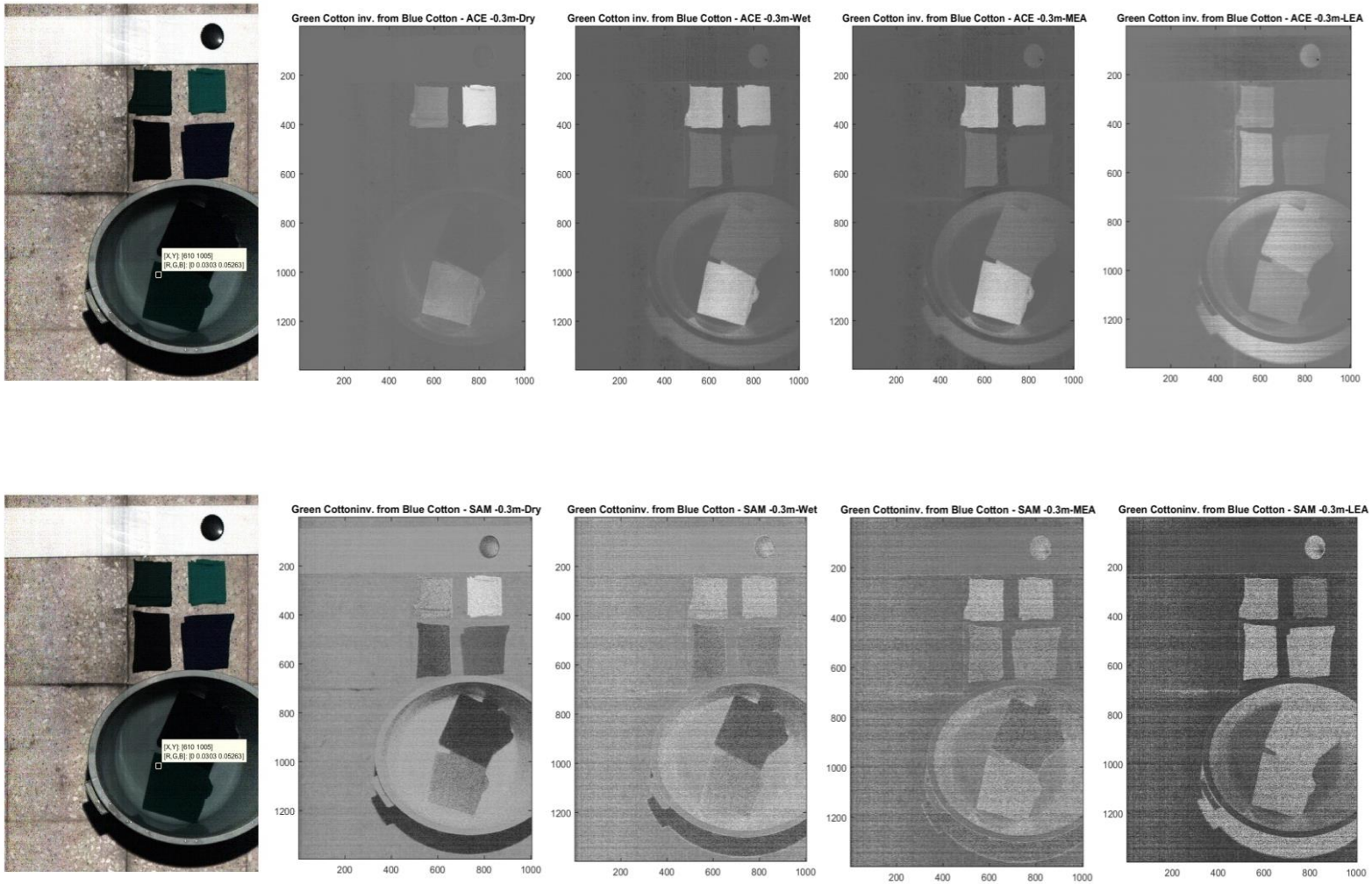

Figure 93: Detection Results of Green Cotton Inverted from Blue Cotton with Different Target Reflectance

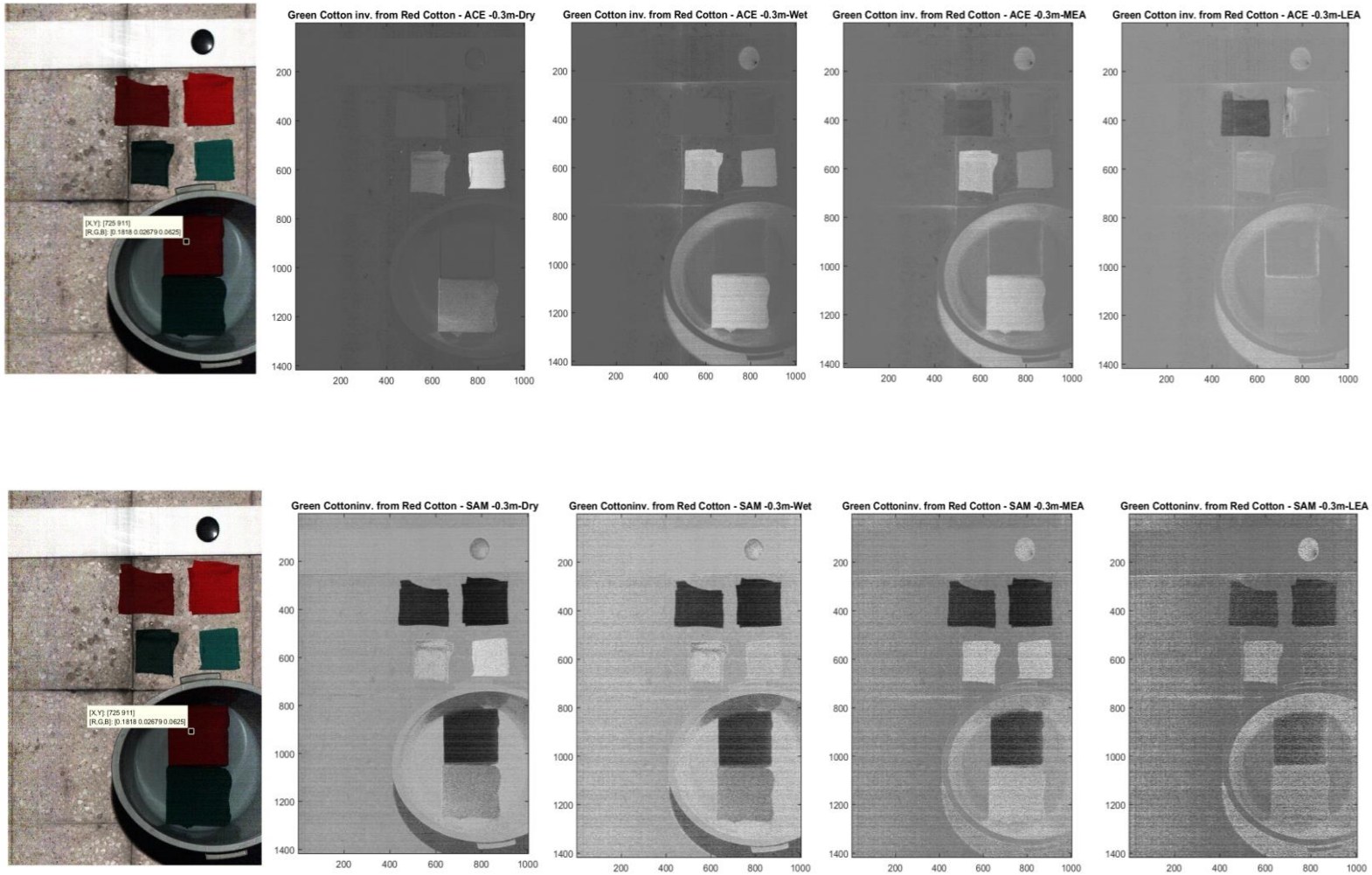

Figure 94: Detection Results of Green Cotton Inverted from Red Cotton with Different Target Reflectance

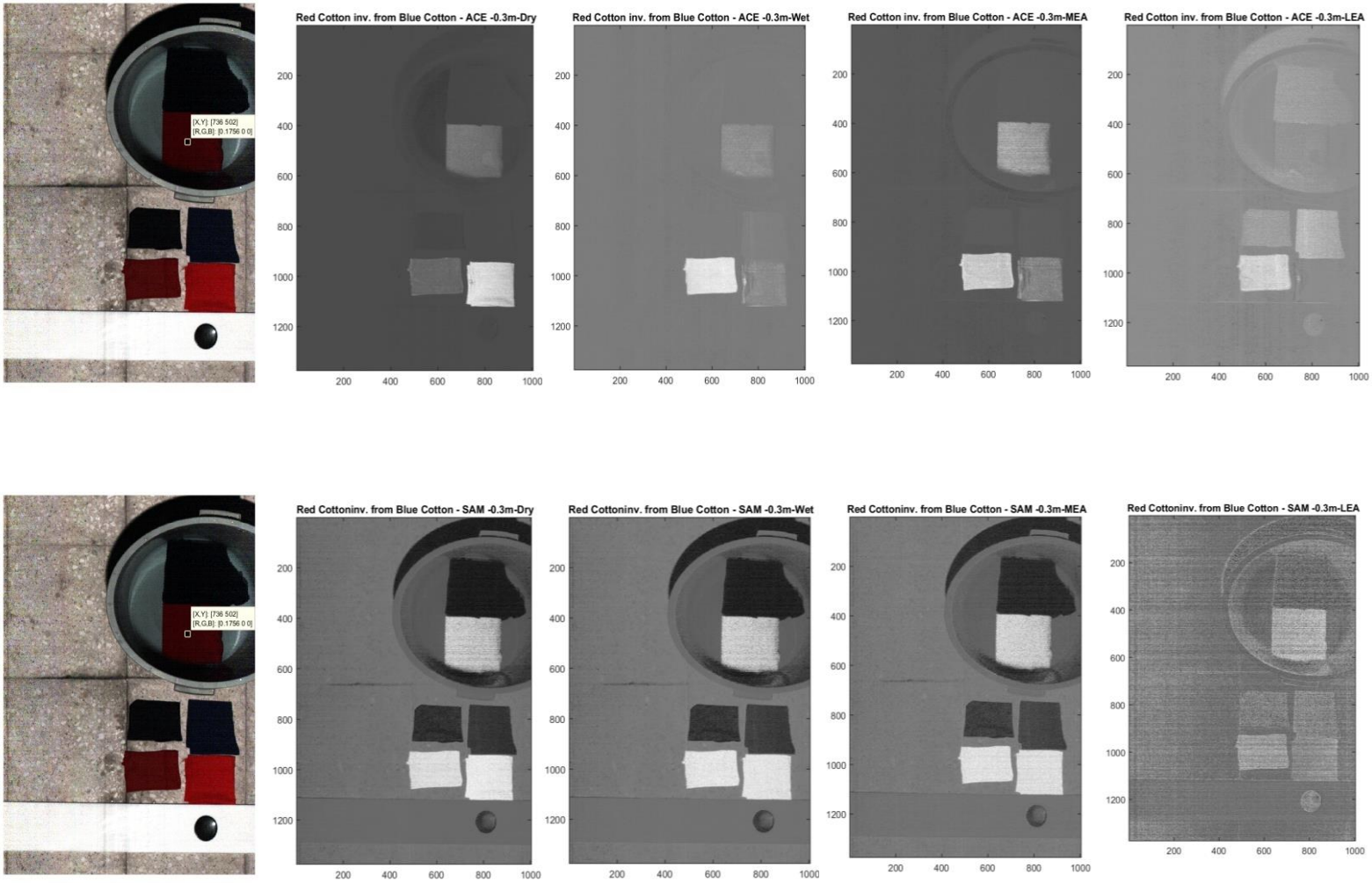

Figure 95: Detection Results of Red Cotton Inverted from Blue Cotton with Different Target Reflectance

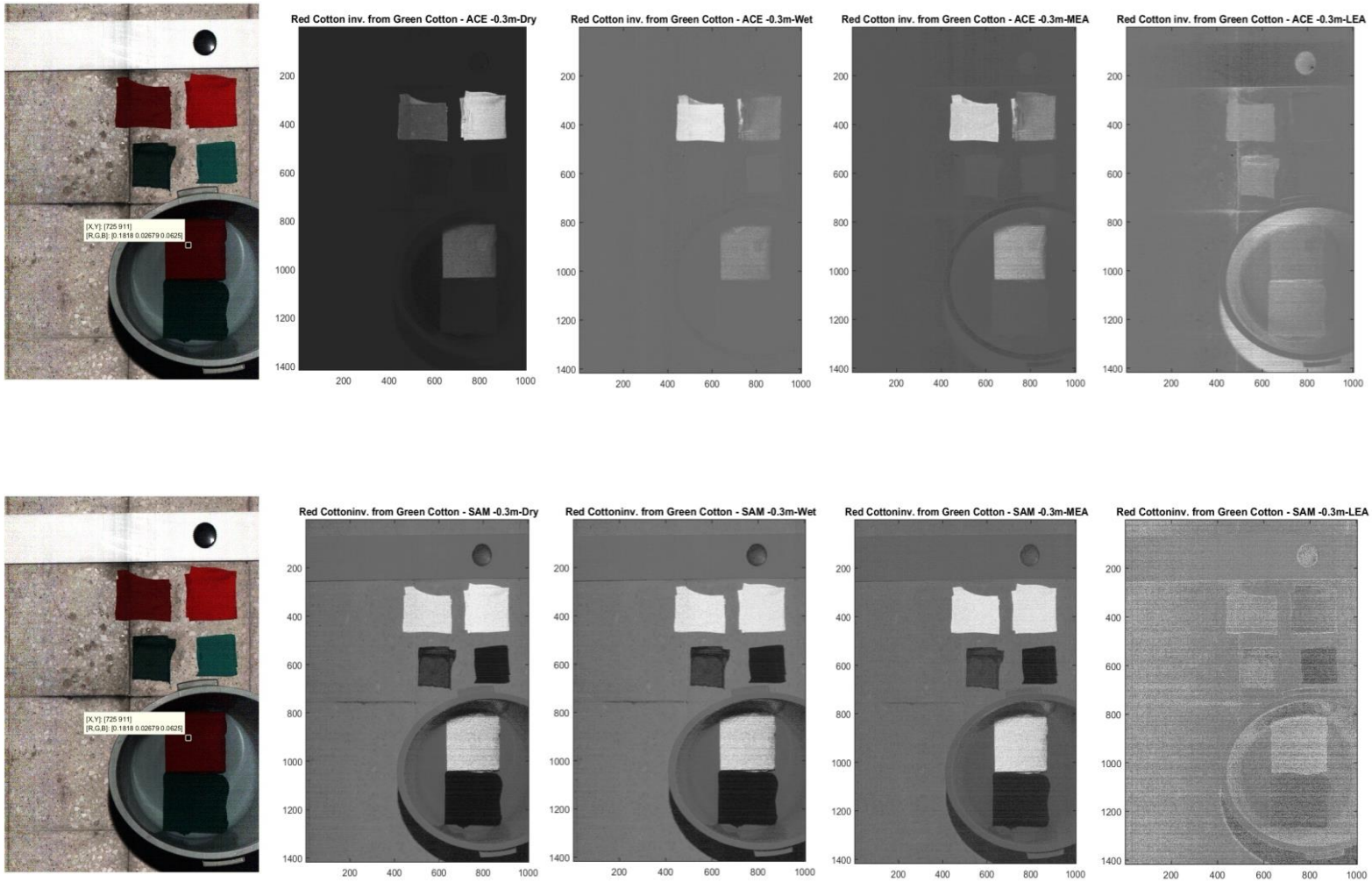

Figure 96: Detection Results of Red Cotton Inverted from Green Cotton with Different Target Reflectance

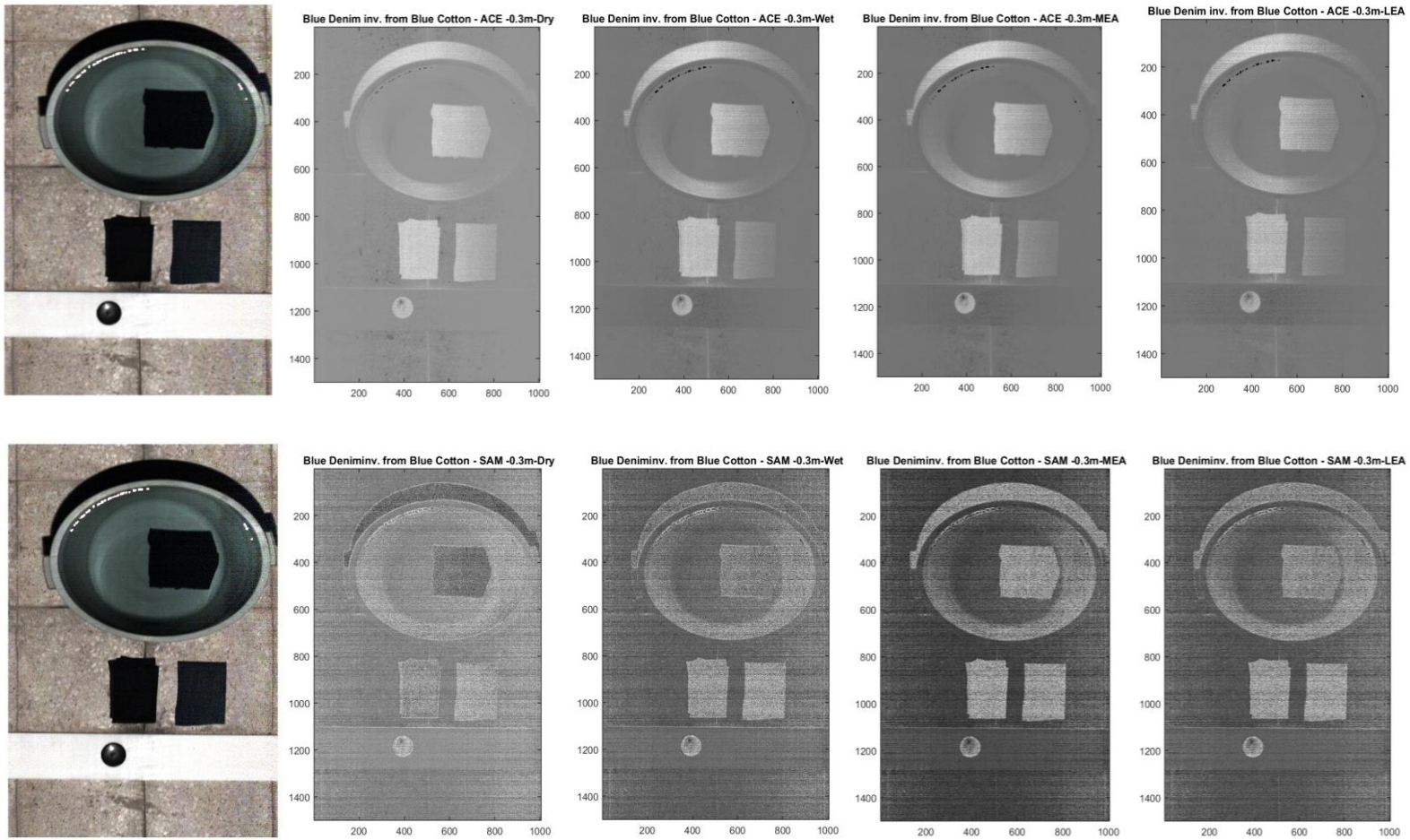

Figure 97: Detection Results of Blue Denim Inverted from Blue Cotton with Different Target Reflectance

TEZ FOTOKOPİ İZİN FORMU

ENSTİTÜ

Fen Bilimleri Enstitüsü ☐

Sosyal Bilimler Enstitüsü ☐

Uygulamalı Matematik Enstitüsü ☐

Enformatik Enstitüsü [X]

Deniz Bilimleri Enstitüsü ☐

YAZARIN

Soyadı : EKEN

Adı : İsa Cem

Bölümü : Bilişim Sistemleri

TEZİNADI (İngilizce): Underwater Target Detection with Hyperspectral Imagery for Search and Rescue Operations

TEZİNTÜRÜ: Yüksek Lisans [X] Doktora ☐

1. Tezimin tamamı dünya çapında erişime açılsın ve kaynak gösterilmek şartıyla tezimin bir kısmı veya tamamının fotokopisi alınsın. [X]

2. Tezimin tamamı yalnızca Orta Doğu Teknik Üniversitesi kullancılarının erişimine açılsın. (Bu seçenekle tezinizin fotokopisi ya da elektronik kopyası Kütüphane aracılığı ile ODTÜ dışına dağıtılmayacaktır.) ☐

3. Tezim bir (1) yıl süreyle erişime kapalı olsun. (Bu seçenekle tezinizin fotokopisi ya da elektronik kopyası Kütüphane aracılığı ile ODTÜ dışına dağıtılmayacaktır.) ☐

Yazarın imzası ..... Tarih 14 Aralık 2017